MATERIALS CHEMISTRY
FRONTIERS

REVIEW

View Article Online
View Journal | View Issue

Cite this: *Mater. Chem. Front.*, 2023, **7**, 567

Self-supported electrocatalysts for the hydrogen evolution reaction

Jin Li,[a] Jian Zhang,[b] Jinke Shen,[a] Honghui Wu,[c] Haipeng Chen,[a] Changzhou Yuan,*[d] Naiteng Wu,*[a] Guilong Liu,[a] Donglei Guo[a] and Xianming Liu*[a]

Electrocatalytic water splitting is a promising technology for producing clean hydrogen fuel. The development of cost-effective, highly efficient, and excellent durable electrocatalysts for the hydrogen evolution reaction (HER) plays an important role in industrial electrolytic water splitting. Using self-supported electrodes is regarded as an impactful strategy for designing electrocatalysts with exceptional activity and high stability, compared with conventional powder electrocatalysts. Herein, recent progress in different substrates including nickel foam (NF), carbon cloth (CC), titanium foil (TF), stainless steel (SS), iron foam (IF), cobalt foam (CF), copper foam (CFM), molybdenum foil (MF), and so on for self-supported electrocatalysts is systematically overviewed, with a special focus on the vacancy engineering, morphological control, heterostructure construction, alloying design, and doping regulation, as well as the design and fabrication route. This review may promote future research and provide a guideline for selecting suitable materials and substrates for fabricating self-supported electrodes with outstanding HER performances, thereby further enhancing the large-scale application of electrolyzing water.

Received 12th September 2022,
Accepted 8th December 2022

DOI: 10.1039/d2qm00931e

rsc.li/frontiers-materials

1 Introduction

Currently, it is an undeniable fact that the depletion of traditional primary energy sources (natural gas, crude oil, and coal) is becoming an increasingly serious problem,[1–5] which needs to be solved immediately. Therefore, high gravimetric energy density hydrogen (H_2) has attracted broad interest in this regard by virtue of its clean, sustainable, zero carbon footprint, and environmentally friendly features.[6–11] H_2 is a perfect medium for energy storage. Hydrogen does not naturally form on Earth, and must be produced by the decomposition of other molecules.

[a] College of Chemistry and Chemical Engineering, and Henan Key Laboratory of Function-Oriented Porous Materials, Luoyang Normal University, Luoyang 471934, P. R. China. E-mail: myclxm@163.com
[b] New Energy Technology Engineering Lab of Jiangsu Province, College of Science, Nanjing University of Posts & Telecommunications (NUPT), Nanjing 210023, P. R. China
[c] School of Materials Science and Engineering, University of Science and Technology Beijing, Beijing 100083, China
[d] School of Materials Science & Engineering, University of Jinan, Jinan, 250022, P. R. China. E-mail: mse_yuancz@ujn.edu.cn

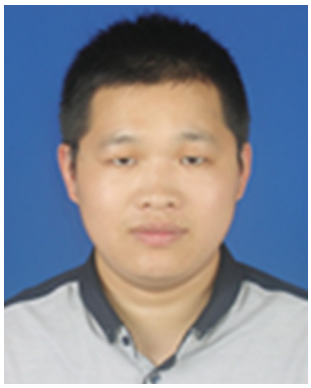

Jin Li

Jin Li is a lecturer at the College of Chemistry and Chemical Engineering, Luoyang Normal University. He received his PhD from Nanjing University of Science and Technology in 2014. His current research focuses on the electrocatalytic material for the hydrogen evolution reaction.

Haipeng Chen

Haipeng Chen received his PhD in 2015 in Mineral Processing Engineering from Shandong University of Science and Technology. He is now an associate professor at Luoyang Normal University. His current research activities include experimental and theoretical studies aimed at the utilization of composite materials in electrocatalysis.

Approximately 95% of the hydrogen yield around 50×10^6 t a^{-1} (around 50 million tonnes per annum) is generated through steam reforming of natural gas and subsequent water–gas shift reactions with electrolysis.[12] The formation of H_2 from natural gas will lead to harmful or polluting side-products. Considering the limited supplies of natural gas and the greenhouse effect of CO_2, producing H_2 from this method does not solve the needs of renewable energy storage. It should be mentioned that on a weight-by-weight basis H_2 produces almost four times more energy than the equivalent weight of gasoline. Fortunately, the production of H_2 from water through electrolysis is a clean and environmentally benign process, resulting in only oxygen being generated as a byproduct. In addition, when H_2 is burned, H_2 as a renewable fuel only generates water without by-products including sulfide, nitric oxide, and carbon dioxide. Furthermore, with the ongoing development of the economy and the global industrialization process, human beings have to deal with the universal threat of global warming and air pollution.[13–19] Thereinto, H_2, a promising energy carrier, is capable of solving the environmental problems caused by the consumption of fossil fuels. However, the strategies of producing H_2 in industry derived from steam methane reforming, biomass conversion, and coal gasification are not energy-efficient and economical.[20] Since water electrolysis was first studied by Troostwijk and Diemann in 1789, it has been extensively investigated by researchers around the world.[21–23] Alternatively, electrolyzing water is a desirable method to yield H_2 with high purity and efficiency.[24–26] Accordingly, efficient and stable electrocatalysts are urgently developed and used for the HER.

Recently, several electrocatalysts have been synthesized for the HER, and most of the electrocatalysts are in the form of powder.

Changzhou Yuan

Changzhou Yuan received his PhD from Nanjing University of Aeronautics and Astronautics in 2009. He is a distinguished professor of Taishan Scholar at the University of Jinan. He was named a Highly Cited Researcher by Clarivate Analysis (2016–2020, 2022) and Most Cited Chinese Researcher by Elsevier (2016–2021). His current research interests are mainly focused on the design and synthesis of micro-/nanostructure materials for energy-related applications including supercapacitors, Li/Na/K-ion batteries, Li–S batteries, and electrocatalysis. He has published more than 150 papers in peer-reviewed Journals with total citations of >12 000 and an h-index of 68.

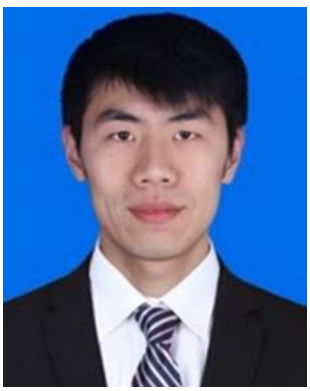

Naiteng Wu

Naiteng Wu is an associate professor at the College of Chemistry and Chemical Engineering, Luoyang Normal University. He received his PhD from Sichuan University in 2016. His current research interests are key materials for electrochemical energy storage and conversion.

Guilong Liu

Guilong Liu received his PhD from Tianjin University in 2016. He is now an associate professor at Luoyang Normal University. His research interests focus on nano-structured materials and hybrid materials for energy-related applications, including industrial catalysis and metal ion batteries.

Xianming Liu

Xianming Liu received his PhD from the Chinese Academy of Sciences in 2006 and worked as a visiting scholar under the supervision of Prof. Jang-Kyo Kim in Hong Kong University of Science and Technology (2008–2010). He is currently a professor and Dean of School of Food and Drug at Luoyang Normal University. His research focuses on transitiona metal oxide and carbon materials for supercapacitors, lithium/sodium/potassium/zinc ion batteries, and electrocatalysis. He has written well over 130 referred journal papers and holds 10 Chinese invention patents. He was named a Highly Cited Researcher 2019 in Materials Science by Royal Society of Chemistry.

Thus, a binder is necessarily adopted to cast catalysts on substrates in electrochemical tests, which is a time- and cost-consuming process. Besides, the binder employed in preparing electrodes can not only increase the interfacial resistance between electrocatalysts and substrates but also block the active sites,[27,28] resulting in reducing their HER activity and stability. Fortunately, the self-supported electrocatalysts directly constructed on conductive substrates have many advantages compared to the powdery-type catalysts such as (1) a simplified electrode preparation process, (2) enriched active sites *via* increasing loading amounts, (3) more active sites exposed by eliminating binders, (4) charge transport favoured through evenly rooting catalysts on the substrates, (5) hydrophilic/hydrophobic surface engineering *via* tuning the morphology and microstructure, and (6) the catalysts can be anchored on the substrates for enhancing stability,[29–34] leading to extraordinary HER performance. As a result, the self-supported electrocatalysts are more suitable for industrial applications compared to conventional powdery electrocatalysts. To date, encouraging improvements have been achieved in the self-supported electrodes.[34] Nevertheless, to meet the industrial standard, it is still significantly challenging to enhance the performance of HER electrocatalysts, and the performance of self-supported electrocatalysts is still far away from meeting the requirements for commercial applications. The challenges in fabricating electrocatalysts for practical applications at large current densities primarily originate from the rigorous need of electron and mass transfer efficiency. More importantly, rationally constructing an electrocatalytic electrode with desirable morphology and structure can improve the electron transfer efficiency, exposure of active sites, ion diffusion rates, reaction kinetics, as well as mechanical stability, and therefore has an important effect on its HER performance at large current densities.[35] Therefore, highly efficient and stable self-supported electrocatalysts are urgently needed for industrial electrolytic water splitting for producing hydrogen. To meet the requirements for commercial use (a low overpotential at 10 mA cm^{-2} for the HER, a small Tafel slope, long-term stability (>1000 h), high operating current densities up to 1000 mA cm^{-2}, and so on), summarizing the recent advances in the designing and fabricating self-supported electrodes is greatly significant.

In this review, we summarize recent developments in the area of self-supported electrodes for the HER (Fig. 1). We comprehensively review many important kinds of self-supported substrates. In the discussion, particular attention is paid to the defect and morphology engineering, interface regulation, doping, and catalytic performance of these HER electrocatalysts. Finally, we briefly point out the critical challenges in HER electrode design and performance.

2. Electrochemical hydrogen evolution reaction

2.1 Mechanisms of electrochemical HER

The electrocatalytic HER involves a two-electron transfer reaction occurring at the electrode/electrolyte interface.[36]

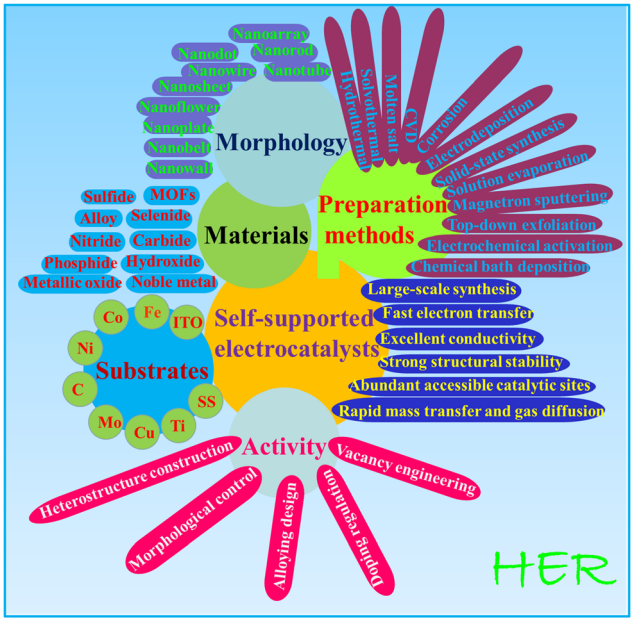

Fig. 1 Overview of the topic covered in this article.

Thereinto, H_2 is produced at the cathode through the reduction of either a proton (H^+) in acidic media or H_2O in alkaline media, both of which contain multiple steps (Fig. 2). It should be noted that the HER process in a neutral solution is similar to that in an alkaline solution. Moreover, electrocatalysts are required to lower the energy barriers in each step.

2.1.1 HER in acidic media. In an acidic solution, first, hydronium ions coupled with electrons form reactive hydrogen intermediates H* at active sites (where * represents an active site on the electrode surface, and H* is the hydrogen atom adsorbed on the active site) *via* the electrochemical adsorption process (Volmer step, eqn (1)). Subsequently, there are two possible reaction pathways: one is the electrochemical desorption process (Heyrovsky step, eqn (2)), where the generated H* combines a new pair of H^+ and electron (e^-) in the solution to produce H_2 molecules, and then desorbed; the second is the chemical desorption process (Tafel step, eqn (3)), in this case, two nearby H* obtained by the Volmer step are recombined directly to yield H_2 molecules. In acidic

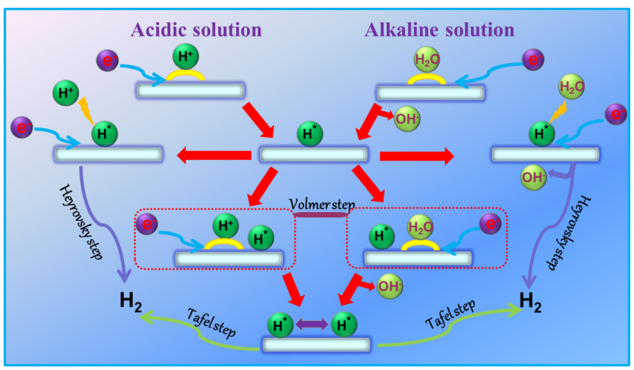

Fig. 2 Schematic process for the HER under acidic and alkaline solutions.

media, the HER pathway with different Tafel slopes is as follows:

$$H_3O^+ + e^- + * \rightarrow H^* + H_2O, \text{ Volmer step } (120 \text{ mV dec}^{-1}) \quad (1)$$

$$H_3O^+ + e^- + H^* \rightarrow H_2 + H_2O, \text{ Heyrovsky step } (40 \text{ mV dec}^{-1}) \quad (2)$$

$$H^* + H^* \rightarrow H_2, \text{ Tafel step } (30 \text{ mV dec}^{-1}) \quad (3)$$

2.1.2 HER in alkaline media. Compared with the HER in acidic media, the HER in alkaline solution shows a slower kinetic rate, because extra energy is required to dissociate H_2O molecules to obtain enough H^+.[37] Therefore, the alkaline HER is first initiated by water adsorption and dissociation process to produce H* on active sites (Volmer step, eqn (4)), which is the rate-determining step (RDS). Then, at low coverage of H* on the catalyst surface, H* will preferably combine with an electron and H_2O molecule to generate an H_2 molecule (Heyrovsky step, eqn (5)); When the H* coverage is high, the H_2 molecule will be formed through binding two adjacent H* atoms (Tafel step, eqn (6)). Additionally, it should be mentioned that the low water adsorption energy and water dissociation are conducive to the effective alkaline HER.[38–41] In an alkaline solution, the reaction formula and Tafel slope for the HER are described as follows:

$$H_2O + e^- + * \rightarrow H^* + OH^-, \text{ Volmer step } (120 \text{ mV dec}^{-1}) \quad (4)$$

$$H_2O + e^- + H^* \rightarrow H_2 + OH^-, \text{ Heyrovsky step } (40 \text{ mV dec}^{-1}) \quad (5)$$

$$H^* + H^* \rightarrow H_2, \text{ Tafel step } (30 \text{ mV dec}^{-1}) \quad (6)$$

2.2 Parameters for evaluating electrocatalysts

As shown in Fig. 3, several significant parameters are usually utilized to evaluate the performance of an electrocatalyst, such as overpotential (η), Tafel slope, exchange current density (j_0), stability, electrochemically active surface area (ECSA), specific and mass activity, turnover frequency (TOF), electrochemical impedance spectroscopy (EIS), and faradaic efficiency (FE). These parameters can furnish penetrative information about the thermodynamics and kinetics of the HER. These parameters are introduced briefly in this section.

2.2.1 Overpotential. Theoretically, the driving thermodynamic potential of the HER is 0 V *versus* the reversible hydrogen electrode (RHE), while the extra potential is routinely required to drive the reaction in a practical reaction system. The extra potential is called overpotential, which is a critical parameter to assess the performance of catalysts. The overpotential value can be determined by linear sweep voltammetry (LSV) with a function between the current density and overpotential. The overpotential mainly comprises the activation overpotential, resistance potential, and concentration overpotential in the electrochemical systems.[42] The activation

Fig. 3 The parameters for evaluating the HER performance.

overpotential, an intrinsic property of the catalyst, can be reduced by using an efficient catalyst. The concentration overpotential derives from a sudden change in the concentration near the electrode/electrolyte interface owing to the sluggish diffusion rate.[43] This can be decreased by distributing the electrolyte *via* stirring the solution. The resistance overpotential can be depressed by employing ohmic drop compensation, which can be realized in many modern electrochemical workstations equipped with automatic compensation for IR loss. For ease of quantifying the overpotential, three η values at the current densities of 1 (η_1), 10 (η_{10}), and 100 (η_{100}) mA cm^{-2} are frequently utilized to compare the activities between different catalysts. η_1 is called an "onset overpotential", which suggests that the current density starts to tremendously increase.[30] η_{10}, an important criterion, corresponds to the solar water-splitting efficiency of 12.3%, which is generally chosen as the comparison standard for different catalysts.[44] A smaller η_{10} implies a better electrocatalytic activity to some extent. However, it cannot directly discriminate the activity of a catalyst by just comparing the η_{10} value, because the loading content of the catalyst on the electrode with the same geometrical area is totally different. Therefore, for evaluating and comparing the real HER activity of catalysts, researchers should load the same amount of a catalyst on a standard glassy carbon electrode with low roughness to achieve the activity per unit mass. η_{100} is another key criterion for catalyst evaluation in practical applications. Furthermore, potentials are frequently measured and quoted regarding reference electrodes other than the RHE,

which is greatly inconvenient from an experimental standpoint. The common references are the saturated calomel electrode (Hg/Hg_2Cl_2) in acidic media or the mercuric oxide electrode (Hg/HgO) in alkaline media. Meanwhile, the counter electrode should be a convenient one, which cannot affect the performance of the working electrode. Over the past few decades, the Pt electrode is prevalently used as the counter electrode due to its outstanding stability and excellent electrical conductivity, which, however, can be dissolved into Pt^{2+} for a long-term test. Then, the produced Pt^{2+} transfers to the working electrode surface, resulting in enhancing the activity of the working electrode.[45] To ensure the authenticity of the test data, some stability electrodes including graphite rod, conductive glass, carbon cloth, and titanium mesh should be served as the counter electrodes. To unify the standard of evaluation, the potentials should be calibrated to the RHE according to the following equations:

$$E(\mathrm{RHE}) = E(\mathrm{Hg/Hg_2Cl_2}) + E^{\circ}(\mathrm{Hg/Hg_2Cl_2}) + 0.0592 \times \mathrm{pH} \quad (7)$$

$$E(\mathrm{RHE}) = E(\mathrm{Ag/AgCl}) + E^{\circ}(\mathrm{Ag/AgCl}) + 0.592 \times \mathrm{pH} \quad (8)$$

$$E(\mathrm{RHE}) = E(\mathrm{Hg/HgO}) + E^{\circ}(\mathrm{Hg/HgO}) + 0.0592 \times \mathrm{pH} \quad (9)$$

2.2.2 Tafel plot and exchange current density. The Tafel plot is often applied to exhibit the relationship between current density and overpotential in the HER.[46] From eqn (10), the Tafel slope and exchange current density can be derived. The Tafel slope is plotted by η as a function of $\log|j|$, and b can be extrapolated from the linear portion of the Tafel plot. The Tafel slope shows the intrinsic property of a catalyst and discerns the charge transfer kinetics and probable reaction pathways, as well as the rate-determining step of the hydrogen evolution process,[47] which generally can be used for explaining the catalyst mechanism of the HER. It has been elaborated that the HER kinetics contains three main steps: Volmer, Heyrovsky, and Tafel as the rate-determining steps with corresponding Tafel slopes of 120, 40, and 30 mV dec^{-1} observed at the low overpotential values/current densities.[48] Note that the above Tafel slope values are not absolute, because the Tafel slope is determined by the coverage of the absorbed hydrogen.[49] The smaller b indicates that less η is required to achieve the same current density increment, signifying faster electron-transfer kinetics. On the other hand, j_0, relying on the reaction activation energy at the surface of the electrocatalyst, is a critical kinetic parameter for revealing the inherent catalytic activity of an electrocatalyst under reversible conditions, which can be valued by assuming η of being zero.[50] In addition, electrolyte composition and temperature also affect the value of j_0.[51] A superior electrocatalyst should possess a high j_0 and a small b simultaneously.

$$\eta = a + b\log j \quad (10)$$

2.2.3 Electrochemical impedance spectroscopy. EIS can provide information about the electrode/electrolyte interface in the catalytic system.[52] The charge transfer resistance (R_{ct}), which exhibits the interface charge transfer process of an electrode, can be gained by fitting the diameter of the semicircle in the high-frequency region.[53] For the HER, a smaller R_{ct} value indicates a faster reaction rate and high charge transfer efficiency, rendering a smaller overpotential. Additionally, the uncompensated ionic and ohmic resistances of the electrochemical measurement process are also obtained based on the EIS Nyquist plots.

2.2.4 Electrochemically active surface area. In electrochemical reactions, the geometric surface area is generally employed to calculate the current density. However, it is difficult to guarantee the standard flat of a catalyst.[54] To reveal the intrinsic activity, ECSA can be used to assess the performance of a catalyst, which reflects the effective catalytic areas of a catalyst.[55] One of the most regularly used ECSA calculation methods is measuring cyclic voltammetry (CV) in the non-faradaic regions at different scanning rates.[56] When conducting the CV test, the variation of non-Faraday current density (j) should be linearly related to the scan rate (ν); thus, it provides the electric double-layer capacitance (C_{dl}) derived from the slope (eqn (11)),[57] where the slope is twice C_{dl}. The large C_{dl} expounds more active sites exposing and current density enhancing. The ECSA is proportional to C_{dl}, thus the ECSA of the catalyst is calculated according to eqn (12). In addition, ECSA can also be measured by underpotential deposition or advanced electron microscopy.[58–60] It should be mentioned that the chemical nature and construction of the electrodes may overestimate ECSA and thus underestimate the catalytic activity.[61] Moreover, although ECSA manifests some information on the number of active sites of the electrocatalyst, it does not mean that all active sites play a catalytic role in the HER. Even so, ECSA can still act as a key reference for the comparison of similar component materials.

$$C_{dl} = \frac{j}{\nu} \quad (11)$$

$$\mathrm{ECSA} = \frac{C_{dl}}{C_s} \quad (12)$$

where C_s is the specific capacitance of a flat standard electrode (1 cm^2), it is usually between 20 and 60 μF cm^{-2}. The average value of 40 μF cm^{-2} is frequently used for flat electrodes.[54,62,63]

2.2.5 Turnover frequency. TOF is an important parameter for evaluating the intrinsic activity of each catalytic site on catalysts, which is defined by the number of H_2 moles per catalytic site per unit of time at a given potential. A high TOF value implies prominent catalytic activity. However, it is a great challenge to obtain a precise number of active sites per unit area for voluminous HER catalysts, because catalysts generally have readily accessible surface atoms/catalytic groups and some unattainable internal atoms/catalytic species. Therefore, various approximate strategies are carried out. For instance, researchers endeavor to measure the TOF value with a reasonable approach that only considers the surface atoms or the easily accessible catalytic sites on the catalysts. In other cases, the TOF is calculated by using the total catalytic species in the

catalysts, which comprise all the accessible catalytic sites and some inaccessible catalytic sites originating from the surface and interior of catalysts. Although the two kinds of methods cannot provide an accurate value compared with the real TOF value of the active sites, they may still furnish a useful way to compare the catalytic activity or efficiency of similar catalysts. A common method to estimate TOF value is according to eqn (13) and (14). Based on eqn (13), the number of active sites (n) is obtained by the CV test from −0.2 V to +0.6 V *vs.* RHE at a scan rate of 20 or 50 mV s^{-1} in 1.0 M phosphate buffer solution (PBS, pH = 7). In addition, other methods for quantifying the number of active sites are also applied, such as the copper underpotential deposition method and estimating the number of molecules on the active surface.[64–67] When the number of active sites is determined, the TOF (s^{-1}) can be calculated with eqn (14).

$$n = \frac{Q}{2F} \tag{13}$$

$$\mathrm{TOF} = \frac{IN_A}{2Fn} \tag{14}$$

where Q is the voltammetric charge calculated by the integral curve of CV, I is the current (A) during the linear sweep measurement, N_A denotes the Avogadro constant (6.023×10^{23} mol^{-1}), F is the Faraday constant (96 485 C mol^{-1}), and n is the number of active sites (mol). The factor 1/2 in the equation means that two electrons are consumed to generate one H_2 molecule.

2.2.6 Specific and mass activities. The specific and mass activities are key quantitative parameters to evaluate the catalytic activity of electrocatalysts at a defined overpotential. The specific activity is the current density per unit real surface area of the catalyst, which can be measured by normalizing the current to the ECSA. The ECSA normalized activity is relatively accurate, because ECSA can reveal the intrinsic surface area of the catalyst.[68,69] The current normalized by the loading mass is the mass activity, which is normally valid for the comparison of a similar material system.[70] The mass activity is positively correlated with the active surface area of catalysts, namely, catalysts with larger surface area usually present a higher mass activity.[71]

2.2.7 Faradaic efficiency. Faradaic efficiency is another crucial parameter to evaluate the performance of an electrocatalyst, which illustrates the proportion of electrons partaking in the HER *versus* total electrons provided by an external circuit in the HER.[72] FE is defined as the ratio of the experimental to the theoretical amount of H_2 production. The theoretical H_2 production can be calculated from the chronoamperometry or chronopotentiometry test, and the experimental H_2 generation can be collected by the gas chromatography or drainage method. The FE of electrons is usually less than 100% due to the by-products forming on the electrode surface during the HER.

2.2.8 Stability. Long-term stability, which shows the long-term ability to retain the initial catalytic activity of the electrocatalysts, is a crucial indicator to evaluate the practical applications of an HER catalyst.[73] Generally speaking, two assessment approaches are performed, such as continuous CV and chronoamperometry (potential-time curve) or chronopotentiometry test (current-time curve). In the case of the CV test, potential cycles usually are consistent with that of the LSV range. The stability is evaluated by comparing the LSV curve change before and after the repetitive CV cycles (normally 1000–10 000 cycles). While the LSV curves remain negligible variation as the initial one or the overpotential marginally increases less than 10% with respect to the initial value, suggesting great durability. With regard to the chronopotentiometry (CP) or chronoamperometric (CA) measurements, which are usually conducted at a constant current density of 10 mA cm^{-2} or applied overpotential for at least ten hours. The longer duration without potential (or current) change presents excellent endurance. Even so, ten hours are not enough for HER. We recommend using a longer time test, such as 100 hours. Additionally, along with the accumulating and releasing of H_2 bubbles on electrodes, the measured current-time curve displays a unique serrate shape.[74] Unfortunately, the produced H_2 bubbles can cover the catalytic sites, leading to slow HER kinetics.[71] Meanwhile, the release of H_2 bubbles may peel the active materials from the electrode surface, resulting in lowering HER performance. To a certain extent, the negative effect of H_2 bubbles can be weakened through stirring or using self-supported electrodes.

2.3 Density functional theory (DFT)

As a vital computational tool, DFT, which is based on quantum mechanics, can not only illuminate the correlations between the electrocatalytic performances and physical/chemical properties of catalysts at an atomic level but also calculate the electronic structure of the whole catalytic system.[75] With the exuberant development of computer technology, DFT calculations have been widely used to explore the electrocatalytic mechanisms, identify the active sites, and predict potential catalysts.[76–78] In particular, it is very hard to probe the intermediate states of electrocatalytic reactions and electron transfer because of their short lifetimes and complex reaction conditions, leading to ambiguous active sites indefinite and inconclusive electrocatalytic mechanisms.[79] Therefore, coupling experiment with DFT calculations is an effective method to identify the active sites, deeply discern the catalytic mechanisms of the HER, as well as rationally design new advanced electrocatalysts.

2.3.1 The Gibbs free energy of hydrogen adsorption (ΔG_{H^*}). The Gibbs free energy of hydrogen adsorption has been extensively regarded as a crucial descriptor for theoretically predicting and evaluating the catalytic activity of the HER catalysts,[80] which can reflect the electronic state of the catalyst surface. As guided by the volcano plot (Fig. 4), an optimal HER catalyst should have a nearly zero ΔG_{H^*}, which not only promotes the charge/mass transfer with fast kinetics but also facilitates adsorbed H (H_{ads}) bond breaking and rapidly release of H_2 molecules under this condition.[81,82] When ΔG_{H^*} is too negative, the intermediate H_{ads} will bind strongly with the electrocatalyst surface, thereby promoting the initial Volmer step, but retarding the subsequent

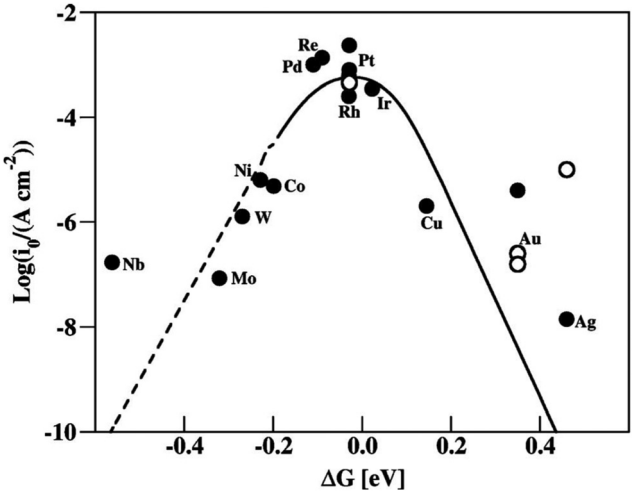

Fig. 4 A volcano plot.[82]

Heyrovsky or Tafel steps. When ΔG_{H^*} is too positive, H_{ads} shows insufficient interaction with the electrocatalyst surface, resulting in a slow Volmer step.[83–85] Therefore, appropriate ΔG_{H^*} is very important for enhancing H_2 evolution. By modeling the possibly produced intermediates of hydrogen adsorption, reduction, and desorption processes, ΔG_{H^*} can be calculated from eqn (15).[86]

$$\Delta G_{H^*} = \Delta E_{H^*} + \Delta E_{ZPE} - T\Delta S \quad (15)$$

where ΔE_{H^*} is the hydrogen chemisorption energy, ΔE_{ZPE} is the zero-point energy difference between the adsorbed and gas phases, T is the room temperature (298.15 K), and ΔS is the entropy change.

2.3.2 The d-band center theory. The d-band center theory was first established by Nørskov and Hammer, which has been successfully used to describe the tendency in the activity of transition metal-based electrocatalysts.[87–90] Particularly, the d-band center theory manifests that the hydrogen or oxygen adsorption strength depends on the d states of metals.[91–93] For instance, when H* adsorbs on the surface of the metal catalysts, the metal–hydrogen (M–H) bond will be formed through hybridizing the H* orbital with the metal d orbital. Basically, the interplay between H* orbital and the metal d orbital can generate a fully filled bonding orbital with low energy and a partially filled anti-bonding orbital with high energy, where the occupancy of the anti-bonding orbital determines the M–H bond strength.[94] Generally speaking, the low anti-bonding orbital occupancy will result in a high M–H bond strength. Therefore, the inherent surface adsorption ability of H* can be qualitatively construed and forecasted through computing the local d-band states of a metal surface.[95] Moreover, the position of the d-band center (ε_d) relative to the metal's Fermi level also has a great impact on the M–H bond strength. When the metal's Fermi level gets close to the d-band center, the anti-bonding orbital becomes higher due to the decreased occupancy, leading to a stronger H* adsorption.[96] Apart from the d-band filling, the bandwidth of the d-band also influences the adsorption strength on the catalyst surface. When fixing the filling level of the d-band, a diminished bandwidth will elevate the level of the d-band center, thereby resulting in a strong adsorption interaction.[97–99] For calculating the effect of ε_d on the adsorption interactions, the corresponding ε_d is defined as the local average of the d electron energies (eqn (16)).

$$\varepsilon_d = \frac{\int_{-\infty}^{+\infty} x\rho(x)\mathrm{d}x}{\int_{-\infty}^{+\infty} \rho(x)\mathrm{d}x} \quad (16)$$

where x is the energy level and $\rho(x)$ is the density of states of the corresponding d-orbital.

3. Design and fabrication of self-supported electrocatalysts

3.1 Carbon-based substrates

Carbon-based substrates mainly contain carbon fiber paper (CFP), graphite plate (GP), and CC, which exhibit augmented conductivity, strong flexibility, and high resistance to strong acidic and alkaline electrolytes.[100–103] To improve the solvent-accessible hydrophilic surface, carbon-based substrates should be treated before use. Several methods of treating carbon-based substrates have already been reported, for instance, CC was cleaned using acetone and ethanol under ultrasonication to remove impurities, respectively, and then dried at 60–80 °C for many hours. Whereafter, CC was treated with concentrated nitric acid with the hydrothermal method or reflux method.[104–107] In addition, chemical oxidation with potassium permanganate, electrochemical oxidation, air calcination treatment, and plasma methods were also utilized.[108–111] Therefore, the carbon-based substrates were widely used to construct the self-supported electrodes for the HER by virtue of their advantages. For example, the Mo–Fe–Ni phosphides nanowires were prepared on carbon cloth, which shows superefficient alkaline HER performance with an overpotential of 75 mV at the current density of 10 mA cm^{-2} and superior long-term electrochemical stability for 20 h electrolysis.[112] The improved HER performance could be attributed to the synergistic effects between multiple catalytic centers (Mo, Fe, and Ni), as well as the facilitated evolved-gas escape. In similar research, Wen *et al.* provided a general strategy for fabricating self-supported nanoporous Cu-doped CoP nanorod arrays on CC (Cu–CoP NRAs/CC) *via* a hydrothermal method followed by a low-temperature phosphatization route, showing enhanced HER performance in a wide pH range.[113] The resultant Cu–CoP NRAs/CC electrode exhibited wonderful HER performance with 44 mV overpotential to reach a current density of 10 mA cm^{-2} in 0.5 M H_2SO_4 solution. Simultaneously, it needed overpotentials of 81 mV in 1.0 M KOH and 137 mV in 1.0 M PBS at the same current density, respectively. It also presented prominent stability under different pH conditions for 40 h. The exceptional HER performance could be ascribed to the strong heteroatomic interactions induced by many lattice distortions and defects. Zheng *et al.* successfully synthesized bimetallic carbide Ni_6Mo_6C nanodots embedded on $NiMoO_x$ nanosheets arrays anchored on an activated carbon cloth ($Ni_6Mo_6C/NiMoO_x$/ACC)

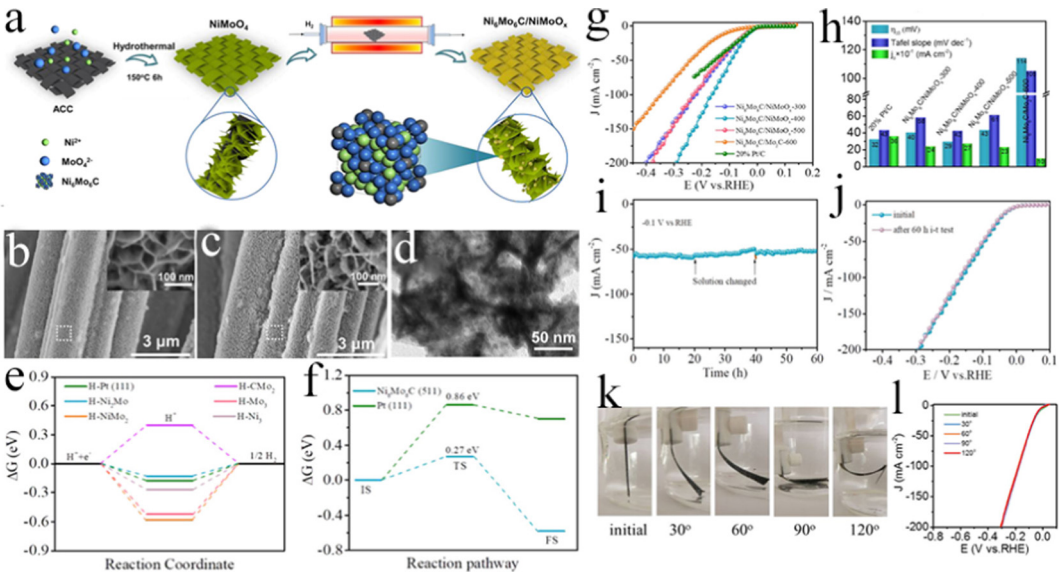

Fig. 5 (a) Schematic illustration of the preparation of $Ni_6Mo_6C/NiMoO_x$-T. (b) Field emission scanning electron microscope (FESEM) images of $NiMoO_4$ nanosheets grown on ACC at different resolutions. (c) FESEM images of $Ni_6Mo_6C/NiMoO_x$-400 at different resolutions. (d) Transmission electron microscope (TEM) images of $Ni_6Mo_6C/NiMoO_x$-400. (e) Calculated ΔG_{H^*} values for H adsorption on different sites of Ni_6Mo_6C (511) and Pt (111). (f) Gibbs free energy diagram of the water dissociation path on Ni_6Mo_6C (511) and Pt (111). (g) HER polarization curves of different electrocatalysts without iR compensation in 1 M KOH solution at 2 mV s^{-1}. (h) Comparison of η_{10}, Tafel slope, and j_0 of various electrocatalysts. (i) i–t curve of $Ni_6Mo_6C/NiMoO_x$-400 at 100 mV overpotential in 1 M KOH solution, and (j) corresponding LSV curves after constant electrolysis for 60 h. (k) Digital images of the distorted $Ni_6Mo_6C/NiMoO_x$-400 electrode under the HER test, and (l) corresponding LSV curves.[114]

via controlling the diffusion of carbon atoms into precursor $NiMoO_4$ nanosheets with carbothermal hydrogen reduction (Fig. 5a).[114] The as-formed $NiMoO_x$ nanosheet arrays grown on ACC with unique hierarchical structures (Fig. 5b–d) could greatly enhance both the mass transport and electric conductivity. In virtue of the moderated hydrogen adsorption ability ($\Delta G_{H^*} = -0.13$ eV) and low water dissociation energy barrier ($\Delta G_b = 0.27$ eV) on Ni_6Mo_6C (Fig. 5e and f), the open microstructure of the $Ni_6Mo_6C/NiMoO_x$ hybrid, and the high conductive ACC support, the $Ni_6Mo_6C/NiMoO_x$/ACC flexible electrode displayed a small overpotential of 29 mV to achieve 10 mA cm^{-2} with long-term stability for 60 h of constant electrolysis, even superior to the benchmark Pt/C and most of the reported nonprecious metal catalysts (Fig. 5g–j). Exclusively, as exhibited in Fig. 5k and l, it showcased excellent flexibility, which could remain unchanged for the HER performance under different bending angles. Therefore, this work provided a good idea to fabricate HER electrocatalysts with highly efficient, inexpensive, and flexible merits for practical application and commercialization. Liu *et al.* synthesized a three-dimensional (3D) self-supported binder-free integrated electrode constructing a few layered N, P dual-doped carbon-encapsulated ultrafine MoP nanocrystal/MoP cluster hybrids on CC (FLNPC@MoP-NC/MoP-C/CC) for attractive HER performance.[115] The FLNPC@MoP-NC/MoP-C/CC electrode was fabricated through an electrodeposition process and an *in situ* phosphatization. The preparation of the FLNPC@MoP-NC/MoP-C/CC electrode with several steps is depicted in Fig. 6a. First, a layer of the polyaniline (PANI) film on CC (PANI/CC) was generated by an electrodeposited method. Second, the MoO_3 microrods (MoO_3-MRs) were *in situ* arrayed on PANI/CC to form MoO_3-MRs/PANI/CC by a hydrothermal route with the predecessors of $(NH_4)_6Mo_7O_{24}$ and tartaric acid. Subsequently, another PANI film layer was further electrodeposited on the MoO_3-MRs/PANI/CC electrode to obtain PANI/MoO_3-MRs/PANI/CC. Finally, the as-formed PANI/MoO_3-MRs/PANI/CC was annealed in a PH_3 atmosphere, achieving a 3D self-supported integrated FLNPC@MoP-NC/MoP-C/CC electrode by means of converting MoO_3-MRs into MoP-NC/MoP-C hybrids and carbonizing PANI films into few layered N, P dual-doped carbon. From Fig. 6b–d, the FLNPC@MoP-NC/MoP-C/CC electrode showed remarkable HER performance with extremely low overpotentials over the entire pH range ($j = 10$ mA cm^{-2} at $\eta = 74$, 69, and 106 mV in 0.5 M H_2SO_4, 1.0 M KOH, and 1.0 M PBS solutions, respectively). Besides, owing to the protection of few layered N, P dual-doped carbon, FLNPC@MoP-NC/MoP-C/CC presented long-term durability for 50 h testing in acidic, neutral, and alkaline media (Fig. 6e–g), indicating the great potential for electrolyzing water application. The excellent electrocatalytic performance could be ascribed to the following virtues: (1) 3D porous structure of the electrode with large specific surface area could furnish more active sites and facilitate electrolyte diffusion, as well as forcefully lower the charge transport resistance;[116] (2) the well-dispersed MoP-NCs embedded in few-layered N, P dual-doped carbon could increase the specific surface area, resulting in exposing more active sites; (3) the N, P dual-doped carbon layer could not only boost the porousness and electroconductivity of the entire electrode, enhancing the contact between the active sites and the electrolyte, and shortening the charge transfer pathway, but

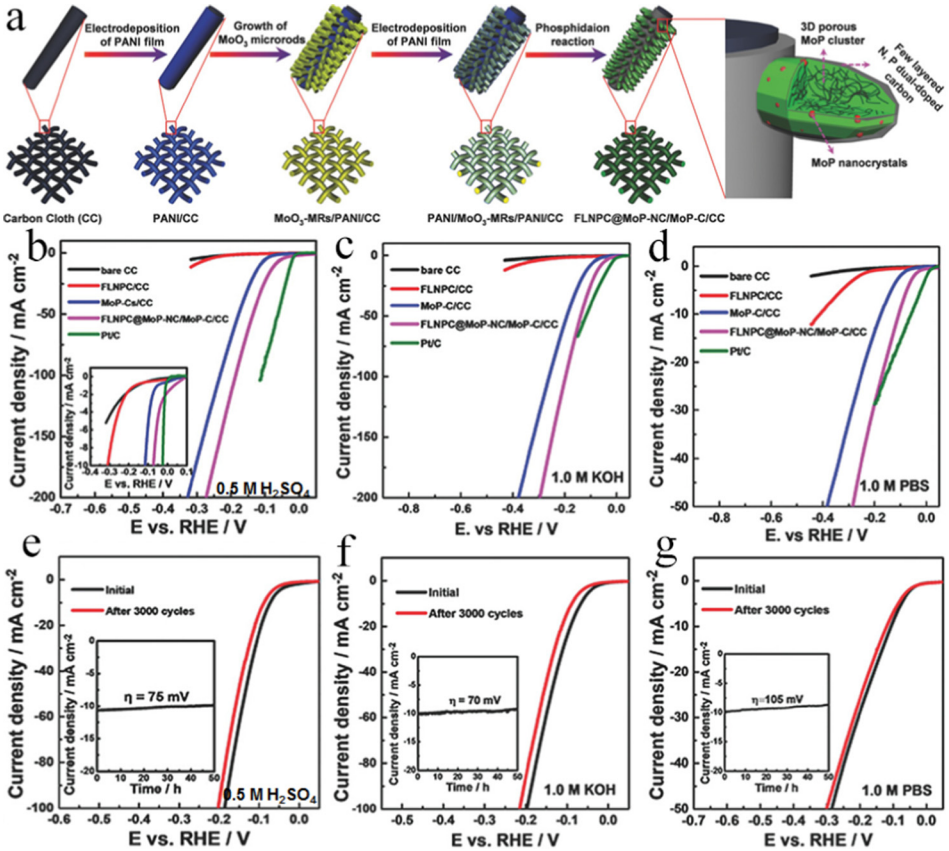

Fig. 6 (a) Fabrication process of few layered N, P dual-doped carbon-encapsulated MoP nanocrystal/MoP cluster hybrids on CC. (b–d) LSV curves of bare CC, FLNPC/CC, MoP-C/CC, FLNPC@MoP-NC/MoP-C/CC, and Pt/C in 0.5 M H_2SO_4, 1.0 M KOH, and 1.0 M PBS electrolytes at 2 mV s^{-1}. (e–g) LSV curves of FLNPC@MoP-NC/MoP-C/CC initially and after 3000 cycles in 0.5 M H_2SO_4, 1.0 M KOH, and 1.0 M PBS medium. Insets of (e–g) are time-dependent current density curves of FLNPC@MoP-NC/MoP-C/CC under a static overpotential for 50 h.[115]

can also prevent MoP-NCs from corrosion and aggregating;[117] (4) N doping of carbon layers could provide extra active sites by changing the electron density in graphitic carbon;[118] (5) the synergistic effect between MoP components and few layered N, P dual-doped carbon could optimize the ΔG_{H^*} values to improve the H* adsorption, resulting in promoting the HER performance. This work put forward a broad strategy for guiding the fabrication of various self-supported electrodes for the HER. Lately, numerous works have been devoted to exploring the economical and efficient alternatives based on transition metal dichalcogenides, which showed potential electrocatalytic HER activities owing to their optimal ΔG_{H^*}.[62,119–122] Among them, molybdenum disulfide (MoS_2) is a well-known electrocatalyst due to its natural abundance, distinct catalytic mechanism, low price, tunable electronic structure, and good chemical stability.[123–128] A 3D self-supported cross-linked (3DSC) Co-doped MoS_2 (Co-MoS_2) nanostructured HER electrocatalyst on CC was designed and synthesized by creative nanostructure engineering.[129] Benefiting from the special structure, MoS_2 nanosheets exposed more copious active sites on the edges, making ion transfer and bubble release easy and smooth. Moreover, the unique structure also enhanced the stability and advanced electron transfer *via* direct bonding with CC. On the other hand, the Co element in MoS_2 could raise the overall conductivity, resulting in optimizing the electron transfer path and activating the adjacent S sites. As a consequence, the 3DSC Co-MoS_2 electrode integrated on CC could reach the current density of 10 and 100 mA cm^{-2} with merely 40 and 119 mV overpotentials, respectively, surpassing other MoS_2-based HER electrocatalysts reported recently. This research exhibited a facile integration strategy and a new method for boosting inexpensive and high-activity electrocatalysts. Pang and co-workers reported a versatile and effective method to synthesize Re/ReS_2 self-supporting array electrodes with abundant S defects on CC (Re/ReS_2/CC).[130] The optimized S-defect-rich Re/ReS_2/CC exhibited outstanding electrocatalytic HER performance, providing ultralow overpotentials of 42 and 44 mV at 10 mA cm^{-2} in acidic and alkaline solutions, respectively, and corresponding small Tafel slopes of 36 and 53 mV dec^{-1}, which were comparable to many promising HER catalysts. Experiments and DFT results demonstrated that the S defects in Re/ReS_2/CC could afford sufficient active sites, boost charge transfer kinetics, and optimize ΔG_{H^*} at the active sites, resulting in high-caliber electrocatalytic HER performance. Sun *et al.* used a simple two-step method of dip-coating and electrochemical reduction to synthesize self-supported molybdenum oxide stabilized ultrafine palladium electrocatalysts on CC (MoO_x-Pd/CC), which showed a small Tafel slope of 45.75 mV dec^{-1},

an ultralow overpotential of 25 mV at 10 mA cm^{-2}, and outstanding durability for at least 7 days in 0.5 M H_2SO_4 solution, surpassing the bare Pd/CC and MoO_x/CC and also comparable to the commercial Pt mesh electrode.[131] The experimental results and DFT calculations presented that MoO_x could not only effectively downsize and disperse Pd nanoparticles by exposing more active sites, but also tune the electronic structure of the Pd surface, boosting their intrinsic catalytic activity. Hu *et al.* fabricated a self-supported economical Ni-doped Mo_2C electrocatalyst with nanoflower morphology on CFP through a molten salt method.[132] Compared to the conventional solid-phase approach, the molten salt method can prepare products with a uniform chemical composition, great crystal morphology, and pure phase by using a low melting point salt as a reaction medium at low temperatures for a short time.[133–137] Based on this method, the as-obtained fluffy and porous nanoflower-like structure showed a large specific surface area, resulting in exposing more active sites and promoting charge transfer. The optimal Ni-doped Mo_2C electrocatalyst exhibited high-efficient HER performance with a low overpotential of 56 mV at 10 mA cm^{-2}, a small Tafel slope of 27.4 mV dec^{-1}, and long-term stability for 35 h electrolysis in 0.5 M H_2SO_4 solution, which is superior to most of the noble-metal-free electrocatalysts. DFT calculations indicated that the Ni doping could cause a down shift of ε_d, which enabled H_{ads} to desorb from the catalyst surface easily, thus enhancing the intrinsic catalytic activity. Recently, metal–organic frameworks (MOFs) have received great attention in the electrocatalytic field due to their intrinsically porous structures, large specific surface areas, and well-dispersed metal sites.[138–144] Unfortunately, the catalytic performance of most MOFs was markedly hampered by their improper adsorption/desorption energy of intermediates generated in electrocatalysis and quite poor electrical conductivity. In view of these issues, Geng *et al.* developed a simple method to directly fabricate novel high conductive Co-doped Cu-catecholate nanorod arrays on CC (CuCo-CAT/CC) as binder-free electrodes for the HER in alkaline and neutral media.[27] Electrochemical results demonstrated that CuCo-CAT/CC showed evidently improved HER performance with low overpotentials of 52 and 143 mV at 10 mA cm^{-2} in alkaline and neutral solutions, respectively, exceeding that of the reported non-noble metal-based electrocatalysts or comparable to the commercial Pt/C electrocatalysts. DFT calculations proved that Co doping could not only optimize ΔG_{H^*} and adsorption energy of water (ΔE_{H_2O}) of Cu-CAT, thereby facilitating the Volmer and Heyrovsky steps, but also boost the electrical conductivity of Cu-CAT. Furthermore, the CuCo-CAT nanorod arrays on CC presented an open porous interconnected structure, resulting in decent stability for the HER in alkaline and neutral solutions. This study elaborated a new strategy to design conductive MOF-based electrocatalysts for highly efficient HER. Besides CC and CFP, graphite plate (GP) was also a distinguished substrate. For example, a superhydrophilic NiCo–CeO_2 nanoparticle array was integrally deposited on GP (NiCo–CeO_2/GP) by simple anion intercalation heightened electrodeposition method and subsequent high-temperature selective reduction.[145] The superhydrophilic self-supported NiCo–CeO_2/GP electrode had many traits, such as boosting electron conduction, accelerating bubble release, and preventing catalyst shedding. Owing to the superhydrophilic self-supported electrode and the synergistic interaction between NiCo and CeO_2, it displayed outstanding HER performance with low overpotentials of 34 mV (140 mV) at 10 mA cm^{-2} (500 mA cm^{-2}) and striking stability in alkaline electrolytes. Notably, the coupled CeO_2 could favor dissociating water and facilitate hydrogen adsorption, drastically enhancing the HER performance of the NiCo alloy. More importantly, CeO_2 was also applied to boost the electrocatalytic activities of NiFe and NiCu alloys, indicating its versatility. Meanwhile, an alkaline electrolyzer with NiCo–CeO_2/GP as the cathode and NiCo$(OH)_x$–CeO_2/GP as the anode exhibited a low voltage of 1.45 V at 10 mA cm^{-2} and a prominent stability at 500 mA cm^{-2}, outperforming that of the Pt/C||RuO_2 electrolyzer. This work presented a simple method to synthesize the low-priced NiCo–CeO_2 electrocatalyst and proved its potential for producing H_2 at large current densities.

3.2 Titanium-based substrates

Titanium materials have been deemed as the optimum substrate candidates due to their natural abundance, excellent corrosion resistance to acidic and alkaline media, processability, and good chemical stability.[146–150] Inspired by the merits, Li *et al.* fabricated Co-doped anatase TiO_2 nanorod arrays on a Ti plate (Co-TiO_2@Ti(H_2)) with 1D structure, abundant oxygen vacancies (OVs), and good hydrophilic feature by ion exchange process and calcination treatment (Fig. 7a–c).[151] As displayed in Fig. 7d–f, the as-formed Co-TiO_2@Ti(H_2) provided a much low overpotential of 78 mV at 10 mA cm^{-2}, a small Tafel plot of 67.8 mV dec^{-1}, and outstanding long-term durability at a large current density of 480 mA cm^{-2} for the alkaline HER. DFT calculations demonstrated that the excellent hydrophilic surface could facilitate water adsorption, the Co atoms could lower the free energy of water adsorption/dissociation and H intermediate, as well as ample OVs could grab OH^- to efficiently promote water dissociation and H intermediate desorption. The work provided a promising electrode for cost-effective and energy-efficient HER. To enhance the HER performance of the Pt catalyst along with minimizing the Pt loading, an effective electrode was designed, which was constructed by using 3D Ti mesh (3D-Ti) as a substrate to yield TiO_2 nanotubes (TiO_2 NTs), followed by implanting a Pt nanocluster *via* an atomic layer deposition method.[152] The as-formed Pt_x/TiO_2 NTs@3D-Ti catalysts showed a low overpotential of 53 mV at 10 mA cm^{-2} in 0.5 M H_2SO_4 solution, which was superior to that of the commercial 20 wt% Pt/C catalysts. The experiments and DFT results implied that the Pt–O–Ti bond between the Pt nanocluster and TiO_2 nanotube could not only boost the durability of the Pt nanocluster anchored on TiO_2 nanotubes but also greatly enhance the HER performance. The improved HER activity may be attributed to the following reasons: (1) the 3D pore structure from Ti mesh could facilitate gas diffusion easily and furnish more surface contact between the electrode and the electrolyte; (2) the regular TiO_2 nanotubes possessed a

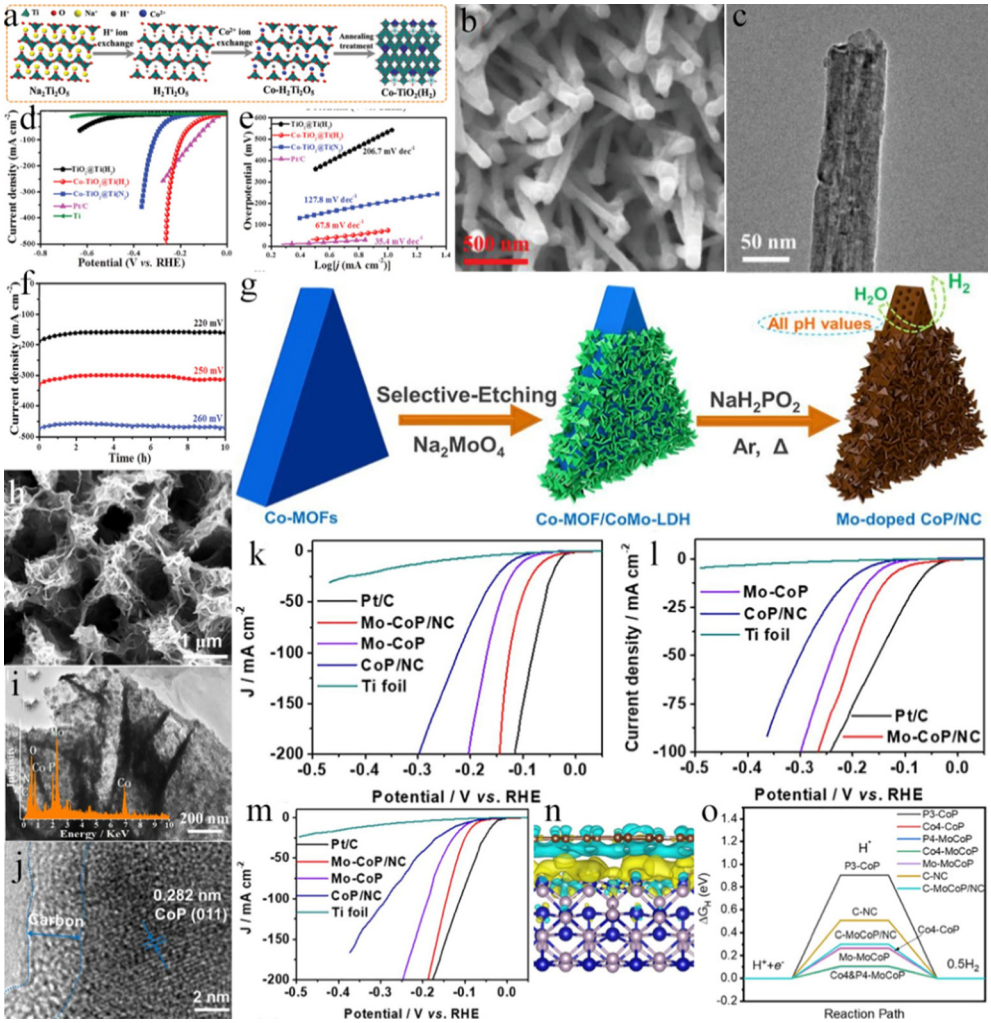

Fig. 7 (a) Schematic illustration of the ion exchange process for Co-TiO_2@Ti(H_2). (b) FESEM, and (c) TEM images of Co-TiO_2@Ti(H_2). (d) LSV curves in 1.0 M KOH solution. (e) Tafel plots derived from (d). (f) *i*–*t* Curves with different potentials in 1.0 M KOH solution.[151] (g) The synthesis process of hierarchical porous Mo-CoP/NC arrays on TF. (h) FESEM, (i) TEM, and (j) high-resolution transmission electron microscopy (HRTEM) images of Mo-CoP/NC/TF. (k–m) LSV curves in 0.5 M H_2SO_4, 1.0 M PBS, and 1.0 M KOH electrolytes. (n) The local charge density difference isosurfaces (±0.0005 e Bohr^{-3} isosurfaces, cyan: −, yellow: +). (o) HER free energy diagrams for various sites.[187]

high specific surface area for scattering Pt nanocluster and offered 1D channel for transferring electron. Besides, Ru species, which are much cheaper than Pt species, have favorable dissociation kinetics of the absorbed water, exhibiting excellent HER performance.[153–156] Consequently, Wang *et al.* provided a strategy to synthesize a hybrid catalyst by decorating TiO_2 nanotube arrays (TNAs) with crystalline $Ru_{0.33}Se$ nanoparticles.[157] Due to the large-specific surface area of TNAs, $Ru_{0.33}Se$ nanoparticles could be evenly distributed without aggregation, exposing more active sites. As a result, the fabricated $Ru_{0.33}Se$@TNA showed an improved HER activity with an overpotential of 57 mV at 10 mA cm^{-2}, a small Tafel slope of 50 mV dec^{-1}, and outstanding catalytic stability. The enhanced HER performance of $Ru_{0.33}Se$@TNA catalysts stemmed from the following aspects: (1) the increased active sites by the good dispersion of $Ru_{0.33}Se$ nanoparticles on the TNAs with large-specific surface area; (2) the boosted charge transfer efficiency because of the contracted electron transport pathway distributed by TNAs; and (3) the strong synergistic effect between $Ru_{0.33}Se$ and TiO_2. Additionally, Li *et al.* forecasted that the defect-rich RuO_2/TiO_2 hybrids could dramatically modulate the electron structure of RuO_2, resulting in boosting the water splitting.[158] More importantly, ε_d of Ru in defective RuO_2/TiO_2 shifted to a low-energy level owing to the strong synergistic effect, and reduced the interaction between the adsorbed oxygen species and Ru sites, benefiting the HER performance. Consequently, defective RuO_2/TiO_2 hybrids on Ti mesh (D-RuO_2/TiO_2/TM) were reasonably developed by impregnating Ru precursor over TM followed by a thermal-oxidative method at high temperatures. As expected, the as-obtained D-RuO_2/TiO_2/TM catalyst presented excellent activity with a low overpotential of 71 mV at 50 mA cm^{-2} for the HER in an alkaline solution. Moreover, because of the partial metallic nature of Se species, $MoSe_2$ shows high electrical conductivity.[159] In addition,

its edge site surface energy is larger than that of the terrace sites, making Mo and Se edges in the $MoSe_2$ atomic layers more active for the HER.[160–163] Zhang's group successfully fabricated few-layered $MoSe_2$ nanosheets with a mixed 1T/2H phase on Ti substrates (1T@2H-$MoSe_2$/Ti) *via* a simple one-step solvothermal method.[164] The 1T@2H-$MoSe_2$/Ti electrode showed great HER catalytic activity with an overpotential of 133 mV at 20 mA cm^{-2} and excellent stability for long-term electrolysis. The good electrocatalytic performance was owing to the synergistic effects of the special few-layered nanosheet morphology, conductive 1T metallic phase, and 1T@2H-$MoSe_2$ directly grown on the Ti substrate. Furthermore, alloy catalysts could result in superior electrocatalytic performance owing to the synergistic effect between different metal atoms.[165–169] In this regard, a 3D NiMo alloy nanowire array on a titanium substrate was successfully constructed by a simple and effective magnetic field-assisted strategy with a short reaction time and low temperature.[170] The 3D NiMo alloy displayed significantly enhanced alkaline HER catalytic activity with ultra-low overpotentials of 17 and 98 mV at 10 and 400 mA cm^{-2}, a small Tafel slope of 28 mV dec^{-1}, and prominent long-term stability, which were better than most non-noble metal-based electrocatalysts and even comparable to the Pt-based electrocatalysts. More importantly, the small Tafel slope suggested that the NiMo electrode could reduce the kinetic energy barrier for the Volmer step, thereby enhancing the alkaline HER activity. The enhanced catalytic activity may come from the lattice distortions induced by Mo incorporation, low contact resistance, more active sites at nanowires surface, as well as superior charge/mass transport and H_2 bubbles abilities. Interestingly, Zhao *et al.* synthesized FeP nanosheets on the Ti foil.[171] After etching in concentrated acid, the native oxide layer on the surface of the FeP nanosheet was removed. The as-treated FeP nanosheet showed significantly enhanced HER performance with the overpotentials 79 (95) and 95 (102) mV at 10 and 20 mA cm^{-2} in 0.5 M H_2SO_4 (1 M KOH) electrolyte, respectively. Oxygen vacancy in transition metal oxides (TMOs) plays a key role in catalytic fields, which have been used to regulate the electron structure for improving the HER activity.[172–176] Liu *et al.* successfully established simple calcination and electrochemical activation strategy to remarkably increase the OVs content and get theoretical insight into how the concentration of OVs influences the activity of spinel TMOs for the alkaline HER.[177] The self-supported spinel $NiCo_2O_4$ nanowire arrays with tunable concentrations of OVs on TMs exhibited extremely great HER performance. Impressively, it only required a low overpotential of 317 mV to achieve a current density of 360 mA cm^{-2}. In addition, the effective route could efficiently produce OVs in $CoFe_2O_4$ and $NiFe_2O_4$ for boosted HER activity. Furthermore, the DFT calculations indicated that the increasing concentration of OVs on the surface of $NiCo_2O_4$ could not only lower the adsorption energy of water molecules but also reduce their dissociation energy barrier on the surface of the catalyst, thus resulting in excellent HER performance. As a typical HER electrocatalyst, the application of pyrite-type cobalt disulfide (CoS_2) is limited by its deficient activity and weak durability because of the slow water dissociation kinetics and oxygen-related corrosion.[178–180] In view of this, an effective electrocatalyst containing a CeO_2-decorated CoS_2 nanowire array on a Ti plate was fabricated through constructing Lewis acid–base Ce···S pairs.[181] Correspondingly, the optimized electrocatalyst showed an enormous HER performance with a low overpotential of 36 mV at 10 mA cm^{-2} and unchanged activity over 1000 h electrolysis in an alkaline solution. Experimental and theoretical results indicated that the improved alkaline HER performance of CoS_2 is induced by the interfacial Lewis acid–base Ce···S pairs with neither too strong nor too weak acidity–basicity. Besides, the interfacial Lewis acid–base Ce···S pairs kinetically promoted interfacial water dissociation, sped the subsequent HER steps, as well as established a special interfacial electronic and geometric configuration for weakening O_2 adsorption on the catalyst surface and thus inhibiting corrosion during the alkaline HER. These above findings could provide guidance to design CeO_2-based electrocatalysts for water splitting. In addition to CoS_2, the CoP electrocatalyst has also received great attention for the HER.[182–186] Likewise, Wang's group utilized a synergistic electronic and geometric tailoring strategy to rationally fabricate hierarchically porous N-doped carbon incorporated Mo-doped CoP nanosheet arrays on the titanium foil (Mo-CoP/NC/TF) *via* etching Co-based MOFs (Fig. 7g–j).[187] From Fig. 7k–m, the synthesized Mo-CoP/NC/TF electrocatalysts exhibited outstanding performance and superior stability for the pH-universal HER, requiring overpotentials of 59, 130, and 78 mV at 10 mA cm^{-2} in acidic, neutral, and alkaline solutions, respectively. DFT calculations (Fig. 7n and o) and experimental results suggested that the excellent catalytic activity of Mo-CoP/NC/TF could be attributed to the following points: (1) a strong synergistic effect between the Mo doping and N-doped carbon could effectively tailor the electronic structures of CoP, resulting in thermo-neutral adsorption of hydrogen-containing intermediates and fast interfacial charge transfer kinetics for Mo-CoP/NC; (2) the hierarchical porous self-supported electrode could not only furnish more accessible active sites, but also facilitate electrolyte diffusion and the gas release.

3.3 Nickel-based substrates

Nickel foam has been widely employed as a substrate for HER electrodes owing to its excellent electrical conductivity, low price, hierarchical porous structure, commercial availability, as well as 3D cross-linked network.[188–193] For example, Chen *et al.* reported a facile and simple one-pot aqueous strategy to synthesize ultrathin rhodium-iridium nanosheets on NF (RhIr NSs/NF) at room temperature.[194] The catalyst exhibited high HER performance in both 1.0 M KOH and 0.5 M H_2SO_4 solutions with the overpotentials of 15 and 14 mV at 10 mA cm^{-2} and long-term durability. The excellent HER performance was mainly attributed to the high conductivity, large ECSA, and strong synergistic effect between the bimetals. Recently, metal nitrides have received widespread attention due to their excellent conductivity, superior chemical stability, excellent mechanical robustness, and special electronic structure.[195–199] Scaly Ni_3N nanosheets were fabricated on 3D NF (Ni_3N NSs/NF) with the high-efficient electrocatalytic property through ammonification engineering.[200] The self-supported

electrodes had many advantages including (1) the Ni_3N NSs *in situ* were formed on NF without using a binder and conducting agent, thus simplifying the electrode preparation process, preventing catalyst shedding, and reducing the cost; (2) high contents of active Ni_3N NSs catalysts could be realized on NF, leading to abundant catalytic active sites; (3) the seamless contact of Ni_3N NSs and NF guaranteed the rapid charge transfer and conductivity of the integrated electrode. As expected, Ni_3N NSs/NF exhibited an ultralow overpotential of 34 mV at 10 mA cm^{-2}, a small Tafel slope of 54 mV dec^{-1}, and long-term durability in 1 M KOH solution. DFT results showed that the synergistic effect between Ni_3N and NF, as well as more effective facets for H_{ads} could accelerate reaction kinetics. Our group successfully fabricated a PVP gel encapsulated Pt/$Ni(OH)_2$ heterojunction on NF (PVP@Pt/$Ni(OH)_2$@NF) by a facile solution evaporation method (Fig. 8a–g).[201] The obtained self-supported PVP@Pt/$Ni(OH)_2$@NF only required overpotentials of 12, 37, and 60 mV to reach current densities of 10, 50, and 100 mA cm^{-2} in 1.0 M KOH electrolyte, respectively, rivaling the Pt/C catalyst (Fig. 8h). Furthermore, the catalysts displayed an extremely low Tafel slope of 21.5 mV dec^{-1} (Fig. 8i) and outstanding long-term durability for 50 h without obvious decay (Fig. 8j). Additionally, the loading of Pt contents in PVP@Pt/$Ni(OH)_2$@NF was very low (0.35 wt%), improving the utilization efficiency of Pt-based catalysts. DFT calculations were applied to investigate the effect of PVP on the alkaline HER. The results indicated that PVP molecules at the interface could lower the water dissociation energy and optimize ΔG_{H^*} on the Pt/$Ni(OH)_2$ heterostructure (Fig. 8k and l), resulting in great activity for the alkaline HER. Furthermore, compared with the Tafel slopes and the electron state of Pt/$Ni(OH)_2$ with and without the PVP gel involved, the PVP gel could not only boost water dissociation to generate enough protons, but also improve the desorption of H_{ad} to enhance the HER kinetics by redistributing the charges of Pt/$Ni(OH)_2$. Our work exhibited a convenient strategy for designing a Pt/$Ni(OH)_2$ heterostructure and enhancing the utilization efficiency of Pt-based catalysts. Analogously, Kong *et al.* reported a facile and simple approach to fabricating Pt-decorated TiO_2/β-$Ni(OH)_2$ nanosheet arrays based on two-dimensional (2D) Ti_3C_2 through anodic electrodeposition coupling with the hydrothermal method (Fig. 9a–h).[202] Initially, few-layered Ti_3C_2 nanoplates were evenly riveted on NF in the anodic electrodeposition process. Ni^{2+} ions were easily yielded from NF in acidic conditions, which could act as the nucleation sites for β-$Ni(OH)_2$ nanosheets on the surface of

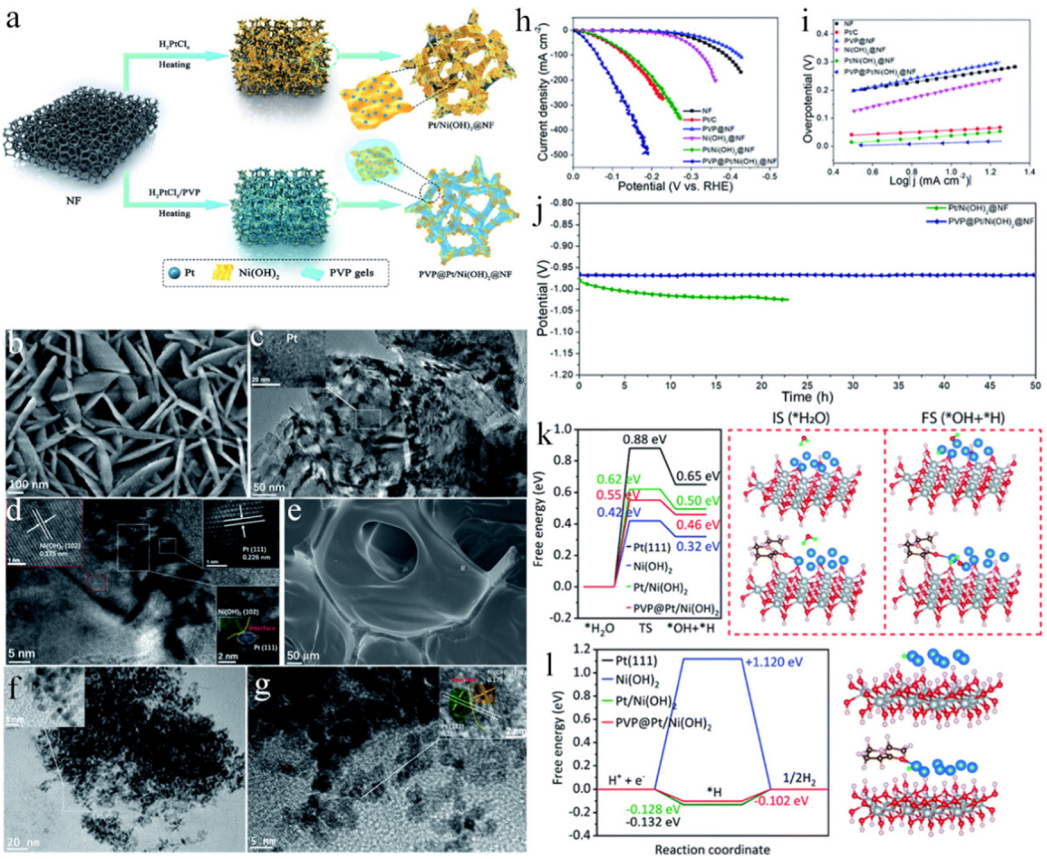

Fig. 8 (a) The preparation procedures of Pt/$Ni(OH)_2$@NF and PVP@Pt/$Ni(OH)_2$@NF. (b) The FESEM, (c) TEM, and (d) HRTEM images of the Pt/$Ni(OH)_2$@NF sample. (e) The FESEM, (f) TEM, and (g) HRTEM images of the PVP@Pt/$Ni(OH)_2$@NF sample. (h) LSV curves. (i) Tafel plots. (j) CP test of Pt/$Ni(OH)_2$@NF and PVP@Pt/$Ni(OH)_2$@NF at 10 mA cm^{-2} for 50 h without IR compensation. (k) H_2O dissociation energy profile for different substrate surfaces. The initial and final optimized configurations of H_2O adsorption and dissociation on the Pt/$Ni(OH)_2$ and PVP@Pt/$Ni(OH)_2$ surfaces are given on the right side. The silver, red, pink, blue, brown, and orange balls display Ni, O, H, Pt, C, and N atoms, respectively. (l) ΔG_{H^*} profile for different substrate surfaces.[201]

2D Ti_3C_2. During the facile hydrothermal reaction, Ti_3C_2 could accelerate dissociating H_2O into hydroxyl anions, subsequently reacting with adsorbed Ni^{2+} to produce $Ni(OH)_2$ species. Meantime, Pt^0 and TiO_2 species were generated *via* the reduction of Pt(IV) and the partial oxidization of Ti_3C_2. The prepared $Pt/TiO_2/Ni(OH)_2/NF$ presented a superior performance for alkaline water electrolysis under large industrial current densities. For the HER (Fig. 9i), the $Pt/TiO_2/Ni(OH)_2/NF$ delivered low overpotentials of 107, 145, and 184 mV at the industrial current densities of 500, 1000, and 1500 mA cm^{-2}, respectively, and excellent electrochemical stability at 500, 700, and 1400 mA cm^{-2} for at least 12 h (Fig. 9j), which far outperformed most reported HER electrocatalysts. In particular, the $Pt/TiO_2/Ni(OH)_2/NF$ electrodes could reach 10, 500, and 1000 mA cm^{-2} at the voltages of 1.37, 1.83, and 1.95 V, respectively, attaining extraordinary overall water splitting performances, which also preserved good long-term durability for at least 25 h. The outstanding electrocatalytic activity was the collaboration of the hydrophilic surface for facilitating the electrolyte wetting, rapid kinetics of water dissociation and H* recombination, a strong synergistic effect of Pt and $TiO_2/Ni(OH)_2$, and unique array architecture for promoting gas bubble releasing. This work developed effective nanoarray support for alkaline water electrolysis under large current densities. Song's group fabricated a MOF-derived Ru doped cobalt–nickel oxide heterostructure nanosheet arrays grown *in situ* on NF (Ru-Co_3O_4-NiO-NF).[203] The synthesized Ru-Co_3O_4-NiO-NF could efficiently preserve the merits of 2D Co-MOF precursors with leaf-shaped nanosheet morphology and simultaneously possess the mechanical strength and skeleton integrity of the 3D NF network, resulting in exposing more active sites and quickening the charge or mass transfer.[204] As a result, the optimized Ru-Co_3O_4-NiO-NF showed a superior HER performance achieving a current density of 10 mA cm^{-2} and 100 mA cm^{-2} at overpotentials of 44 mV and 115 mV in 1 M KOH solution, respectively, superior to that of the commercial 20 wt% Pt/C catalysts. Furthermore, the self-supported electrode maintained electrocatalytic activity over 60 h at 100 mA cm^{-2} without apparent decrease. Experiments and DFT calculation results indicated that Ru-doping and Co_3O_4-NiO heterointerface could cooperatively adjust the electronic state of Ni and Co sites, thereby optimizing the H_2O adsorption/desorption and hydrogen adsorption in the alkaline HER. This work not only afforded an effective and scalable synthesis method to design a MOF-derived self-supported electrode, but also raised a new strategy to synthesize the excellent alkaline HER electrocatalysts through engineering morphology and regulating electronic structure. Nickel phosphide catalysts have attracted considerable attention owing to their great catalytic activities for the HER.[205–210] Yan *et al.* constructed 3D self-supported, hierarchical, and edge-rich Ni_2P nanosheet arrays on NF (Ni_2P NSs-NF) for the HER.[211] Several in-plane nanopores were produced on the Ni_2P NSs in the phosphatization step, benefiting from the electrolyte soakage and H_2 molecules release. Meanwhile, abundant

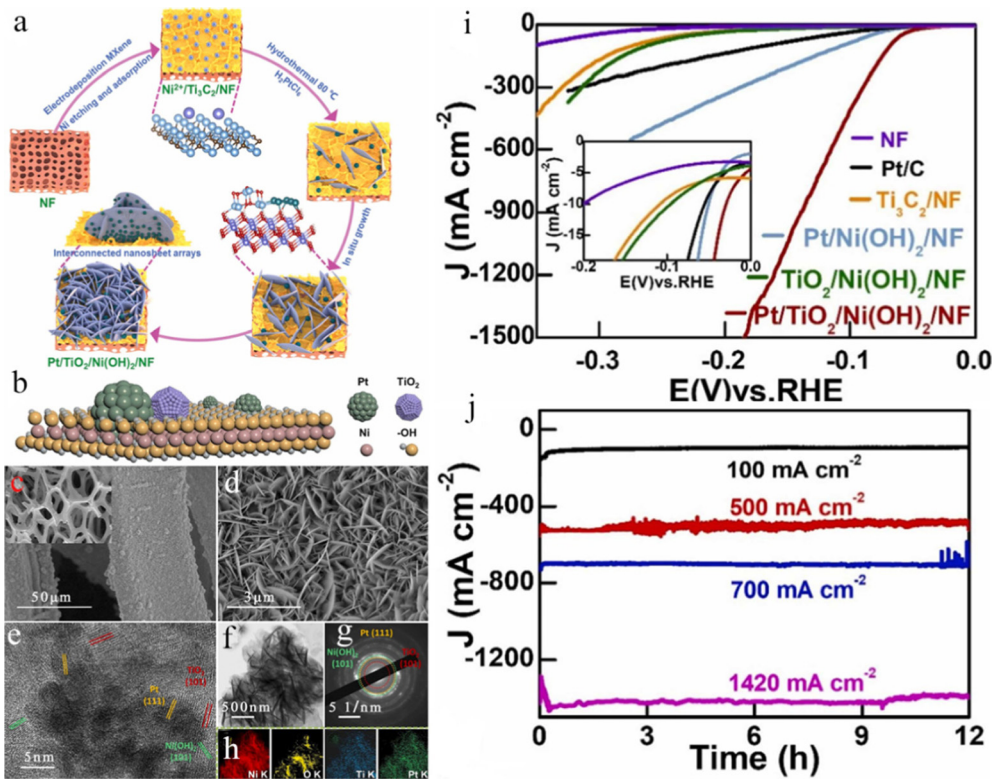

Fig. 9 (a) Fabrication process of $Pt/TiO_2/Ni(OH)_2/NF$ nanosheet arrays. (b) Schematic illustration of $Pt/TiO_2/Ni(OH)_2$ nanosheets. (c) FESEM image of $Pt/TiO_2/Ni(OH)_2/NF$. (d) Corresponding magnified FESEM image. (e) TEM image of $Pt/TiO_2/Ni(OH)_2$ arrays, and corresponding (f) HRTEM image, (g) selected area electron diffraction (SAED) pattern, (h) elemental mapping. (i) LSV curves. (j) CP test of $Pt/TiO_2/Ni(OH)_2/NF$ in 1.0 M KOH solution at different overpotentials.[202]

active edges on the Ni_2P NSs could expose more active sites. Owing to the 3D open nanostructure with abundant edges in the Ni_2P NSs, the Ni_2P NSs-NF electrode displayed superior HER performance both in alkaline and acidic solutions, which needed low overpotentials of 89 mV in 1 M KOH solution and 67 mV in 0.5 M H_2SO_4 solution to reach 10 mA cm^{-2} with low Tafel slopes of 82 and 57 mV dec^{-1}, respectively. Additionally, the self-supported Ni_2P NSs-NF electrode exhibited good cycling stability for the HER both in alkaline and acidic solutions even after 10 000 runs. Similarly, Wang *et al.* developed a new method for fabricating tripod-like Ni_xP nanowires on NF (Ni_xP/NF).[212] The method contained the processes of removing Mo cations in nickel molybdate nanowires *via* electrochemical oxidation and the following phosphorization. The optimized self-supported Ni_xP/NF presented a small 71 mV overpotential at 10 mA cm^{-2}. More significantly, the overpotential of Ni_xP/NF was only increased by about 4 mV at 200 mA cm^{-2} after 2000 CV runs, and the activity above 360 mA cm^{-2} showed little loss after 40 h electrolysis, outshining the benchmark Pt/C catalyst. Therefore, this self-supported electrode could be used practically for H_2 production *via* water electrolysis. The HER performance of transition-metal phosphides was affected greatly by the phosphorus content.[213–217] Zhou *et al.* provided a facile strategy to integrate P-rich NiP_2 and P-poor Ni_5P_4 into self-supported in-plane heterostructures *via* anion substitution of S in NiS/NiS_2 by P, in which P atoms at the in-plane interfaces served as active sites to adsorb H*, thereby favoring the HER by tuning the electron distribution between NiP_2 and Ni_5P_4.[218] The self-supported NiP_2/Ni_5P_4 heterostructures were synthesized through gas-phase sulfurization and phosphorization processes using the precursors of commercial NF, sulfur, and red phosphorous. Initially, the NF reacted with sulfur to produce high-crystalline NiS/NiS_2 nanoparticles on NF at an optimal annealing temperature. Subsequently, the NiS/NiS_2 nanoparticle acted as a sacrificial template for *in situ* forming in-plane NiP_2/Ni_5P_4 heterostructures on conductive NF by thermal phosphorization with red phosphorus powder. The resultant NiP_2/Ni_5P_4 heterostructure only required ultralow overpotentials of 30 and 76 mV to reach 10 and 100 mA cm^{-2} with a Tafel slope of 30.2 mV dec^{-1} in acidic solution, which outperformed most of the earth-abundant electrocatalysts and was comparable to Pt catalysts (30/72 mV at 10/100 mA cm^{-2}). Specifically, it could be used at a large current density and only needed 247 mV to achieve 2 A cm^{-2}, showing great potential for the commercialization of water electrolysis. DFT calculations elucidated that the interfacial hybridization between P 2p and H 1s orbitals at the interface of the NiP_2/Ni_5P_4 catalyst led to an optimal H-adsorption strength and a fast kinetic process. This work furnished a new design principle for fabricating excellent electrocatalysts for industrial water electrolysis.

3.4 Copper-based substrates

Compared with NF, CFM possesses a lower cost and higher electrical conductivity and therefore acts as a highly favourable substrate for the HER.[219] However, the corrosion resistance and electrocatalytic activity of CFM are generally lower than those of NF. As reported, platinum-based catalysts showed the benchmark activity;[220–222] however, there were fewer studies on their HER performance under high current densities in neutral electrolytes. Tan *et al.* proposed a simple synthetic strategy to directly *in situ* deposit blackberry-shaped Pt nanocrystals with low contents on CFM for the HER in a neutral solution.[223] Compared with the commercial 20 wt% Pt/C electrocatalysts pasted on CFM, the self-standing Pt@Cu foam exhibited low overpotentials of 35 and 438 mV at 10 and 1000 mA cm^{-2}, respectively. Meantime, due to the strong interaction between Cu and Pt, it showed outstanding durability in CA measurement at high current densities (100 to 400 mA cm^{-2}) and 1000 cycles LSV tests achieving 1000 mA cm^{-2}. DFT calculations revealed that the optimized ΔG_{H^*} on the Pt@Cu interface could facilitate efficient proton adsorption and rapid release of produced H_2. Moreover, Pt@Cu displayed effective water dissociation owing to the existence of a small amount of $Cu(OH)_2$ on CFM, which could easily adsorb OH^- in a neutral solution, thus further facilitating dissociating water.[224–226] This work provides a new strategy for designing self-supported electrocatalysts by establishing strong metal-metal interactions between active materials and substrates. Furthermore, Ru-doped $Cu_{2+1}O$ vertically arranged nanotube arrays *in situ* prepared on CFM (Ru/$Cu_{2+1}O$ NT/CFM) were reported by Cao's group, which presented a small overpotential of 32 mV at 10 mA cm^{-2} in the alkaline HER.[227] Dramatically, the alkaline electrolyzer employing Ru/$Cu_{2+1}O$ NT/CFM as a bifunctional electrocatalyst only required 1.53 V voltage to reach a current density of 10 mA cm^{-2}, superior to the benchmark of IrO_2(+)/Pt(−) counterpart (1.64 V at 10 mA cm^{-2}). The remarkable performance of the Ru/$Cu_{2+1}O$ NT/CFM catalyst originated from its high conductive substrate and special Ru-doped nanotube structure, which offered a high electrochemically active surface area and 3D gas diffusion channel. Song *et al.* reported a simple one-pot solution method to fabricate a self-standing 3D CFM electrode integrated with *in situ* grown Ag nanodots decorated Cu_2O porous nanobelts at room-temperature, which exhibited an overpotential of 108 mV at 10 mA cm^{-2}, a low Tafel slope of 58 mV dec^{-1}, and high durability for at least 20 h at 200 mV.[228] The good performance could be ascribed to the porous nanobelts with abundant active sites and the fast electron transfer between Ag@Cu_2O and conductive CFM support. Moreover, the low-cost, high-efficient, and long-durable electrocatalysts that operated well at high current densities are strongly demanded by industry H_2 production.[229–234] Therefore, the high-throughput scalable preparation method should be developed. Based on this, Zhang *et al.* synthesized high-performance and low-cost 2D MoS_2-based HER electrocatalysts on CFM through a scalable top-down exfoliation method followed by a thermal treatment.[235] The catalysts possessed a great acidic HER activity with an overpotential of 412 mV at a high current density of 1000 mA cm^{-2}, a small Tafel slope of 60 mV dec^{-1}, and good durability for 24 h. In addition, an inexpensive mineral-based catalyst with outstanding performance for the high-current-density HER was also fabricated using the same approach. Noteworthy, except for the cost of the CFM, the price of MoS_2 mineral-based catalyst was only 10 US$ m^{-2}, which is almost 30 times lower than the commercial Pt/C catalysts, highlighting a magnificent potential for large-scale industry

H_2 production. Li *et al.* utilized a simple electrochemical method to successfully synthesize a grass-like Ni/Cu nanosheet array on CFM (Ni/Cu/CFM).[236] First, a grass-like Cu nanosheet array was produced *via* partially electrochemical oxidizing CFM in 3 M NaOH solution and then an electrochemical reduction in 1 M Na_2SO_4 solution at room temperature. Finally, the grass-like Ni/Cu/CFM was fabricated by electrochemically reducing $NiSO_4$ solution on the surface of the Cu nanosheet array at room temperature. The resultant grass-like Ni/Cu/CFM electrode showed excellent HER performance with a Tafel slope of 42.7 mV dec^{-1} and an overpotential of 38 mV at 10 mA cm^{-2}, which was far lower than 156 mV of Ni/CFM and 246 mV of Cu nanosheet array/CFM electrode. Meanwhile, the as-prepared Ni/Cu/CFM electrode also exhibited superior catalytic durability because of its solid structure, which displayed 50 h stability at the current density of 30 mA cm^{-2}, indicating outstanding durability. The excellent electrocatalytic activity should be ascribed to the unique grass-like structure, which could expose more effective active sites and facilitate electrolyte penetration and gas diffusion. Yao *et al.* fabricated mesoporous Cu nanowires shelled with ultrathin WC layer self-supported on CFM through the chemical oxidation and *in situ* electro-reduction route followed by a simple and rapid magnetron sputtering (Fig. 10a–e).[237] The as-obtained Cu@WC/CFM catalyst exhibited low overpotentials of 92, 119, and 173 mV at 10 mA cm^{-2} in acidic, alkaline, and neutral solutions with high stability over 12 h (Fig. 10f and g). The enhanced HER performance could be attributed to the following reasons: (1) the large surface area of the mesoporous structure with exposed active sites boosted the H^+ transfer and the bubbles release; (2) the small work function between Cu (core) and WC (shell) reduced the contact potential; (3) the lattice mismatch of WC and Cu optimized both the atomic and electronic structures of WC. Tong *et al.* successfully synthesized a bamboo leaves-like amorphous FeO_x coated Cu_3P on CFM, and the bamboo leaves-like morphology facilitated the mass transfer and more active site exposing.[238] As a result, the binder-free FeO_x coated Cu_3P@Cu exhibited a low overpotential of 48 mV at 10 mA cm^{-2} for the alkaline HER, even exceeding the Pt/C catalyst at a large current density. Benefiting from the special hierarchical hollow nanowire array nanostructure with large surface area, good conductivity, abundant active sites, as well as fast mass/transport ability, a two-step synthetic route to synthesize hierarchical Cu_2S hollow nanowire arrays grown on CFM (Cu_2S HNAs-CFM) was proposed (Fig. 10h).[239] The obtained hierarchical Cu_2S HNAs-CFM electrode showed admirable alkaline HER activity with a low overpotential of 125 mV at 100 mA cm^{-2} (Fig. 10i), which was comparable to the performance of Pt/C-CFM

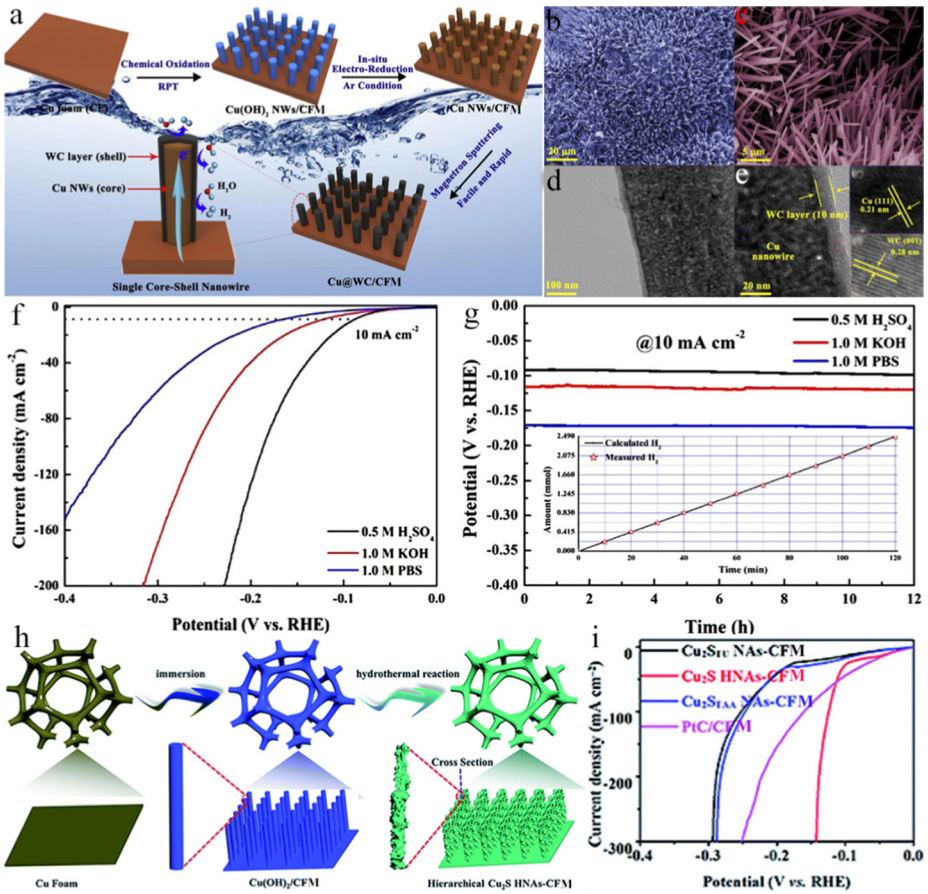

Fig. 10 (a) Schematic illustration for the formation mechanism of Cu@WC/CFM. (b and c) FESEM, (d) TEM, and (e) HRTEM images of Cu@WC/CFM. (f) LSV curves for Cu@WC/CFM in 0.5 M H_2SO_4, 1.0 M KOH, and 1.0 M PBS solutions. (g) CP tests of Cu@WC/CFM. The inset is the line of the amount of H_2 gas.[237] (h) Preparation of a hierarchical Cu_2S HNAs-CFM electrode. (i) LSV plots.[239]

and most reported electrocatalysts. Altogether, these meaningful works demonstrated the practicability of synthesizing high-performance HER electrode based on CFM.

3.5 Stainless steel substrates

Stainless steel is not only more resistant to corrosion in acid and alkaline solutions, but also cheaper than CC, NF, titanium-based substrates, and CFM, which have been more emphasized heavily.[240–246] Recently, Zhu *et al.* fabricated an efficient bifunctional electrocatalytic electrode of nanoporous nickel–iron hydroxides ($NiFe(OH)_x$) nanosheet arrays combined metal Ni/Fe *in situ* grown on stainless steel fiber felt (SSF) by a facile electrodeposition method at room temperature.[247] The constructed electrode showed distinguished electrocatalytic activity for water splitting, requiring overpotentials of 100 and 210 mV at 10 mA cm^{-2} in 1 M KOH media for the HER and oxygen evolution reaction (OER), respectively. Served as both anode and cathode for overall water splitting, the synthesized electrode also displayed extraordinary performance, achieving an overall cell voltage of 1.80 V to gain a current density of 100 mA cm^{-2}. Moreover, no obvious potential drop was observed after a long-term stability test. The improved water splitting performance was attributed to the special vertically ultrathin nanosheets with abundant active sites, more dangling bonds, and a synergistic effect between the $NiFe(OH)_x$ nanosheets and SSF substrate. The exceptional dual-functional catalyst could not only effectively lower the total cost but also simplify the electrolytic device. The strong metal–support interaction has been used to design and fabricate metal–support catalysts, which is a simple and effective approach to forming unique electronic structures and modifying the interface on the surface of the catalyst for enhancing HER performance.[248–253] Ascertaining that, our group directly fabricated Na_xWO_3 nanotube bundle support on a stainless mesh (SM) substrate *via* a facile hydrothermal method, followed by anchoring Pt nanoparticles with a low load-level (1.44%) on the as-prepared Na_xWO_3 nanotube bundles (Pt/R-Na_xWO_3@SM) *via* the *in situ* chemical reduction, successfully establishing Pt-sodium tungsten bronze hybrid electrocatalysts.[254] Specially, the Na_xWO_3 nanotube bundles were synthesized without using additives and surfactants, and $Na_2S_2O_8$ reagent was employed as an acid source instead of the strong corrosive including HCl, HNO_3, as well as H_2SO_4. As expected, owing to the nanotube bundle morphology with 3D structure and the strong metal–support interaction between Pt and Na_xWO_3, the optimized Pt/R-Na_xWO_3@SM-170 catalyst exhibited excellent HER performance with low overpotentials of 20 and 46 mV at 10 and 100 mA cm^{-2}, a small Tafel slope of 18.6 mV dec^{-1}, as well as good stability over 3000 CV runs and CA test for 25 h in 0.5 M H_2SO_4 media. Additionally, its activity even exceeded the benchmark 20 wt% Pt/C catalysts at a high current density (69 mV at 100 mA cm^{-2}). Impressively, it showed 10.8-fold higher mass activity than the Pt/C catalyst at 20 mV overpotential. DFT calculations manifested that the charge transfer between the R-Na_xWO_3 nanotube bundle and Pt nanoparticles could increase the electrons on the surface of the Pt nanoparticle, and thus negatively shift ε_d, leading to fast desorbing hydrogen intermediate and re-exposing the active sites on the Pt surface, eventually achieving outstanding the HER activity. This work provided a reliable route to synthesize sodium tungsten bronze for feasible support. Edison *et al.* electrochemically synthesized ruthenium nanoparticles on cathodically treated stainless-steel mesh. The experimental results showed that its acidic HER performance is very close to that of the bare Pt.[255] Moreover, Balogun's group developed a simple method to improve the HER performance of Co-based heterojunction catalysts with dual nanostructures on 3D stainless steel mesh (SSM) *via* non-oxygen anionic modifying CoO.[256] The compounds including CoO–CoP (SSM/CoOP), CoO–Co_xN (SSM/CoON), and CoO–CoS_x (SSM/CoOS) could be produced after phosphorizing, nitriding, and sulfuring CoO, respectively, where SSM/CoOP exhibited the best HER performance with a small overpotential of 21 mV at a current density of 10 mA cm^{-2}, comparable to the benchmark Pt/C catalysts (19 mV) and superior to that of SSM/CoON (44 mV) and SSM/CoOS (142 mV), evincing the non-oxygen treatment route benefitting for enhancing the HER activity. The excellent activity of SSM/CoOP could arrive from the following merits: (1) the strong electronic interaction between CoO and CoP and (2) the 1D nanowires and 2D nanosheets dual nanostructures, which could forcefully increase active surface, expose more active sites, and boost the ion/electron transfer, and thus significantly optimizing ΔG_{H^*}, resulting in improving catalytic activity. Hu *et al.* incorporated iron oxyhydroxide (FeOOH) on Co_4N nanowires supported on 3D SSM (FeOOH@Co_4N/SSM) by a facile hydrothermal and chemical bath deposition process.[257] The as-synthesized FeOOH@Co_4N/SSM hybrid electrocatalyst showed a low overpotential of 92 mV at 10 mA cm^{-2}, a small Tafel slope of 34 mV dec^{-1}, and excellent stability for the alkaline HER. DFT analyses indicated that the enhanced HER performance of FeOOH@Co_4N was owing to the suitable ε_d of Co_4N adjusted by the strong electronic interaction between Co_4N and FeOOH. Yao *et al.* synthesized self-supported $(Ni,Co)_3C$ mesoporous nanosheets/N-doped carbon ($(Ni,Co)_3CNSs$@NC) on a conductive SSM with controllable sizes from 1 cm × 1 cm to 25 cm × 25 cm through a simple and fast electrodeposition method followed by carbonization (Fig. 11a–e).[258] The as-fabricated catalyst exhibited small overpotentials of 58, 118, and 71 mV at 10 mA cm^{-2} in acidic, neutral, and basic solutions, respectively, with high stability (Fig. 11f–i), which outperformed that of most non-noble metal carbide-based catalysts in a pH-universal solution. The eminent activity could be attributed to the special ultrathin nanosheet-like morphology, large specific surface area, and strong synergetic effect of Ni and Co. As shown in Fig. 11j–l, DFT calculations revealed that the bimetallic NiCo carbide was favorable for the HER due to its good metallic conductivity, appropriate ΔG_{H^*}, and downshifted ε_d. This work provided a facile and viable strategy to prepare large-scale excellent catalysts for the HER in a wide pH electrolyte.

3.6 Molybdenum-based substrates

Compared to the common conductive substrates including CFP, CC, and GP, the monolithic Mo foil or plate can be directly utilized as a molybdenum source and self-supported substrate.[259–266] In addition, due to the chemically inert Mo substrate, the

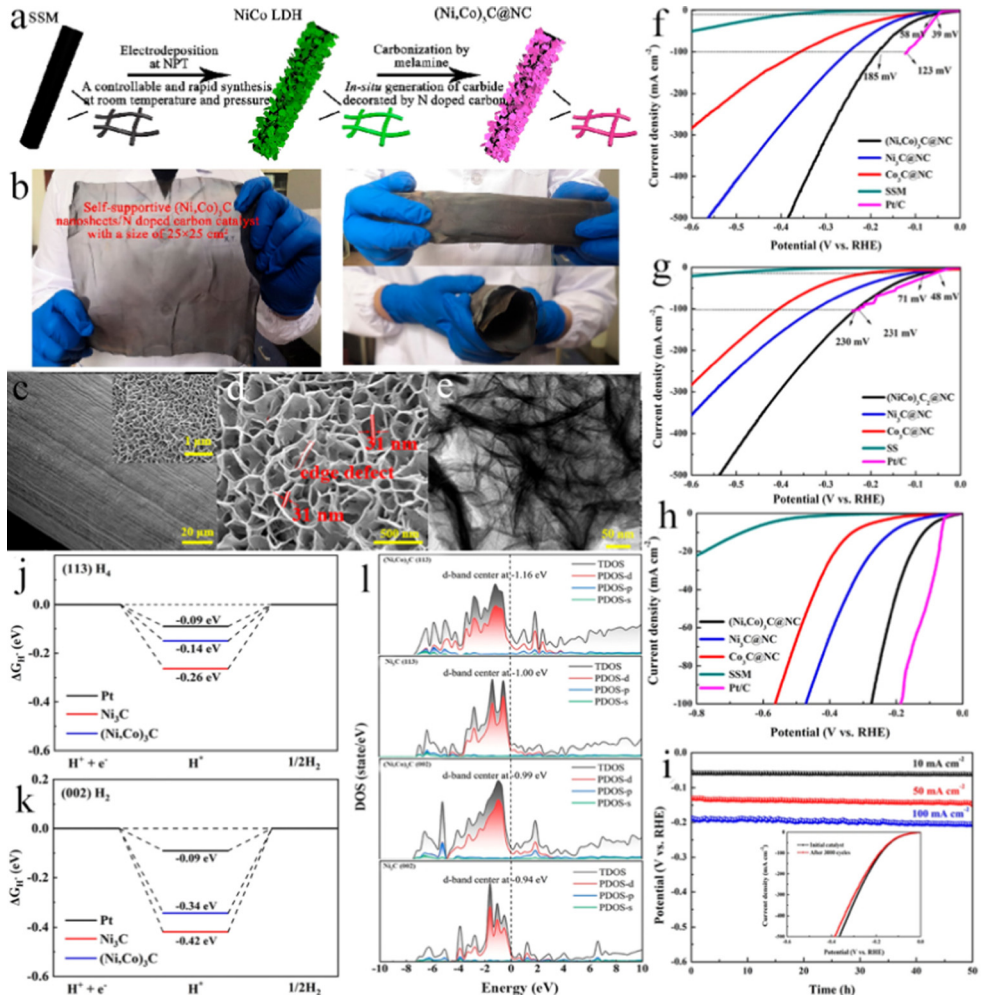

Fig. 11 (a) Schematic illustration of the formation mechanism. (b) Digital images of the catalyst with flexible property (size of 25 cm × 25 cm). (c and d) FESEM, and (e) TEM images of $(Ni,Co)_3C$ NSs@NC. (f–h) LSV curves for $(Ni,Co)_3C$ NSs@NC in 0.5 M H_2SO_4, 1.0 M KOH, and 1.0 M PBS solutions. (i) CP test at different current densities in 0.5 M H_2SO_4 solution; (i inset) LSV curves before and after the stability test. Schematic energy profiles for the HER (j) (113) and (k) (002). (l) Total and partial electronic density of states (TDOS and PDOS) calculated for $(Ni,Co)_3C$ (113), Ni_3C (113), $(Ni,Co)_3C$ (002), and Ni_3C (002).[258]

Mo-based electrode can be applied directly in both acidic and alkaline solutions.[267] Recently, Guo *et al.* reported the large-scale fabrication of vertically standing MoP nanosheet arrays (NSAs) on the Mo substrate through topotactically phosphorizing MoS_2 by a facile two-step chemical vapor deposition (CVD) method.[268] Initially, MoS_2 NSAs on the Mo substrate (MoS_2 NSAs/Mo) were synthesized by the CVD process using MoO_3 and S powders as the evaporation precursors. Subsequently, the formed MoS_2 NSAs/Mo precursor was topotactically switched to MoP NSAs/Mo. The as-synthesized MoP NSAs/Mo possessed excellent structural robustness, completely exposed active sites, and much adjoining space, benefiting for boosting the electrochemical kinetics and releasing the H_2 bubbles during the HER. As a result, the self-supported MoP NSAs/Mo electrode exhibited outstanding acidic and alkaline HER performance with overpotentials of 95 and 106 mV at 10 mA cm^{-2}, respectively, and small Tafel slopes of 50 and 56 mV dec^{-1}. Moreover, its activity remained unchanged even after 5000 cycles of repeating the CV test at 100 mV s^{-1}, as well as 36 h electrolysis at a high current density in both acidic and alkaline solutions. Zhao *et al.* provided a simple bottom-up approach to synthesizing heterostructured CoP nanoarray/MoO_2 films on the Mo foil (CoP–MoO_2/MF) employing pre-oxidized MF supported cobalt hydroxide-carbonate nanoneedles as the precursor.[269] The CoP–MoO_2/MF heterostructure exhibited superior HER activity with low overpotentials of 65 and 42 mV at 10 mA cm^{-2} in acidic and alkaline electrolytes, prosperous long-term stability, large exchange current density, and high turnover frequency. The experiments and DFT results indicated that MoO_2 was in favor of adsorbing water, cleaving H–O bonds, and facilitating hydrogen transfer. Moreover, heterointerfacial charge redistribution could optimize the ΔG_{H^*} on the heterointerface of CoP–MoO_2, which could be reduced from 0.08 eV on CoP (011) and 0.78 eV on MoO_2 (011) to 0.02 eV on CoP–MoO_2, significantly enhancing the HER performance and accelerating the catalytic kinetics. The large-scale synthesis of cheap, efficient, and stable electrocatalysts used

at high current densities in HER is very important and indispensable for industrial H_2 generation.[270–272] Liu's group developed a large-scale strategy to efficiently and economically fabricate $MoSe_2$–Mo_2N Schottky heterojunction flakes on inexpensive industrial-grade molybdenum substrates through a simple solid-state synthesis method.[273] The preparation process was as follows, first, MoO_3 prisms were seamlessly synthesized on Mo substrates *via* a controlled calcination process, and then the $MoSe_2$–Mo_2N Schottky heterojunction catalyst was achieved by a facile thermal treatment under the H_2/NH_3 mixture atmosphere. As a result, the as-formed $MoSe_2$–Mo_2N/Mo electrode showed a low overpotential of 76 mV at the current density of 10 mA cm^{-2} for the alkaline HER. Besides, it delivered a high current density of 1000 mA cm^{-2} at the overpotential of 462 mV, superior to that of a commercial Pt/C catalyst. DFT results demonstrated that the formed Schottky heterojunction between $MoSe_2$ and Mo_2N could prompt self-driven electron transfer that not only optimized the electronic structure at heterointerfaces but also adjusted the free energy of hydrogen adsorption and dissociation. Subsequently, they also successfully constructed a molybdenum oxide–phosphide (MoO_2–MoP) seamless electrode on Mo substrate using the same method.[274] The MoO_2–MoP mesh electrode achieved an industrial current density of 800 mA cm^{-2} at a low overpotential of 362 mV and showed excellent stability at high current densities for 200 h in an alkaline electrolyte. Additionally, it yielded a current density of 1000 mA cm^{-2} at 293 mV in 1.0 M KOH solution, but required an overpotential of only 215 mV to reach the same current density in 5.0 M KOH solution, which was practical for industrial alkaline HER. Similarly, a self-standing MoC–Mo_2C heterojunction was also constructed on a Mo sheet utilizing CO_2 as the carbon resource and electrons as the reducer in molten carbonate *via* a one-step electrodeposition method (Fig. 12a–d).[275] The as-prepared MoC–Mo_2C heterojunction exhibited outstanding HER performances (Fig. 12e–j) with low overpotentials of 256 and 292 at a high current density of 500 mA cm^{-2} in acidic and alkaline solutions, respectively, with long-term stability for at least 1000 h, a large TOF, and a high industrial operating temperature of about 70 °C, indicating a cost-effective catalyst for the HER operating at industry-level conditions. Experiments and DFT calculations (Fig. 12k–m) verified that the decent HER activity of the MoC–Mo_2C heterojunction self-supported electrode in acidic and alkaline electrolytes was due to the profitable ΔG_{H^*}, low water dissociation energy, hydrophilic surface, and special 3D porous structure. This work proposed a facile strategy to fabricate large-scale electrodes (3 cm × 11.5 cm), which could be expanded to the preparation of diverse carbide electrodes with sensibly designed microstructures, adjustable compositions, and excellent performances for practical applications.

3.7 Cobalt-based substrates

The strategy of nitrogen doping into metal phosphides has been extensively utilized to tune electronic structure, hydrogen adsorption free energy and water dissociation free energy, *etc.*, thereby enhancing their HER performance.[2,276–280] By virtue of this phenomenon, a nitrogen-doped CoP nanoarray grown on 3D porous CF was prepared for the HER and OER in water electrolysis.[281] The as-obtained CoP–N/CF required overpotentials of 100 and 260 mV for the HER and OER to reach a current density of 50 mA cm^{-2}, respectively, in alkaline conditions. Furthermore, as a bifunctional catalyst for the electrolyzing water reaction in a two-electrode system, it needed a cell voltage of 1.61 V to achieve a current density of 50 mA cm^{-2}, even exceeding the benchmark catalyst system of RuO_2/CF@Pt/C/CF (1.78 V). Additionally, the electrolyzer showed outstanding stability after 25 h of continuous operation at 50 mA cm^{-2}. The results revealed that doping of non-metallic nitrogen into CoP could greatly boost its catalytic activity, durability, kinetics, and catalytic efficiency for the HER and the OER. Similarly, the interface-strengthened CoP nanosheet array with Co_2P nanoparticles on CF as a self-supported electrocatalyst exhibited low overpotentials of 68 and 256 mV at 10 mA cm^{-2} for the HER and the OER, respectively.[282] Meanwhile, the CoP/Co_2P/CF as both anode and cathode for overall splitting water delivered a low voltage of 1.57 V to achieve 10 mA cm^{-2} with stability for over 58 h. Zhang's group elaborately fabricated flower-like Fe–Ni bimetallic layered double hydroxide on ultrahigh porosity CF (FeNi LDH/CF), and then flower-like FeNiP-LDH/CF was obtained through a phosphorization process in a tube furnace.[283] The hierarchical FeNiP-LDH/CF catalyst offered a current density of 10 mA cm^{-2} at a low overpotential of 39 mV for the alkaline HER, which was superior to that of the Pt catalyst (53 mV). In addition, the electrode could keep steady HER performance over 16 h during CA measurement at an industrial-level current density of 500–600 mA cm^{-2}. This decent HER performance could be assigned to several advantages, including the special porous nature of CF, the strong synergistic effect of bimetallic electrocatalysis, unique nanoflower-like morphology constructed by LDHs, as well as coupling interaction of transition metals and phosphorus. Subsequently, they also fabricated NiCoP/CF electrocatalysts, which only required overpotentials of 47 and 126 mV to reach 10 and 100 mA cm^{-2}, and retained excellent stability at a current density higher than 500 mA cm^{-2} for over 16 h.[284] Additionally, other bimetallic phosphides also exhibited highly efficient overall water splitting under a large current density in industries. A seamless integrated Fe_2P–Co_2P/CF electrode was successfully fabricated (Fig. 13a), which only required 145(243), 208(291), and 254(317) mV for alkaline HER(OER) to reach current densities of 100, 500, and 1000 mA cm^{-2}, respectively (Fig. 13b and c).[285] Remarkably, using Fe_2P–Co_2P/CF for overall water splitting at room (25 °C) and quasi-industrial (65 °C) temperatures, the operating voltages were 1.87 and 1.71 V to deliver 500 mA cm^{-2}, respectively, along with long-term stability for at least 300 h (Fig. 13d and e). The outstanding performance was owing to the *in situ* grown seamless integrated electrode with excellent conductivity and good stability, as well as the strong coupling effect between Fe_2P and Co_2P, indicating it met the application of industrial water splitting for large-scale renewable H_2 production. Interface engineering is an effective strategy for enhancing the water adsorption and

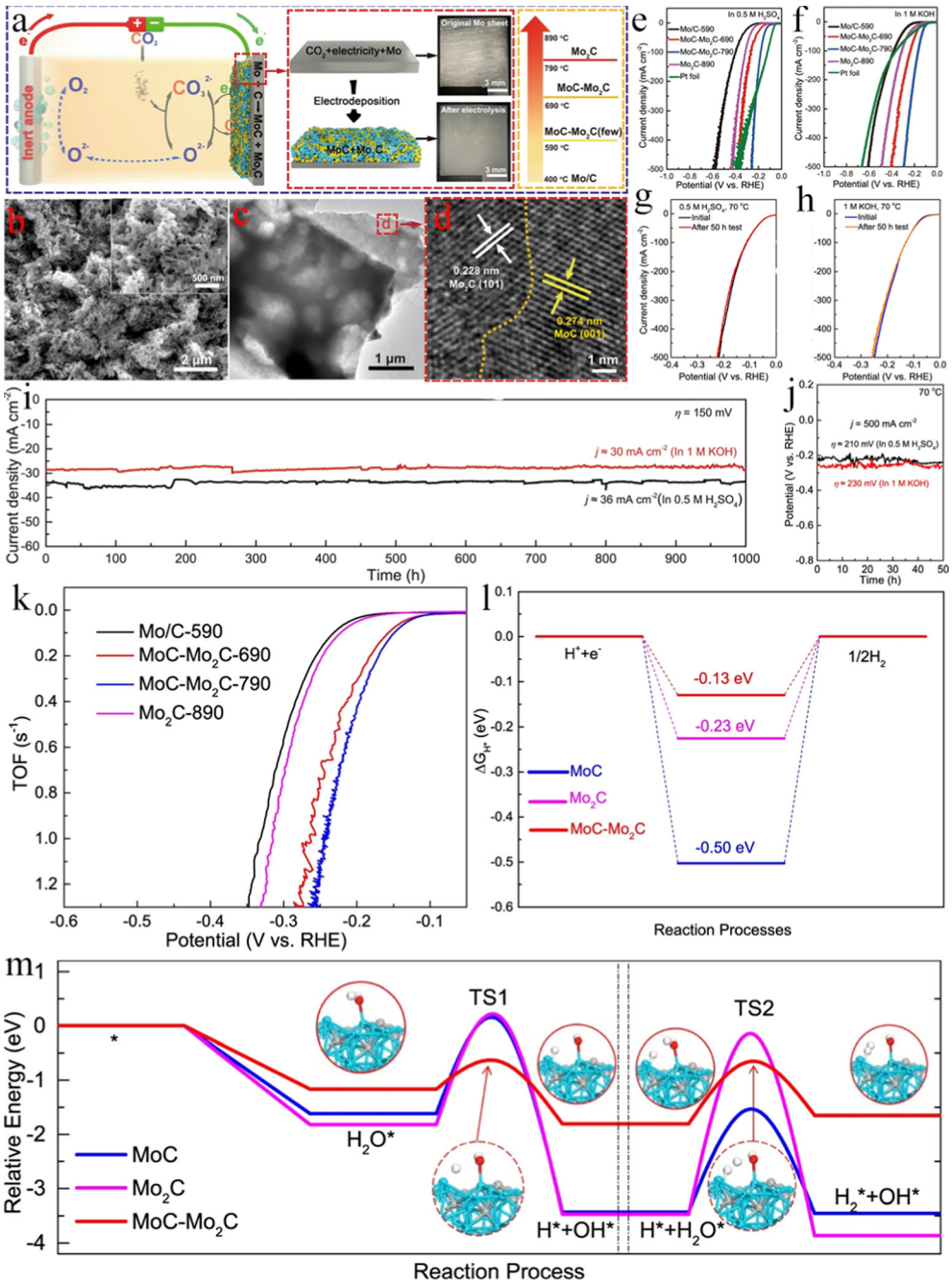

Fig. 12 (a) Schematic of synthesizing MoC–Mo_2C in molten carbonate and digital pictures of the Mo electrode before and after electrolysis. (b) FESEM, (c) TEM, and (d) HRTEM images of the synthesized MoC–Mo_2C. (e and f) LSV curves for MoC–Mo_2C in 0.5 M H_2SO_4 and 1 M KOH solutions. (g and h) LSV curves before and after stability tests in 0.5 M H_2SO_4 and 1 M KOH solutions at 70 °C. (i) The long-term electrolysis stability test of MoC–Mo_2C at 150 mV overpotential in 0.5 M H_2SO_4 and 1 M KOH solutions. (j) Stability test in both 0.5 M H_2SO_4 and 1 M KOH medium at 500 mA cm^{-2} and 70 °C. (k) TOF curves of different electrodes. (l) Calculated ΔG_{H^*} diagram of the HER in an acidic solution. (m) Relative energy diagram of water dissociation on MoC, Mo_2C, and MoC-Mo_2C, including the two steps of water dissociation, in alkaline solution, TS: transition state.[275]

dissociation and optimizing the ΔG_{H^*}, thereby improving the heterostructured catalyst's HER performance in acidic and alkaline solutions.[286–290] The low-cost interfacial Co_2N/Co grown on CF was reported, which displayed superior HER activity with overpotentials of only 12 and 64 mV to produce 10 and 100 mA cm^{-2}, respectively, substantially lower than those of Pt/CF (20 and 98 mV).[291] In addition, it showed exceedingly robust stability after the 10 000 CV and CP test at 10 and 100 mA cm^{-2} for at least 100 h. The ΔG_{H^*} values at two interfacial sites of Co_2N/Co were computed to be only −0.02 and −0.04 eV. In the contrast, both Co_2N and Co presented strong hydrogen affinity (−0.27 to −0.40 eV). The DFT computational results indicated that the interfacial sites of Co_2N/Co could improve the HER activity. Correspondingly, a

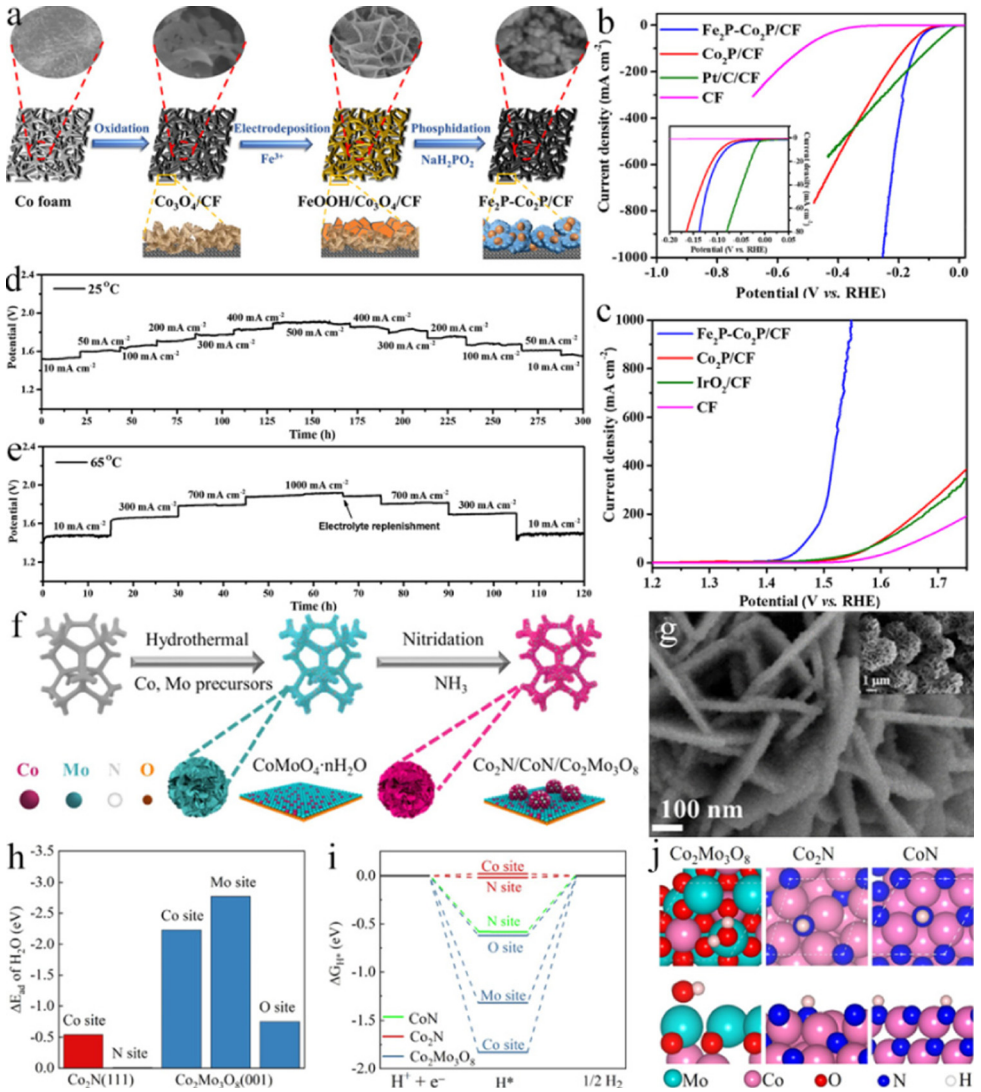

Fig. 13 (a) Schematic illustration of preparing a seamlessly integrated electrode of Fe_2P–Co_2P/CF. (b and c) LSV curves of different catalysts for the alkaline HER and OER. (d) Multistep CP curves of Fe_2P–Co_2P/CF under different current densities for overall water splitting at 25 °C. (e) Multistep CP curves of Fe_2P–Co_2P/CF under different current densities for overall water splitting at 65 °C.[285] (f) Schematic illustration to fabricate the Co_2N/CoN/$Co_2Mo_3O_8$/CF catalyst. (g) FESEM images of Co_2N/CoN/$Co_2Mo_3O_8$/CF catalyst. (h) Adsorption energies (ΔE_{ad}) of H_2O and (i) ΔG_{H^*} for the HER on different sites of the Co_2N (111), CoN (111), and $Co_2Mo_3O_8$ (001) surfaces. (j) Top and side views of the optimal adsorption structures of H_2O and H on Co_2N (111), CoN (111), and $Co_2Mo_3O_8$ (001) surfaces, respectively.[292]

CF-supported Co_2N/CoN/$Co_2Mo_3O_8$ heterostructure with hierarchical and nanoporous architecture was fabricated by a hydrothermal route followed by nitridation treatment (Fig. 13f and g), which exhibited high activity and excellent durability for the alkaline HER, exceeding most reported non-precious catalysts.[292] DFT calculations (Fig. 13h–j) indicated that the $Co_2Mo_3O_8$ component facilitated H_2O dissociation and Co_2N promoted the hydrogen adsorption and recombination. Wang *et al.* built super-hybrid metal sulfide nanoarrays on CF (super-Co_3S_4/P-WS_2/Co_9S_8/CF) by a simple one-step method.[293] The as-synthesized super-Co_3S_4/P-WS_2/Co_9S_8/CF consisted of a metallic Co_3S_4 nanosheet, a P doped WS_2 nanosheet and Co_9S_8 nanoparticles, which just required 58, 70, and 129 mV in alkaline, acidic, and neutral solutions, respectively, to achieve 10 mA cm^{-2}, and showed rapid kinetics and good long-term durability. The experimental and theoretical results demonstrated that the robust activity in super-Co_3S_4/P-WS_2/Co_9S_8/CF mainly originated from the unique electronic structure, special nanoarray morphology, and multiple heterointerfaces, which not only boosted the electric conductivity for electron transfer but also maximized the active heterointerfaces exposing for mass transport, resulting in Pt-like ΔG_{H^*} and favorable H_2O adsorption and dissociation energy for all-pH HER. For instance, the interface between Co_3S_4/WS_2 could enhance the HER activity *via* optimizing ΔG_{H^*}, and the Co_3S_4/WS_2 and Co_9S_8/WS_2 heterostructures were in favor of H_2O adsorption and dissociation, thereby enabling the outstanding HER performance in a wide pH range. The strategy in this work could

inspire the future synthesis of high-performance metal sulfide-based heterostructures for the HER. Like WS_2, the CeO_2 nanorod array was also employed to decorate Co_3S_4 nanosheets, forming a heterogeneous hierarchical Co_3S_4/CeO_2 nanorod array on CF (Co_3S_4/CeO_2-CF) through a simple ionic liquid-assisted one-step hydrothermal approach.[294] The as-synthesized Co_3S_4/CeO_2-CF with the favorable heterointerfaces and hierarchical core–shell structures demonstrated high-performance HER and OER activity, which only required overpotentials of 74.9 mV and 213 mV to reach the current density of 10 mA cm^{-2} in 1.0 M KOH electrolyte. To attain the current density of 10 mA cm^{-2}, the Co_3S_4/CeO_2-based electrolytic water device merely needed 1.64 V in an alkaline solution, lower than that of the Pt/C and RuO_2-assembled electrolysis device (1.70 V).

3.8 Iron-based substrates

The corrosion method has been widely used to synthesize self-supported electrodes on metal surfaces without electricity input, intricate synthetic process, and high temperature, and the metals served as substrates and precursors.[295–298] Consequently, a simple and industrially-compatible one-pot corrosion route for the fast preparation of amorphous RuO_2-decorated FeOOH nanosheets on iron foam (FF-Na-Ru) within 60 min was developed.[299] The as-fabricated electrode could rapidly release the generated gas bubbles owing to its super-hydrophilic and aerophobic feature, ensuring fast HER kinetics. Therefore, the FF-Na-Ru electrocatalyst presented a superior performance for the HER (30 mV at 10 mA cm^{-2}) and electrolyzer (1.46 V at 10 mA cm^{-2}) with high operational stability in 1 M KOH solution. DFT calculations confirmed that the strong electronic interactions between RuO_2 and FeOOH could enhance the electrocatalytic HER activity. The metastable FeS with ultrathin nano fan-like morphology on the 3D porous IF was prepared by the *in situ* sulfurization method (Fig. 14a–c), which showed efficient and long-term HER performance in alkaline simulated seawater and neutral electrolyte with low

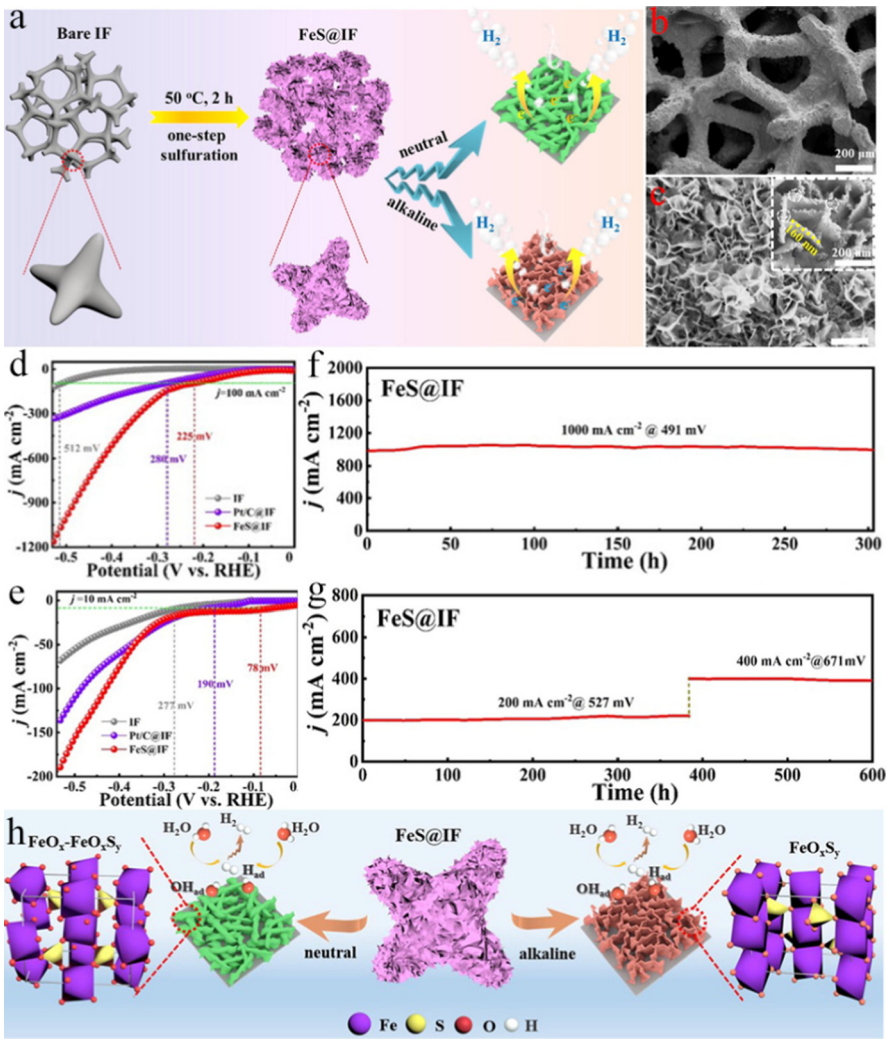

Fig. 14 (a) The synthesis of the FeS@IF electrode, and tested the electrochemical performance in both neutral and alkaline solutions. (b and c) FESEM images of the FeS@IF electrode. (d and e) LSV curves of the FeS@IF electrode in alkaline simulated seawater solution and 1.0 M PBS solution. (f and g) CP tests for the FeS@IF electrode in alkaline simulated seawater and 1.0 M PBS medium. (h) Schematic mechanism of the FeS@IF electrode in the HER process.[300]

overpotentials of 63 and 78 mV at 10 mA cm^{-2}, respectively (Fig. 14d and e).[300] Strikingly, it also exhibited outstanding stability for at least 300 h in alkaline simulated seawater solution at 1 A cm^{-2} with neglect deterioration (Fig. 14f). Surprisingly, the FeS@IF electrode was continuously electrolyzed for over 600 h at an industrial-grade current density in a neutral solution (Fig. 14g). The decent activity and robustness were attributed to the fast gas release and mass transfer induced by the highly-dispersed fan-like structure and the strong interaction between corrosion-resistant FeO_xS_y protection layers and 3D porous IF (Fig. 14h). Based on the doping effect, Ru, Ni dual-doped Fe_2O_3 catalyst with a lily-shaped morphology was constructed on IF (RuNi-Fe_2O_3/IF) through a simple one-step hydrothermal method for alkaline water electrolysis.[301] The RuNi-Fe_2O_3/IF electrode produced a large current density of 100 mA cm^{-2} at overpotentials of 75 and 329 mV for the HER and the OER, respectively. Besides, the overall water splitting needed cell voltages of 1.66 and 1.73 V to achieve 100 mA cm^{-2} in 1.0 M KOH and 1.0 M KOH seawater solutions, respectively. Moreover, the electrode displayed excellent long-term stability, retaining 100 mA cm^{-2} for over 100 h, which was superior to the two-electrode cell assembled by noble catalysts. The excellent activity and durability of RuNi-Fe_2O_3/IF could be ascribed to the intact lily-shaped morphology and the strong electronic coupling between the Ru/Ni doping and Fe_2O_3 host. Chai's group fabricated phosphorus doped inverse spinel Fe_3O_4 on IF (P-Fe_3O_4/IF) for the alkaline HER, which exhibited an ultralow overpotential of 138 mV at 100 mA cm^{-2}.[302] More inspiringly, coupling NiFe LDH/IF with P-Fe_3O_4/IF for splitting water showed excellent durability for over 1000 h at 1 A cm^{-2}, and even for 25 000 s at 10 A cm^{-2} in 6.0 M KOH at 60 °C, exhibiting great potential for the industrial H_2 production. DFT calculations suggested that the octahedral Fe site with excellent conductivity facilitated the water dissociation through a biomolecule Volmer reaction mechanism, greatly boosting the proton supply.[303] Meanwhile, ΔG_{H^*} of the P atom in inverse spinel Fe–O–P as an active site was theoretically calculated to be 0.01 eV, benefitting the alkaline HER. They also investigated the effect of F doping on bimetallic phosphide, and the results showed that F doping could affect the valence state and electronic structure of Co and Fe ions, thereby enhancing HER performance.[304] As a result, the as-synthesized F-Co_2P/Fe_2P/IF exhibited outstanding HER catalytic activity, which required low overpotentials of 229.8, 260.5, 292.2, and 304.4 mV to deliver 500, 1000, 2000, and 3000 mA cm^{-2}, respectively. Meantime, it could retain a long-term durability in 1.0 and 6.0 M KOH electrolytes at different high current densities for industrial water splitting. For further improving the HER performance of the bimetallic phosphide, they fabricated a self-supported CoFeOH/CoFeP on the IF substrate (CoFeOH/CoFeP/IF) with superior alkaline HER performance, requiring overpotentials of 114.9, 194.9, 221.8, 249.7, and 266.1 mV in 1.0 M KOH (25 °C) to reach 100, 500, 1000, 2000, and 3000 mA cm^{-2}, together with over 100 h durability (at 500 and 1000 mA cm^{-2}).[305] When integrating with NiFe-LDH/IF in a two-electrode cell, the voltage of NiFe-LDH/IF (+)||CoFeOH/CoFeP/IF (−) is only 1.57 V (7.6 M KOH 70 °C) at 2500 mA cm^{-2}. Even in 1.0 M KOH (25 °C) media, it merely demanded 1.88 V. The outstanding HER performance of CoFeOH/CoFeP/IF showed great potential for large-scale H_2 production.

3.9 Other substrates

Besides the substrates discussed above, other substrates including W foils, indium tin oxide (ITO) glass, SiO_2/Si, Au/Si, and MoNi foam have also been used as HER electrode substrates. For instance, Li *et al.* developed a WS_2 nanosheet electrocatalyst fabricated on the W foil (WS_2/W) by a mild bottom-up method (Fig. 15a).[306] The vertically arranged WS_2 ultra-thin nanosheets formed on the W substrate could reduce the effect of the contact resistance and improve the conductivity of WS_2 (Fig. 15b–d). Moreover, the W and S vacancies in the WS_2/W heterostructure could offer more active sites for the HER. DFT calculations demonstrated that the chemical bonds could be formed between the W foil and WS_2, leading to fast electron transport. This electrocatalyst exhibited HER activity with an overpotential of 108 mV for 10 mA cm^{-2}, a low Tafel slope of 45.5 mV dec^{-1}, and good stability. Xie *et al.* fabricated a vertically aligned defect-rich MoS_2 (DR-MoS_2) nanowall (NW) on the highly conductive ITO glass with a facile hydrothermal reaction (Fig. 15e and f).[307] Benefiting from the more exposed active edge sites, the coarse surface, as well as the potent nanowall structure, the DR-MoS_2 NW catalyst with an optimized thickness displayed a low overpotential of 95 mV to reach 10 mA cm^{-2} in an acidic solution. Furthermore, the HER stability of DR-MoS_2 NW could be maintained due to the close contact between the NW structure and the conductive ITO substrate. Vikraman *et al.* synthesized the metal-doped $MoSe_2$ layers on SiO_2/Si and Au/Si substrates using the solution bath technique (Fig. 15g), which exhibited improved acidic HER activity due to the more edge facets and enhanced electrical conductivity, requiring overpotentials of 86, 87, and 88 mV at 10 mA cm^{-2} for Cu-, Mn-, and Fe-doped $MoSe_2$, respectively.[308] Considering the advantages of nickel and molybdenum substrates, Zhou *et al.* fabricated a self-supported NiO/MoO_2 heterostructure with large crystal-amorphous interfaces utilizing MoNi foam as the metal source and substrate by a mild and practical anodizing-assisted molten-salt strategy (Fig. 15h).[309] The prepared diamond-like NiO/MoO_2-100-2 catalyst exhibited excellent alkaline HER activity with a low overpotential of 48 mV at 10 mA cm^{-2}, a small Tafel slope of 51.5 mV dec^{-1}, and good stability, which could be derived from three main factors: (1) the activated substrate by a pre-anodizing process facilitated the etching of subsequent molten salt, exposing more available active sites; (2) the NiO crystal/amorphous MoO_2 heterojunction with high-density distribution modified the electron density and d-band structure near the Fermi level, resulting in optimizing hydrogen adsorption/desorption energy and boosting charge transfer. In detail, the NiO crystals promoted the alkaline water dissociation to fast produce active hydrogen (Volmer step), thereby benefitting for the subsequent Heyrovsky and Tafel steps on the amorphous MoO_2 region; (3) the modulated electron state of NiO and MoO_2 was also

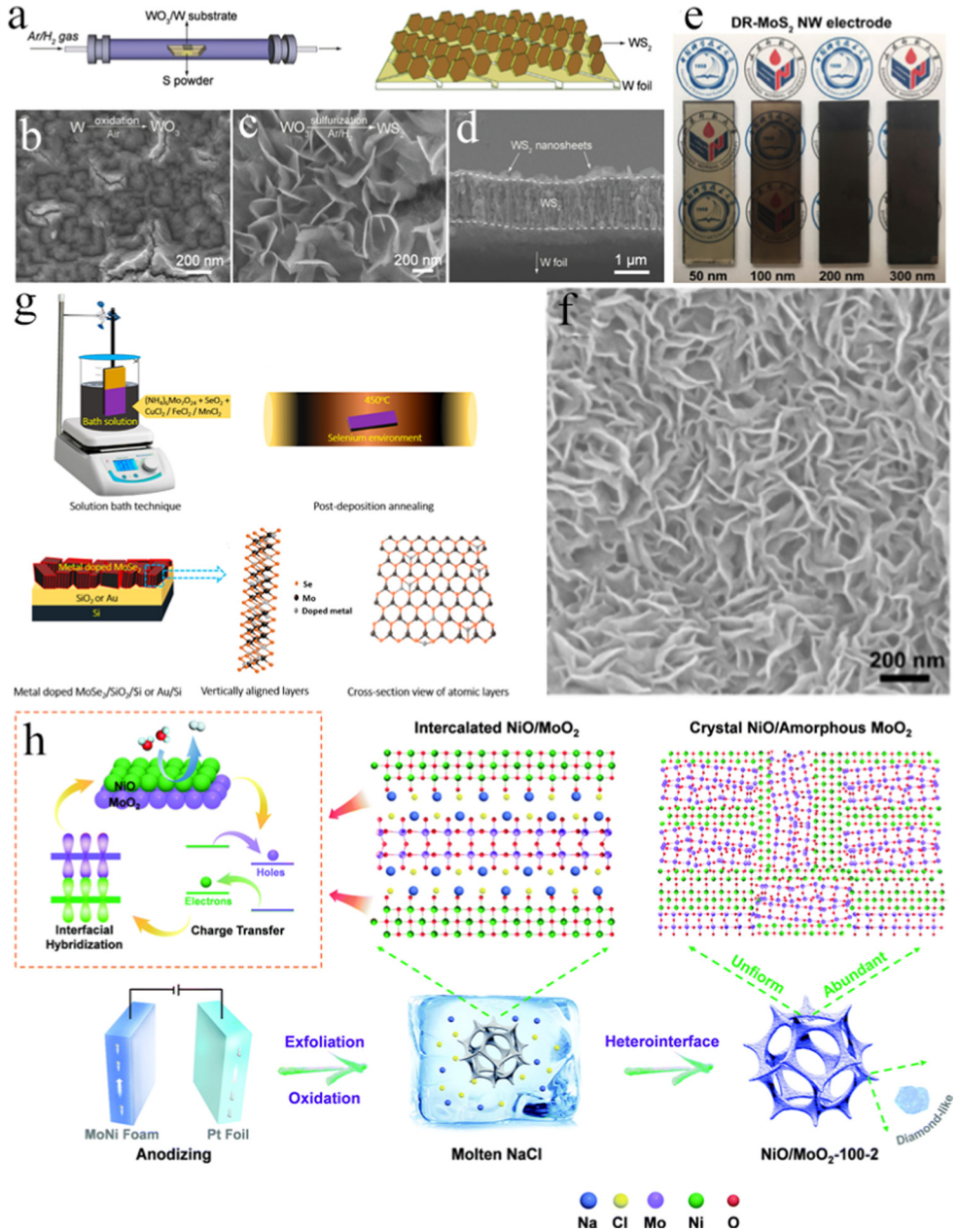

Fig. 15 (a) Fabrication of WS_2 process. (b and c) FESEM images of WO_3 and WS_2 nanosheets on the W foil. (d) Side-view FESEM.[306] (e) Digital photograph of the DR-MoS_2 NW catalysts with different thicknesses and variable transparency. (f) FESEM image of the DR-MoS_2 NW.[307] (g) Illustrations of metal-doped $MoSe_2$ deposition.[308] (h) Illustration of preparation of the NiO/MoO_2 sample.[309]

propitious to improve conductivity and optimize hydrogen adsorption.

4. Future perspectives

In this review, we comprehensively summarized the latest advances in various substrates for supporting electrocatalysts. Compared to the published reviews on the design or modification of electrocatalyst materials, this article focuses on substrates and their impacts on electrolytic water, which can provide an innovative strategy or guidance to develop high-efficient electrocatalytic electrodes. The investigations on self-supported electrodes have received great attention and have achieved a series of progress in the field of electrocatalytic water splitting. Notwithstanding, how to keep the advantages of the self-supported electrodes for large-scale fabrication and application is still a great challenge. To boost electrocatalytic activity and achieve wide applications in the industry, there are some suggestions for developing self-supported electrodes as exhibited in Fig. 16. For instance, (1) It is important to develop advanced substrates, which is the base on the self-supported electrodes; (2) large-scale synthetic methods are explored to serve for electrocatalytic water splitting; (3) the fundamental

Fig. 16 Challenges and future perspectives of self-supported electrodes.

reaction mechanisms of HER need more experimental data and theory analysis; (4) *in situ* spectroscopic technologies are used to evaluate the electrocatalytic performance and investigate interface effects and stability of self-supported electrodes; and (5) appropriate evaluation methods need to be established for evaluating the performance of electrocatalysts.

Currently, 3D macroporous metal foams (especially NF, CF, CFM, IF, and so on) are widely used to support electrocatalysts. Although these substrates exhibit relatively excellent conductivity, their mechanical strength cannot meet the practical long-term test at a large current density and high temperature.[33] In addition, these metal foams may become extremely fragile and broken during the pyrolysis of precursors under a high temperature. Accordingly, the synthesis method for self-supported electrocatalysts will be limited. Furthermore, CC is a preferential alternative to metal foam, which possesses not only good mechanical flexibility and elasticity, but also high-temperature stability. Nevertheless, its conductivity is weaker than that of metal foam, adversely affecting the catalytic performance of self-supported electrodes.[310] Whereas, most of the present attention is mainly paid to designing and tailoring electrocatalysts, the study on substrates is rarely reported. Therefore, more studies should be conducted to develop efficient and advanced substrates, which can not only enhance the catalytic activity of the self-supported electrodes but firmly operate for a long time in practical applications. Moreover, the chemical and physical properties of substrates essentially determine their performances and applications. Thus, the effect of substrate properties on the electrocatalytic performance needs to be further clarified. For instance, the interface between the active materials and the conductive substrates has a crucial impact on the electron transfer and durability properties, which are merely studied. Therefore, their relationship should be intensively investigated to get more information about the adhesive force between active materials and substrates, which may include the electrostatic attraction, van der Waals interaction, and covalent bonding.[311] For enhancing the HER performance, effective strategies should be used to tailor the interface. Besides, tedious procedures and low yield usually appear in the process of constructing self-supported electrocatalysts. Therefore, it is essential to exploit facile and easily scalable synthetic methods. In addition, the mass of the catalyst loaded on substrates shows dramatic effects on the HER performance. When the catalyst loading is high with a large thickness, the catalysts will easily dissolve in the electrolyte during testing due to their delamination from the substrate. On the other hand, when the loading is small with thin active layers, low catalytic activity will be observed.[31] Therefore, it is necessary to ensure the optimal amount of catalysts for efficient water splitting.

For developing advanced HER electrocatalysts, it is necessary to investigate the fundamental reaction mechanism. Theoretical calculations and *in situ* spectroscopic investigations are effective and powerful tools to reveal the catalysis mechanism and structural transformation of electrodes. *In situ operando* analytic techniques such as Raman, X-ray photoelectron spectroscopy, X-ray diffraction, and Fourier-transform infrared spectroscopy have been successfully employed to probe the surface species in the HER, facilitating simultaneously

determining the real catalytic active sites and mechanisms.[312–315] Meanwhile, transmission electron microscopy can give insight into the morphology, microstructure, and chemical properties of catalysts at the nanoscale. With *in situ* transmission electron microscopy, dynamic processes of catalytic reactions in both gas and liquid environments can be deeply investigated in real time.[316–318] Additionally, more refined characterization should be utilized at an atomic level. For instance, *ex situ* and *in situ* synchrotron radiation-based characterizations can study the electronic structure, oxidation states, and coordination environment.[319–321] Besides, more high-resolution techniques should be rapidly and timely developed to investigate the reaction processes and the evolution of surface/interface/bulk. For instance, near-ambient pressure X-ray photoelectron spectroscopy (NAP-XPS) and synchrotron radiation-based vacuum ultraviolet photoionization mass spectrometry (SVUV-PIMS) are useful tools to analyze the surface information under working conditions, as well as detect the active intermediates and radicals in the combustion field, respectively.[322–324] However, these techniques are rarely utilized in the field of electrocatalysis to probe the active intermediates during the HER. Therefore, multi-techniques should be exhaustively developed to probe simultaneously the structural information and reaction intermediates in the catalysis field, visualizing the HER pathways. Furthermore, the self-supported electrode with well-aligned nanostructures can remarkably influence the efficiency of mass transport during the HER.[325–327] In particular, the property of the nanostructure surface plays a key role in the microscale mass transport for the multi-phase system. For example, the 1D/2D nanostructured electrode can quickly remove the produced gas bubble, promoting the HER.[328–330] However, it is difficult to systematically investigate the mass transport effects and mechanisms for different surface nanostructures and active materials. The coupling of computational modeling with experiments will help to comprehend the mass transport mechanisms. Therefore, developing effective computational modeling should be taken into account in detail.

For stability performance, most of the reported self-supported electrodes work well under a current density below 10 mA cm^{-2} for dozens of hours, but cannot satisfy the requirement of industrial water electrolysis, which needs overpotentials of less than 300 mV at 500 mA cm^{-2} with stability for thousands of hours.[331] To obtain a tough self-supported electrode, the catalysts with an optimal adsorption energy of intermediates and porous structure are feasibly designed and fabricated, which can promote releasing H_2 bubbles from the surface and boost mass transfer.[332] Meanwhile, the stability-affecting factors should be focused on and investigated in-depth, such as substrate material, catalyst structure/phase, electrode/electrolyte hydrophilic performance, catalyst/substrate interface property, mechanical behavior, and so on. The intrinsic stability of most electrocatalysts in acid/alkaline solutions is not yet completely comprehended. Thus, the chemical and structural durability upon long-term testing and polarizing in strong acidic/alkaline electrolytes should be paid more attention. Furthermore, the decline mechanisms of electrocatalysts deserve to be further investigated, which can be understood in the following respect especially, such as the electrocatalysts dissolving, active materials converting, substrate corroding, active materials peeling, catalyst surface covering, and catalyst size increasing. In addition, the decline mechanism in different testing conditions ought to be studied separately. For a better understanding of the decline mechanisms, effective mitigation strategies should be proposed, and *in situ* characterization technique and chemical modeling also need to be developed. Furthermore, a reliable evaluation of the catalytic performance should be urgently addressed for different electrocatalysts. To compare the electrocatalyst performance, the presently used current density based on geometric electrode area may not reflect some dominant factors including substrate effect, catalyst dimension and size, mass loading, morphology, specific surface area, and testing condition. Therefore, comprehensive evaluation standards comprising η, Tafel slope, j_0, TOF value, specific activity based on mass and ECSA, and FE should be formulated for convincing comparison.

5. Conclusions

Exploring low-cost, highly efficient and extremely robust HER electrocatalysts is greatly crucial for industrial electrolytic water splitting for sustainable H_2 production. Compared to the conventional coated electrodes in the powder form, the self-supported electrodes with *in situ* integrated catalytically active phase on appropriate substrates are propitious for simplifying the fabrication of electrodes, decreasing interface resistance, exposing more abundant active sites and improving stability, and they have promising potential for practical applications in water splitting. In this review, we systematically summarized the state-of-the-art development of self-supported electrodes using different substrates for effective HER. The efficient strategies for enhancing electrocatalyst performance, such as heteroatomic doping, improving conductivity, building heterostructures, tuning wettability, surface/defect engineering, and so on, are emphasized. Meanwhile, the synthesis routes, including hydrothermal/solvothermal, electrodeposition, molten salt, calcination, CVD, thermal-oxidative, magnetic field assisted, electrochemical activation, solution evaporation, top-down exfoliation, bottom-up, magnetron sputtering, chemical bath deposition, solid-state synthesis, corrosion, and anodizing-assisted molten-salt methods, are also discussed. Furthermore, various electrocatalysts containing Fe_2O_3, Fe_3O_4, Co_3O_4, $Co_2Mo_3O_8$, CoO, NiO, $NiCo_2O_4$, $Cu_{2+1}O$, Cu_2O, TiO_2, RuO_2, CeO_2, MoO_2, Na_xWO_3, FeS, CoS_2, Co_3S_4, Co_9S_8, Cu_2S, MoS_2, WS_2, ReS_2, $MoSe_2$, $Ru_{0.33}Se$, NiMo alloy, NiCo alloy, RhIr alloy, Co, Ag, Ru, Pd, Pt, $Ni(OH)_2$, $NiFe(OH)_x$, FeOOH, Ti_3C_2, Ni_6Mo_6C, $(Ni,Co)_3C$, MoC, Mo_2C, WC, Co_2N, CoN, Co_4N, Ni_3N, Mo_2N, Fe_2P, CoP, Co_2P, Ni_2P, Ni_5P_4, Cu_3P, MoP, and MOFs with nanowire, nanorod, nanodot, nanosheet, nanoflower, nanotube, nanoplate, porous nanobelt, nanoarray, and nanowall morphologies are also introduced. Although significant progress towards materials design/synthesis and property investigation has been made, great challenges remain in the further development of self-supported electrodes.

In summary, we hope that the strategies discussed in this work can provide a background and a better insight into self-supported electrodes utilized in catalytically electrolyzing water. We believe that constructing a self-supported electrocatalyst is a promising and challenging strategy to develop a hydrogen economy.

Author contributions

Jin Li: conceptualization; writing-original draft; visualization. Jian Zhang: data curation; visualization. Jinke Shen: data curation; visualization. Haipeng Chen: data curation; visualization. Honghui Wu: words and sentence editing. Guilong Liu: data curation; visualization. Donglei Guo: data curation; visualization. Changzhou Yuan: funding acquisition; supervision; writing-review & editing. Naiteng Wu: funding acquisition; supervision; writing-review & editing. Xianming Liu: funding acquisition; supervision; writing-review & editing.

Conflicts of interest

There are no conflicts to declare.

Acknowledgements

This work was supported by the National Natural Science Foundation of China (Grant No. 51804156, No. 51904152, No. 22008098), the Program for Science & Technology Innovation Talents in Universities of Henan Province (No. 20HASTIT020, No. 22HASTIT008), the Programs for Science and Technology Development of Henan Province, China (No. 222102320065), and the Key Specialized Research and Development Breakthrough (Science and Technology) in Henan Province (No. 212102210214) and the key scientific research projects of University in Henan Province (No. 23B430002).

References

1 S. Xu, H. Zhao, T. Li, J. Liang, S. Lu, G. Chen, S. Gao, A. M. Asiri, Q. Wu and X. Sun, Iron-based phosphides as electrocatalysts for the hydrogen evolution reaction: recent advances and future prospects, *J. Mater. Chem. A*, 2020, **8**, 19729–19745.

2 S. Chandrasekaran, C. Zhang, Y. Shu, H. Wang, S. Chen, T. Nesakumar, J. I. Edison, Y. Liu, N. Karthik, R. D. K. Misra, L. Deng, P. Yin, Y. Ge, O. A. Al-Hartomy, A. Al-Ghamdi, S. Wageh, P. Zhang, C. Bowen and Z. Han, Advanced opportunities and insights on the influence of nitrogen incorporation on the physico-/electro-chemical properties of robust electrocatalysts for electrocatalytic energy conversion, *Coord. Chem. Rev.*, 2021, **449**, 214209.

3 J. Li, H. Huang, X. Cao, H.-H. Wu, K. Pan, Q. Zhang, N. Wu and X. Liu, Template-free fabrication of MoP nanoparticles encapsulated in N-doped hollow carbon spheres for efficient alkaline hydrogen evolution, *Chem. Eng. J.*, 2021, **416**, 127677.

4 G. Liu, F. Xiao, T. Zhang, Y. Gu, J. Li, D. Guo, M. Xu, N. Wu, A. Cao and X. Liu, In-situ growth of MoO_2@N doped carbon on Mo_2C-MXene for superior lithium storage, *Appl. Surf. Sci.*, 2022, **597**, 153688.

5 Q. Pan, X. Chen, H. Liu, W. Gan, N. Ding and Y. Zhao, Crystalline porphyrin-based graphdiyne for electrochemical hydrogen and oxygen evolution reactions, *Mater. Chem. Front.*, 2021, **5**, 4596–4603.

6 Y. Yang, Y. Yu, J. Li, Q. Chen, Y. Du, P. Rao, R. Li, C. Jia, Z. Kang, P. Deng, Y. Shen and X. Tian, Engineering ruthenium-based electrocatalysts for effective hydrogen evolution reaction, *Nanomicro. Lett.*, 2021, **13**, 160.

7 Z. Zhou, Z. Pei, L. Wei, S. Zhao, X. Jian and Y. Chen, Electrocatalytic hydrogen evolution under neutral pH conditions: current understandings, recent advances, and future prospects, *Energy Environ. Sci.*, 2020, **13**, 3185–3206.

8 Y. Zhao, S. Wei, K. Pan, Z. Dong, B. Zhang, H.-H. Wu, Q. Zhang, J. Lin and H. Pang, Self-supporting transition metal chalcogenides on metal substrates for catalytic water splitting, *Chem. Eng. J.*, 2021, **421**, 129645.

9 M. Chatenet, B. G. Pollet, D. R. Dekel, F. Dionigi, J. Deseure, P. Millet, R. D. Braatz, M. Z. Bazant, M. Eikerling, I. Staffell, P. Balcombe, Y. Shao-Horn and H. Schafer, Water electrolysis: from textbook knowledge to the latest scientific strategies and industrial developments, *Chem. Soc. Rev.*, 2022, **51**, 4583–4762.

10 J. Li, X. Liu and J. Zhang, Smart assembly of sulfide heterojunction photocatalysts with well-defined interfaces for direct Z-scheme water splitting under visible light, *ChemSusChem*, 2020, **13**, 2996–3004.

11 D. S. Baek, J. Lee, J. S. Lim and S. H. Joo, Nanoscale electrocatalyst design for alkaline hydrogen evolution reaction through activity descriptor identification, *Mater. Chem. Front.*, 2021, **5**, 4042–4058.

12 G. Chisholm, T. Zhao and L. Cronin, Hydrogen from water electrolysis, *Storing Energy*, 2022, **24**, 559–591.

13 M. Lu, M. Zhang, J. Liu, Y. Chen, J. P. Liao, M. Y. Yang, Y. P. Cai, S. L. Li and Y. Q. Lan, Covalent organic framework based functional materials: important catalysts for efficient CO_2 utilization, *Angew. Chem., Int. Ed.*, 2022, **61**, 202200003.

14 Y. Zhang, L. Z. Dong, S. Li, X. Huang, J. N. Chang, J. H. Wang, J. Zhou, S. L. Li and Y. Q. Lan, Coordination environment dependent selectivity of single-site-Cu enriched crystalline porous catalysts in CO_2 reduction to CH_4, *Nat. Commun.*, 2021, **12**, 6390.

15 L. Zhang, X. X. Li, Z. L. Lang, Y. Liu, J. Liu, L. Yuan, W. Y. Lu, Y. S. Xia, L. Z. Dong, D. Q. Yuan and Y. Q. Lan, Enhanced cuprophilic interactions in crystalline catalysts facilitate the highly selective electroreduction of CO_2 to CH_4, *J. Am. Chem. Soc.*, 2021, **143**, 3808–3816.

16 J. Zhang, R. Cui, C. Gao, L. Bian, Y. Pu, X. Zhu, X. Li and W. Huang, Cation-modulated HER and OER activities of hierarchical VOOH hollow architectures for high-efficiency and stable overall water splitting, *Small*, 2019, **15**, 1904688.

17 H. Huang, Y. Xue, Y. Xie, Y. Yang, L. Yang, H. He, Q. Jiang and G. Ying, MoS_2 quantum dot-decorated MXene nanosheets as efficient hydrogen evolution electrocatalysts, *Inorg. Chem. Front.*, 2022, **9**, 1171–1178.
18 H. Wu, F. Zhuo, H. Qiao, L. Kodumudi Venkataraman, M. Zheng, S. Wang, H. Huang, B. Li, X. Mao and Q. Zhang, Polymer-/ceramic-based dielectric composites for energy storage and conversion, *Energy Environ. Mater.*, 2022, **5**, 486–514.
19 S. Chandrasekaran, C. Bowen, P. Zhang, Z. Li, Q. Yuan, X. Ren and L. Deng, Spinel photocatalysts for environmental remediation, hydrogen generation, CO_2 reduction and photoelectrochemical water splitting, *J. Mater. Chem. A*, 2018, **6**, 11078–11104.
20 S. Chu and A. Majumdar, Opportunities and challenges for a sustainable energy future, *Nature*, 2012, **488**, 294–303.
21 S. Trasatti, ''Water electrolysis: who first?'', *J. Electroanal. Chem.*, 2000, **481**, 112.
22 H. H. Wu, H. Huang, J. Zhong, S. Yu, Q. Zhang and X. C. Zeng, Monolayer triphosphates MP_3 (M = Sn, Ge) with excellent basal catalytic activity for hydrogen evolution reaction, *Nanoscale*, 2019, **11**, 12210–12219.
23 W. Liu, Z. Xiao, S. Chandrasekaran, D. Fan, W. Li, H. Lu and Y. Liu, Insights into the effect of sulfur incorporation into tungsten diphosphide for improved hydrogen evolution reaction, *ACS Appl. Mater. Interfaces*, 2022, **14**, 16157–16164.
24 Y. Zhu, Q. Lin, Y. Zhong, H. A. Tahini, Z. Shao and H. Wang, Metal oxide-based materials as an emerging family of hydrogen evolution electrocatalysts, *Energy Environ. Sci.*, 2020, **13**, 3361–3392.
25 T. Sun, W. Zhong, M. Zhang, Y. Tang, J. Wang, C. Xu, L. Hu and M. Wang, A low-cost 2D WO_3/Ni_3S_2 heterojunction for highly stable hydrogen evolution, *Mater. Chem. Front.*, 2021, **5**, 8248–8254.
26 S. Chandrasekaran, N. Li, Y. Zhuang, L. Sui, Z. Xiao, D. Fan, V. Aravindan, C. Bowen, H. Lu and Y. Liu, Interface charge density modulation of a lamellar-like spatially separated Ni_9S_8 nanosheet/Nb_2O_5 nanobelt heterostructure catalyst coupled with nitrogen and metal (M = Co, Fe, or Cu) atoms to accelerate acidic and alkaline hydrogen evolution reactions, *Chem. Eng. J.*, 2022, **431**, 134073.
27 B. Geng, F. Yan, X. Zhang, Y. He, C. Zhu, S. L. Chou, X. Zhang and Y. Chen, Conductive CuCo-based bimetal organic framework for efficient hydrogen evolution, *Adv. Mater.*, 2021, **33**, 2106781.
28 Y. Zhao, S. Wei, L. Xia, K. Pan, B. Zhang, H. Huang, Z. Dong, H.-H. Wu, J. Lin and H. Pang, Sintered Ni metal as a matrix of robust self-supporting electrode for ultrastable hydrogen evolution, *Chem. Eng. J.*, 2022, **430**, 133040.
29 J. Jiang, Y. Li, J. Liu, X. Huang, C. Yuan and X. W. Lou, Recent advances in metal oxide-based electrode architecture design for electrochemical energy storage, *Adv. Mater.*, 2012, **24**, 5166–5180.
30 J. Wang, F. Xu, H. Jin, Y. Chen and Y. Wang, Non-noble metal-based carbon composites in hydrogen evolution reaction: fundamentals to applications, *Adv. Mater.*, 2017, **29**, 1605838.
31 S. Chandrasekaran, M. Khandelwal, F. Dayong, L. Sui, J. S. Chung, R. D. K. Misra, P. Yin, E. J. Kim, W. Kim, A. Vanchiappan, Y. Liu, S. H. Hur, H. Zhang and C. Bowen, Developments and perspectives on robust nano- and microstructured binder-free electrodes for bifunctional water electrolysis and beyond, *Adv. Energy Mater.*, 2022, **12**, 2200409.
32 H. Sun, Z. Yan, F. Liu, W. Xu, F. Cheng and J. Chen, Self-supported transition-metal-based electrocatalysts for hydrogen and oxygen evolution, *Adv. Mater.*, 2020, **32**, 1806326.
33 H. Yang, M. Driess and P. W. Menezes, Self-supported electrocatalysts for practical water electrolysis, *Adv. Energy Mater.*, 2021, **11**, 2102074.
34 S. Chandrasekaran, M. Khandelwal, F. Dayong, L. Sui, J. S. Chung, R. D. K. Misra, P. Yin, E. J. Kim, W. Kim, A. Vanchiappan, Y. Liu, S. H. Hur, H. Zhang and C. Bowen, Developments and perspectives on robust nano- and microstructured binder-free electrodes for bifunctional water electrolysis and beyond, *Adv. Energy Mater.*, 2022, **12**, 2200409.
35 C. Liang, P. Zou, A. Nairan, Y. Zhang, J. Liu, K. Liu, S. Hu, F. Kang, H. J. Fan and C. Yang, Exceptional performance of hierarchical Ni–Fe oxyhydroxide@NiFe alloy nanowire array electrocatalysts for large current density water splitting, *Energy Environ. Sci.*, 2020, **13**, 86–95.
36 J. Wei, M. Zhou, A. Long, Y. Xue, H. Liao, C. Wei and Z. J. Xu, Heterostructured electrocatalysts for hydrogen evolution reaction under alkaline conditions, *Nanomicro. Lett.*, 2018, **10**, 75.
37 T. Tang, L. Ding, Z. C. Yao, H. R. Pan, J. S. Hu and L. J. Wan, Synergistic electrocatalysts for alkaline hydrogen oxidation and evolution reactions, *Adv. Funct. Mater.*, 2021, **32**, 2107479.
38 Y. Zheng, Y. Jiao, A. Vasileff and S. Z. Qiao, The hydrogen evolution reaction in alkaline solution: from theory, single crystal models, to practical electrocatalysts, *Angew. Chem., Int. Ed.*, 2018, **57**, 7568–7579.
39 S. Anantharaj, S. Noda, V. R. Jothi, S. Yi, M. Driess and P. W. Menezes, Strategies and perspectives to catch the missing pieces in energy-efficient hydrogen evolution reaction in alkaline media, *Angew. Chem., Int. Ed.*, 2021, **60**, 18981–19006.
40 L. Fu, Y. Li, N. Yao, F. Yang, G. Cheng and W. Luo, IrMo nanocatalysts for efficient alkaline hydrogen electrocatalysis, *ACS Catal.*, 2020, **10**, 7322–7327.
41 Y. Men, Y. Tan, P. Li, X. Cao, S. Jia, J. Wang, S. Chen and W. Luo, Tailoring the 3d-orbital electron filling degree of metal center to boost alkaline hydrogen evolution electrocatalysis, *Appl. Catal., B*, 2021, **284**, 119718.
42 H. Wang, W. Fu, X. Yang, Z. Huang, J. Li, H. Zhang and Y. Wang, Recent advancements in heterostructured interface engineering for hydrogen evolution reaction electrocatalysis, *J. Mater. Chem. A*, 2020, **8**, 6926–6956.
43 Z. Wang, H. H. Wu, Q. Li, F. Besenbacher, Y. Li, X. C. Zeng and M. Dong, Reversing interfacial catalysis of ambipolar WSe_2 single crystal, *Adv. Sci.*, 2020, **7**, 1901382.

44 J. Luo, J. H. Im, M. T. Mayer, M. Schreier, M. K. Nazeeruddin, N. G. Park, S. D. Tilley, H. J. Fan and M. Gratzel, Water photolysis at 12.3% efficiency via perovskite photovoltaics and earth-abundant catalysts, *Science*, 2014, **345**, 1593–1596.
45 R. Chen, C. Yang, W. Cai, H.-Y. Wang, J. Miao, L. Zhang, S. Chen and B. Liu, Use of platinum as the counter electrode to study the activity of nonprecious metal catalysts for the hydrogen evolution reaction, *ACS Energy Lett.*, 2017, **2**, 1070–1075.
46 J. K. Nørskov, T. Bligaard, A. Logadottir, J. R. Kitchin, J. G. Chen, S. Pandelov and U. Stimming, Trends in the exchange current for hydrogen evolution, *J. Electrochem. Soc.*, 2005, **152**, 23.
47 B. V. Tilak and C. P. Chen, Generalized analytical expressions for Tafel slope, reaction order and a.c. impedance for the hydrogen evolution reaction (HER): mechanism of HER on platinum in alkaline media, *J. Appl. Electrochem.*, 1993, **23**, 631–640.
48 G. Zhao, K. Rui, S. X. Dou and W. Sun, Heterostructures for electrochemical hydrogen evolution reaction: a review, *Adv. Funct. Mater.*, 2018, **28**, 1803291.
49 W. Feng, W. Pang, Y. Xu, A. Guo, X. Gao, X. Qiu and W. Chen, Transition metal selenides for electrocatalytic hydrogen evolution reaction, *ChemElectroChem*, 2019, **7**, 31–54.
50 Y. Zheng, Y. Jiao, M. Jaroniec and S. Z. Qiao, Advancing the electrochemistry of the hydrogen-evolution reaction through combining experiment and theory, *Angew. Chem., Int. Ed.*, 2015, **54**, 52–65.
51 J. O. M. Bockris and E. C. Potter, The mechanism of the cathodic hydrogen evolution reaction, *J. Electrochem. Soc.*, 1952, **99**, 169.
52 S. I. Perez Bakovic, P. Acharya, M. Watkins, H. Thornton, S. Hou and L. F. Greenlee, Electrochemically active surface area controls HER activity for Fe_xNi_{100-x} films in alkaline electrolyte, *J. Catal.*, 2021, **394**, 104–112.
53 P. Su, W. Pei, X. Wang, Y. Ma, Q. Jiang, J. Liang, S. Zhou, J. Zhao, J. Liu and G. Q. M. Lu, Exceptional electrochemical HER performance with enhanced electron transfer between Ru nanoparticles and single atoms dispersed on a carbon substrate, *Angew. Chem., Int. Ed.*, 2021, **60**, 16044–16050.
54 B. Dutta, Y. Wu, J. Chen, J. Wang, J. He, M. Sharafeldin, P. Kerns, L. Jin, A. M. Dongare, J. Rusling and S. L. Suib, Partial surface selenization of cobalt sulfide microspheres for enhancing the hydrogen evolution reaction, *ACS Catal.*, 2018, **9**, 456–465.
55 M. Lao, K. Rui, G. Zhao, P. Cui, X. Zheng, S. X. Dou and W. Sun, Platinum/nickel bicarbonate heterostructures towards accelerated hydrogen evolution under alkaline conditions, *Angew. Chem., Int. Ed.*, 2019, **58**, 5432–5437.
56 Y. Yan, R. Zhang, Y. Yu, Z. Sun, R. Che, B. Wei, A. P. LaGrow, Z. Wang and W. Zhou, Interfacial optimization of PtNi octahedrons@Ti_3C_2 MXene with enhanced alkaline hydrogen evolution activity and stability, *Appl. Catal., B*, 2021, **291**, 120100.
57 F. Zhou, Y. Zhou, G.-G. Liu, C.-T. Wang and J. Wang, Recent advances in nanostructured electrocatalysts for hydrogen evolution reaction, *Rare Met.*, 2021, **40**, 3375–3405.
58 J. Wang, Z. Wei, S. Mao, H. Li and Y. Wang, Highly uniform Ru nanoparticles over N-doped carbon: pH and temperature-universal hydrogen release from water reduction, *Energy Environ. Sci.*, 2018, **11**, 800–806.
59 S. Fletcher, Tafel slopes from first principles, *J. Solid State Electrochem.*, 2008, **13**, 537–549.
60 P. Yu, F. Wang, T. A. Shifa, X. Zhan, X. Lou, F. Xia and J. He, Earth abundant materials beyond transition metal dichalcogenides: a focus on electrocatalyzing hydrogen evolution reaction, *Nano Energy*, 2019, **58**, 244–276.
61 D. Voiry, M. Chhowalla, Y. Gogotsi, N. A. Kotov, Y. Li, R. M. Penner, R. E. Schaak and P. S. Weiss, Best practices for reporting electrocatalytic performance of nanomaterials, *ACS Nano*, 2018, **12**, 9635–9638.
62 L. Wu and J. P. Hofmann, Comparing the intrinsic her activity of transition metal dichalcogenides: pitfalls and suggestions, *ACS Energy Lett.*, 2021, **6**, 2619–2625.
63 J. Wordsworth, T. M. Benedetti, S. V. Somerville, W. Schuhmann, R. D. Tilley and J. J. Gooding, The influence of nanoconfinement on electrocatalysis, *Angew. Chem., Int. Ed.*, 2022, **61**, 202200755.
64 D. Voiry, H. Yamaguchi, J. Li, R. Silva, D. C. Alves, T. Fujita, M. Chen, T. Asefa, V. B. Shenoy, G. Eda and M. Chhowalla, Enhanced catalytic activity in strained chemically exfoliated WS_2 nanosheets for hydrogen evolution, *Nat. Mater.*, 2013, **12**, 850–855.
65 H. Li, C. Tsai, A. L. Koh, L. Cai, A. W. Contryman, A. H. Fragapane, J. Zhao, H. S. Han, H. C. Manoharan, F. Abild-Pedersen, J. K. Nørskov and X. Zheng, Activating and optimizing MoS_2 basal planes for hydrogen evolution through the formation of strained sulphur vacancies, *Nat. Mater.*, 2015, **15**, 48–53.
66 J. Kibsgaard, T. F. Jaramillo and F. Besenbacher, Building an appropriate active-site motif into a hydrogen-evolution catalyst with thiomolybdate $[Mo_3S_{13}]^{2-}$ clusters, *Nat. Chem.*, 2014, **6**, 248–253.
67 S. Anantharaj, P. E. Karthik and S. Noda, The significance of properly reporting turnover frequency in electrocatalysis research, *Angew. Chem., Int. Ed.*, 2021, **60**, 23051–23067.
68 Z. Chen, X. Duan, W. Wei, S. Wang and B.-J. Ni, Recent advances in transition metal-based electrocatalysts for alkaline hydrogen evolution, *J. Mater. Chem. A*, 2019, **7**, 14971–15005.
69 S. Anantharaj, S. R. Ede, K. Sakthikumar, K. Karthick, S. Mishra and S. Kundu, Recent trends and perspectives in electrochemical water splitting with an emphasis on sulfide, selenide, and phosphide catalysts of Fe, Co, and Ni: a review, *ACS Catal.*, 2016, **6**, 8069–8097.
70 S. Anantharaj, S. R. Ede, K. Karthick, S. Sam Sankar, K. Sangeetha, P. E. Karthik and S. Kundu, Precision and correctness in the evaluation of electrocatalytic water splitting: revisiting activity parameters with a critical assessment, *Energy Environ. Sci.*, 2018, **11**, 744–771.

71 Z. Y. Yu, Y. Duan, X. Y. Feng, X. Yu, M. R. Gao and S. H. Yu, Clean and affordable hydrogen fuel from alkaline water splitting: past, recent progress, and future prospects, *Adv. Mater.*, 2021, **33**, 2007100.
72 D. H. Kweon, M. S. Okyay, S. J. Kim, J. P. Jeon, H. J. Noh, N. Park, J. Mahmood and J. B. Baek, Ruthenium anchored on carbon nanotube electrocatalyst for hydrogen production with enhanced Faradaic efficiency, *Nat. Commun.*, 2020, **11**, 1278.
73 Q. He, D. Tian, H. Jiang, D. Cao, S. Wei, D. Liu, P. Song, Y. Lin and L. Song, Achieving efficient alkaline hydrogen evolution reaction over a Ni_5P_4 catalyst incorporating single-atomic Ru sites, *Adv. Mater.*, 2020, **32**, 1906972.
74 Y. Li, H. Zhang, T. Xu, Z. Lu, X. Wu, P. Wan, X. Sun and L. Jiang, Under-water superaerophobic pine-shaped Pt nanoarray electrode for ultrahigh-performance hydrogen evolution, *Adv. Funct. Mater.*, 2015, **25**, 1737–1744.
75 X. Liao, R. Lu, L. Xia, Q. Liu, H. Wang, K. Zhao, Z. Wang and Y. Zhao, Density functional theory for electrocatalysis, *Energy Environ. Mater.*, 2021, **5**, 157–185.
76 D. Tian, S. R. Denny, K. Li, H. Wang, S. Kattel and J. G. Chen, Density functional theory studies of transition metal carbides and nitrides as electrocatalysts, *Chem. Soc. Rev.*, 2021, **50**, 12338–12376.
77 T. F. Jaramillo, K. P. Jorgensen, J. Bonde, J. H. Nielsen, S. Horch and I. Chorkendorff, Identification of active edge sites for electrochemical H_2 evolution from MoS_2 nanocatalysts, *Science*, 2007, **317**, 100–102.
78 L. I. Ugwu, Y. Morgan and H. Ibrahim, Application of density functional theory and machine learning in heterogenous-based catalytic reactions for hydrogen production, *Int. J. Hydrogen Energy*, 2022, **47**, 2245–2267.
79 Y. Cui, X. Guo, J. Zhang, X. A. Li, X. Zhu and W. Huang, Di-defects synergy boost electrocatalysis hydrogen evolution over two-dimensional heterojunctions, *Nano Res.*, 2021, **15**, 677–684.
80 F. Li, G. F. Han, H. J. Noh, J. P. Jeon, I. Ahmad, S. Chen, C. Yang, Y. Bu, Z. Fu, Y. Lu and J. B. Baek, Balancing hydrogen adsorption/desorption by orbital modulation for efficient hydrogen evolution catalysis, *Nat. Commun.*, 2019, **10**, 4060.
81 J. Greeley, T. F. Jaramillo, J. Bonde, I. B. Chorkendorff and J. K. Norskov, Computational high-throughput screening of electrocatalytic materials for hydrogen evolution, *Nat. Mater.*, 2006, **5**, 909–913.
82 E. Skúlason, V. Tripkovic, M. E. Björketun, S. Gudmundsdóttir, G. Karlberg, J. Rossmeisl, T. Bligaard, H. Jónsson and J. K. Nørskov, Modeling the electrochemical hydrogen oxidation and evolution reactions on the basis of density functional theory calculations, *J. Phys. Chem. C*, 2010, **114**, 18182–18197.
83 J. Liu, C. Tang, Z. Ke, R. Chen, H. Wang, W. Li, C. Jiang, D. He, G. Wang and X. Xiao, Optimizing hydrogen adsorption by d-d orbital modulation for efficient hydrogen evolution catalysis, *Adv. Energy Mater.*, 2022, **12**, 2103301.
84 S. Shen, Z. Lin, K. Song, Z. Wang, L. Huang, L. Yan, F. Meng, Q. Zhang, L. Gu and W. Zhong, Reversed active sites boost the intrinsic activity of graphene-like cobalt selenide for hydrogen evolution, *Angew. Chem., Int. Ed.*, 2021, **60**, 12360–12365.
85 C. Cai, K. Liu, Y. Zhu, P. Li, Q. Wang, B. Liu, S. Chen, H. Li, L. Zhu, H. Li, J. Fu, Y. Chen, E. Pensa, J. Hu, Y. R. Lu, T. S. Chan, E. Cortes and M. Liu, Optimizing hydrogen binding on Ru sites with RuCo alloy nanosheets for efficient alkaline hydrogen evolution, *Angew. Chem., Int. Ed.*, 2022, **61**, 202113664.
86 J. Cui, X. Liu, Y. Wang, D. Song, Y. Ren and X. Shen, Hydrogen evolution reaction on transition metal nanoparticles from first-principles, *Appl. Surf. Sci.*, 2021, **570**, 151211.
87 T. Bligaard and J. K. Nørskov, Ligand effects in heterogeneous catalysis and electrochemistry, *Electrochim. Acta*, 2007, **52**, 5512–5516.
88 B. Hammer, Y. Morikawa and J. K. Norskov, CO chemisorption at metal surfaces and overlayers, *Phys. Rev. Lett.*, 1996, **76**, 2141–2144.
89 S. Joo, K. Kim, O. Kwon, J. Oh, H. J. Kim, L. Zhang, J. Zhou, J. Q. Wang, H. Y. Jeong, J. W. Han and G. Kim, Enhancing thermocatalytic activities by upshifting the d-band center of exsolved Co-Ni-Fe ternary alloy nanoparticles for the dry reforming of methane, *Angew. Chem., Int. Ed.*, 2021, **60**, 15912–15919.
90 J. L. Lansford, S. J. Kurdziel and D. G. Vlachos, Scaling of transition state vibrational frequencies and application of d-band theory to the Brønsted-evans-polanyi relationship on surfaces, *J. Phys. Chem. C*, 2021, **125**, 7119–7129.
91 J. K. Nørskov, T. Bligaard, J. Rossmeisl and C. H. Christensen, Towards the computational design of solid catalysts, *Nat. Chem.*, 2009, **1**, 37–46.
92 Y. Xu, A. V. Ruban and M. Mavrikakis, Adsorption and dissociation of O_2 on Pt-Co and Pt-Fe alloys, *J. Am. Chem. Soc.*, 2004, **126**, 4717–4725.
93 J. K. Norskov, F. Abild-Pedersen, F. Studt and T. Bligaard, Density functional theory in surface chemistry and catalysis, *Proc. Natl. Acad. Sci. U. S. A.*, 2011, **108**, 937–943.
94 B. Hammer and J. K. Norskov, Why gold is the noblest of all the metals, *Nature*, 1995, **376**, 238–240.
95 T. Meng, Y. Chen, Z. Xing and X. Yang, Tuning phase structure of nickel-ruthenium alloys via MOFs in situ hydrolysis toward enhanced hydrogen evolution performance in alkaline, *Small Methods*, 2022, **6**, 2101188.
96 J. Yu, J. Li, C.-Y. Xu, Q. Li, Q. Liu, J. Liu, R. Chen, J. Zhu and J. Wang, Modulating the d-band centers by coordination environment regulation of single-atom Ni on porous carbon fibers for overall water splitting, *Nano Energy*, 2022, **98**, 107266.
97 H. Xin, A. Vojvodic, J. Voss, J. K. Nørskov and F. Abild-Pedersen, Effects of d-band shape on the surface reactivity of transition-metal alloys, *Phys. Rev. B: Condens. Matter Mater. Phys.*, 2014, **89**, 115114.
98 E. Santos and W. Schmickler, d-Band catalysis in electrochemistry, *Chem. Phys. Chem.*, 2006, **7**, 2282–2285.
99 T. K. Sham, A. Bzowski, M. Kuhn and C. C. Tyson, Observations on the d-bandwidth of Au-Ag and Au-Cu alloys, *Solid State Commun.*, 1991, **80**, 29–32.

100 F. N. I. Sari and J. M. Ting, MoS_2/MoO_x-nanostructure-decorated activated carbon cloth for enhanced supercapacitor performance, *ChemSusChem*, 2018, **11**, 897–906.
101 D. Kong, H. Wang, Z. Lu and Y. Cui, $CoSe_2$ nanoparticles grown on carbon fiber paper: an efficient and stable electrocatalyst for hydrogen evolution reaction, *J. Am. Chem. Soc.*, 2014, **136**, 4897–4900.
102 T. Y. Ma, J. Ran, S. Dai, M. Jaroniec and S. Z. Qiao, Phosphorus-doped graphitic carbon nitrides grown in situ on carbon-fiber paper: flexible and reversible oxygen electrodes, *Angew. Chem., Int. Ed.*, 2015, **54**, 4646–4650.
103 S. Chen, J. Zhang, Z. Wang, L. Nie, X. Hu, Y. Yu and W. Liu, Electrocatalytic $NiCo_2O_4$ nanofiber arrays on carbon cloth for flexible and high-loading lithium-sulfur batteries, *Nano Lett.*, 2021, **21**, 5285–5292.
104 Y. Ma, Z. Wei, Y. Wang, Y. Ding, L. Jiang, X. Fu, Y. Zhang, J. Sun, W. Zhu and J. Wang, Surface oxygen functionalization of carbon cloth toward enhanced electrochemical dopamine sensing, *ACS Sustainable Chem. Eng.*, 2021, **9**, 16063–16072.
105 X. Ma, J. Xia, X. Wu, Z. Pan and P. K. Shen, Remarkable enhancement in the electrochemical activity of maricite $NaFePO_4$ on high-surface-area carbon cloth for sodium-ion batteries, *Carbon*, 2019, **146**, 78–87.
106 H. Sun, F. Niu, P. Yuan, X. He, J. Sun, Z. Liu, Q. Li and Z. Lei, Lithium storage in carbon cloth-supported KNb_3O_8 nanorods toward a high-performance lithium-ion capacitor, *Small Str.*, 2021, **2**, 2100029.
107 D. Wang, N. He, L. Xiao, F. Dong, W. Chen, Y. Zhou, C. Chen and S. Wang, Coupling electrocatalytic nitric oxide oxidation over carbon cloth with hydrogen evolution reaction for nitrate synthesis, *Angew. Chem., Int. Ed.*, 2021, **60**, 24605–24611.
108 X. Liu, W. Xu, D. Zheng, Z. Li, Y. Zeng and X. Lu, Carbon cloth as an advanced electrode material for supercapacitors: progress and challenges, *J. Mater. Chem. A*, 2020, **8**, 17938–17950.
109 Z. Tabti, R. Ruiz-Rosas, C. Quijada, D. Cazorla-Amoros and E. Morallon, Tailoring the surface chemistry of activated carbon cloth by electrochemical methods, *ACS Appl. Mater. Interfaces*, 2014, **6**, 11682–111691.
110 C. Huang, X. Zhao, Y. Xu, Y. Zhang, Y. Yang, A. Hu, Q. Tang, X. Song, C. Jiang and X. Chen, Sewable and cuttable flexible zinc-ion hybrid supercapacitor using a polydopamine/carbon cloth-based cathode, *ACS Sustainable Chem. Eng.*, 2020, **8**, 16028–16036.
111 S.-H. Chang, J.-S. Liou, J.-L. Liu, Y.-F. Chiu, C.-H. Xu, B.-Y. Chen and J.-Z. Chen, Feasibility study of surface-modified carbon cloth electrodes using atmospheric pressure plasma jets for microbial fuel cells, *J. Power Sources*, 2016, **336**, 99–106.
112 M. Zhao, L. Yang, Z. Cai, H. Guo and Z. Zhao, Design of binder-free hierarchical Mo-Fe-Ni phosphides nanowires array anchored on carbon cloth with high electrocatalytic capability toward hydrogen evolution reaction, *J. Alloys Compd.*, 2022, **891**, 162064.
113 L. Wen, Y. Sun, C. Zhang, J. Yu, X. Li, X. Lyu, W. Cai and Y. Li, Cu-doped CoP nanorod arrays: efficient and durable hydrogen evolution reaction electrocatalysts at all pH values, *ACS Appl. Energy Mater.*, 2018, **1**, 3835–3842.
114 X. Zheng, Y. Chen, X. Bao, S. Mao, R. Fan and Y. Wang, In situ formed bimetallic carbide Ni_6Mo_6C nanodots and $NiMoO_x$ nanosheet array hybrids anchored on carbon cloth: efficient and flexible self-supported catalysts for hydrogen evolution, *ACS Catal.*, 2020, **10**, 11634–11642.
115 B. Liu, H. Li, B. Cao, J. Jiang, R. Gao and J. Zhang, Few layered N, P dual-doped carbon-encapsulated ultrafine MoP nanocrystal/MoP cluster hybrids on carbon cloth: an ultrahigh active and durable 3D self-supported integrated electrode for hydrogen evolution reaction in a wide pH range, *Adv. Funct. Mater.*, 2018, **28**, 1801527.
116 W. Liu, P. Geng, S. Li, R. Zhu, W. Liu, H. Lu, S. Chandrasekaran, Y. Pang, D. Fan and Y. Liu, Self-supported three-dimensional WP_2 (WP) nanosheet arrays for efficient electrocatalytic hydrogen evolution, *Int. J. Hydrogen Energ.*, 2020, **45**, 28576–28585.
117 J.-T. Ren, L. Chen, C.-C. Weng and Z.-Y. Yuan, Self-supported MoP nanocrystals embedded in N,P-codoped carbon nanofibers via a polymer-confinement route for electrocatalytic hydrogen production, *Mater. Chem. Front.*, 2019, **3**, 1872–1881.
118 S. Yu, Y. C. Rao, H. H. Wu and X. M. Duan, C_2N: an excellent catalyst for the hydrogen evolution reaction, *Phys. Chem. Chem. Phys.*, 2018, **20**, 27970–27974.
119 N. Ran, B. Sun, W. Qiu, E. Song, T. Chen and J. Liu, Identifying metallic transition-metal dichalcogenides for hydrogen evolution through multilevel high-throughput calculations and machine learning, *J. Phys. Chem. Lett.*, 2021, **12**, 2102–2111.
120 Q. Fu, J. Han, X. Wang, P. Xu, T. Yao, J. Zhong, W. Zhong, S. Liu, T. Gao, Z. Zhang, L. Xu and B. Song, 2D transition metal dichalcogenides: design, modulation, and challenges in electrocatalysis, *Adv. Mater.*, 2021, **33**, 1907818.
121 L. Tang, R. Xu, J. Tan, Y. Luo, J. Zou, Z. Zhang, R. Zhang, Y. Zhao, J. Lin, X. Zou, B. Liu and H. M. Cheng, Modulating electronic structure of monolayer transition metal dichalcogenides by substitutional Nb-doping, *Adv. Funct. Mater.*, 2020, **31**, 2006941.
122 Z. Liu, K. Nie, X. Qu, X. Li, B. Li, Y. Yuan, S. Chong, P. Liu, Y. Li, Z. Yin and W. Huang, General bottom-up colloidal synthesis of nano-monolayer transition-metal dichalcogenides with high 1T'-phase purity, *J. Am. Chem. Soc.*, 2022, **144**, 4863–4873.
123 S. Niu, J. Cai and G. Wang, Two-dimensional MoS_2 for hydrogen evolution reaction catalysis: the electronic structure regulation, *Nano Res.*, 2020, **14**, 1985–2002.
124 Y. Cao, Roadmap and direction toward high-performance MoS_2 hydrogen evolution catalysts, *ACS Nano*, 2021, **15**, 11014–11039.
125 B. Pattengale, Y. Huang, X. Yan, S. Yang, S. Younan, W. Hu, Z. Li, S. Lee, X. Pan, J. Gu and J. Huang, Dynamic evolution and reversibility of single-atom Ni(II) active site in 1T-MoS_2

electrocatalysts for hydrogen evolution, *Nat. Commun.*, 2020, **11**, 4114.

126 X. Liu, B. Li, X. Li, A. R. Harutyunyan, J. Hone and D. V. Esposito, The critical role of electrolyte gating on the hydrogen evolution performance of monolayer MoS_2, *Nano Lett.*, 2019, **19**, 8118–8124.

127 W. Chen, J. Gu, Y. Du, F. Song, F. Bu, J. Li, Y. Yuan, R. Luo, Q. Liu and D. Zhang, Achieving rich and active alkaline hydrogen evolution heterostructures via interface engineering on 2D 1T-MoS_2 quantum sheets, *Adv. Funct. Mater.*, 2020, **30**, 2000551.

128 S. Chandrasekaran, L. Yao, L. Deng, C. Bowen, Y. Zhang, S. Chen, Z. Lin, F. Peng and P. Zhang, Recent advances in metal sulfides: from controlled fabrication to electrocatalytic, photocatalytic and photoelectrochemical water splitting and beyond, *Chem. Soc. Rev.*, 2019, **48**, 4178–4280.

129 Y. Xiao, J. Yao, T. Zhang, X. Ma, D. Xu and H. Gao, Three-dimensional cross-linked Co-MoS_2 catalyst on carbon cloth for efficient hydrogen evolution reaction, *Dalton Trans.*, 2022, **51**, 638–644.

130 Q. Q. Pang, Z. L. Niu, S. S. Yi, S. Zhang, Z. Y. Liu and X. Z. Yue, Hydrogen-etched bifunctional sulfur-defect-rich ReS_2/CC electrocatalyst for highly efficient HER and OER, *Small*, 2020, **16**, 2003007.

131 J. Sun, X. Zhang, M. Jin, Q. Xiong, G. Wang, H. Zhang and H. Zhao, Robust enhanced hydrogen production at acidic conditions over molybdenum oxides-stabilized ultrafine palladium electrocatalysts, *Nano Res.*, 2020, **14**, 268–274.

132 Z. Hu, L. Zhang, J. Huang, Z. Feng, Q. Xiong, Z. Ye, Z. Chen, X. Li and Z. Yu, Self-supported nickel-doped molybdenum carbide nanoflower clusters on carbon fiber paper for an efficient hydrogen evolution reaction, *Nanoscale*, 2021, **13**, 8264–8274.

133 Y.-N. Zhou, F.-L. Wang, S.-Y. Dou, Z.-N. Shi, B. Dong, W.-L. Yu, H.-Y. Zhao, F.-G. Wang, J.-F. Yu and Y.-M. Chai, Motivating high-valence Nb doping by fast molten salt method for NiFe hydroxides toward efficient oxygen evolution reaction, *Chem. Eng. J.*, 2022, **427**, 131643.

134 D. Liu, L. Yang, J. Wu and C. Li, Gaseous elemental mercury capture by magnetic FeS_2 nanorods synthesized via a molten salt method, *ACS Appl. Nano Mater.*, 2022, **5**, 2626–2635.

135 Z. Xie, X. Tang, J. Shi, Y. Wang, G. Yuan and J.-M. Liu, Excellent piezo-photocatalytic performance of $Bi_4Ti_3O_{12}$ nanoplates synthesized by molten-salt method, *Nano Energy*, 2022, **98**, 107247.

136 F. Lv, Y. Zhang, M. Wu and Y. Gu, A molten-salt method to synthesize ultrahigh-nickel single-crystalline LiNi0.92-Co0.06Ni0.02O2 with superior electrochemical performance as cathode material for lithium-ion batteries, *Small*, 2022, **18**, 2201946.

137 Z. Zhou, X. Li, T. Hu, B. Xue, H. Chen, L. Ma, R. Liang and C. Tan, Molybdenum-based nanomaterials for photothermal cancer therapy, *Adv. NanoBiomed Res.*, 2022, **2**, 2200065.

138 H. Huang, Y. Zhao, Y. Bai, F. Li, Y. Zhang and Y. Chen, Conductive metal-organic frameworks with extra metallic sites as an efficient electrocatalyst for the hydrogen evolution reaction, *Adv. Sci.*, 2020, **7**, 2000012.

139 H. F. Wang, L. Chen, H. Pang, S. Kaskel and Q. Xu, MOF-derived electrocatalysts for oxygen reduction, oxygen evolution and hydrogen evolution reactions, *Chem. Soc. Rev.*, 2020, **49**, 1414–1448.

140 H. Furukawa, K. E. Cordova, M. O'Keeffe and O. M. Yaghi, The chemistry and applications of metal-organic frameworks, *Science*, 2013, **341**, 1230444.

141 Y. P. Wu, W. Zhou, J. Zhao, W. W. Dong, Y. Q. Lan, D. S. Li, C. Sun and X. Bu, Surfactant-assisted phase-selective synthesis of new cobalt MOFs and their efficient electrocatalytic hydrogen evolution reaction, *Angew. Chem., Int. Ed.*, 2017, **56**, 13001–13005.

142 X. Deng, S.-L. Zheng, Y.-H. Zhong, J. Hu, L.-H. Chung and J. He, Conductive MOFs based on thiol-functionalized linkers: challenges, opportunities, and recent advances, *Coord. Chem. Rev.*, 2022, **450**, 214235.

143 A. Radwan, H. Jin, D. He and S. Mu, Design engineering, synthesis protocols, and energy applications of MOF-derived electrocatalysts, *Nanomicro. Lett.*, 2021, **13**, 132.

144 J. H. Qin, W. J. Qin, Z. Xiao, J. K. Yang, H. R. Wang, X. G. Yang, D. S. Li and L. F. Ma, Efficient energy-transfer-induced high photoelectric conversion in a dye-encapsulated ionic pyrene-based metal-organic framework, *Inorg. Chem.*, 2021, **60**, 18593–18597.

145 H. Sun, C. Tian, Y. Li, J. Wu, Q. Wang, Z. Yan, C. P. Li, F. Cheng and M. Du, Coupling NiCo alloy and CeO_2 to enhance electrocatalytic hydrogen evolution in alkaline solution, *Adv. Sustain. Syst.*, 2020, **4**, 2000122.

146 M. Thukkaram, P. Cools, A. Nikiforov, P. Rigole, T. Coenye, P. Van Der Voort, G. Du Laing, C. Vercruysse, H. Declercq, R. Morent, L. De Wilde, P. De Baets, K. Verbeken and N. De Geyter, Antibacterial activity of a porous silver doped TiO_2 coating on titanium substrates synthesized by plasma electrolytic oxidation, *App. Surf. Sci.*, 2020, **500**, 144235.

147 Y. Xiong, X. Liu, T. C. Zhang and S. Yuan, MnO_2/TiO_2 nanotube array-coated titanium substrates as anodes for electrocatalytic oxidation of As(III) in aqueous solution, *ACS Appl. Nano Mater.*, 2021, **4**, 7404–7415.

148 M. Reggente, P. Masson, C. Dollinger, H. Palkowski, S. Zafeiratos, L. Jacomine, D. Passeri, M. Rossi, N. E. Vrana, G. Pourroy and A. Carrado, Novel alkali activation of titanium substrates to grow thick and covalently bound pmma layers, *ACS Appl. Mater. Interfaces*, 2018, **10**, 5967–5977.

149 J. Jeon, J. Kim, J. Ahn and D. R. Kim, Direct growth of hierarchical nanoneedle arrays with branched nanotubes from titanium foil with excellent anti-corrosion and superhydrophilicity, *Chem. Eng. J.*, 2019, **372**, 616–623.

150 N. Jiménez-Arévalo, F. Leardini, I. J. Ferrer, J. R. Ares, C. Sánchez, M. M. Saad Abdelnabi, M. G. Betti and C. Mariani, Ultrathin transparent B–C–N layers grown on titanium substrates with excellent electrocatalytic activity for the oxygen evolution reaction, *ACS Appl. Energy Mater.*, 2020, **3**, 1922–1932.

151 R. Li, B. Hu, T. Yu, Z. Shao, Y. Wang and S. Song, New TiO_2-based oxide for catalyzing alkaline hydrogen evolution reaction with noble metal-like performance, *Small Methods*, 2021, **5**, 2100246.

152 Y. Chen, Y. Wang, L. Zheng, Y. Chang, S. Xu, Y. Wu, W. Zhou, Y. Lu, J. Wang and H. Li, Platinum nanoclusters by atomic layer deposition on three-dimensional TiO_2 nanotube array for efficient hydrogen evolution, *Mater. Today Energy*, 2022, **27**, 101042.

153 T. Wu, M. M. Melander and K. Honkala, Coadsorption of NRR and HER intermediates determines the performance of Ru-N_4 toward electrocatalytic N_2 reduction, *ACS Catal.*, 2022, **12**, 2505–2512.

154 Z. Liu, Z. Li, J. Li, J. Xiong, S. Zhou, J. Liang, W. Cai, C. Wang, Z. Yang and H. Cheng, Engineering of Ru/Ru_2P interfaces superior to Pt active sites for catalysis of the alkaline hydrogen evolution reaction, *J. Mater. Chem. A*, 2019, **7**, 5621–5625.

155 W. Li, Y. Zhao, Y. Liu, M. Sun, G. I. N. Waterhouse, B. Huang, K. Zhang, T. Zhang and S. Lu, Exploiting Ru-induced lattice strain in CoRu nanoalloys for robust bifunctional hydrogen production, *Angew. Chem., Int. Ed.*, 2021, **60**, 3290–3298.

156 D. Chen, Z. Pu, R. Lu, P. Ji, P. Wang, J. Zhu, C. Lin, H. W. Li, X. Zhou, Z. Hu, F. Xia, J. Wu and S. Mu, Ultralow Ru loading transition metal phosphides as high-efficient bifunctional electrocatalyst for a solar-to-hydrogen generation system, *Adv. Energy Mater.*, 2020, **10**, 2000814.

157 K. Wang, Q. Chen, Y. Hu, W. Wei, S. Wang, Q. Shen and P. Qu, Crystalline Ru0.33Se nanoparticles-decorated TiO2 nanotube arrays for enhanced hydrogen evolution reaction, *Small*, 2018, **14**, 1802132.

158 W. Li, H. Zhang, M. Hong, L. Zhang, X. Feng, M. Shi, W. Hu and S. Mu, Defective RuO_2/TiO_2 nano-heterostructure advances hydrogen production by electrochemical water splitting, *Chem. Eng. J.*, 2022, **431**, 134072.

159 C. Xu, S. Peng, C. Tan, H. Ang, H. Tan, H. Zhang and Q. Yan, Ultrathin S-doped $MoSe_2$ nanosheets for efficient hydrogen evolution, *J. Mater. Chem. A*, 2014, **2**, 5597–5601.

160 D. Gao, B. Xia, Y. Wang, W. Xiao, P. Xi, D. Xue and J. Ding, Dual-native vacancy activated basal plane and conductivity of $MoSe_2$ with high-efficiency hydrogen evolution reaction, *Small*, 2018, **14**, 1704150.

161 D. Xiao, D.-L. Bao, X. Liang, Y. Wang, J. Shen, C. Cheng and P. K. Chu, Experimental and theoretical investigation of the control and balance of active sites on oxygen plasma-functionalized $MoSe_2$ nanosheets for efficient hydrogen evolution reaction, *Appl. Catal., B*, 2021, **288**, 119983.

162 L. Zhang, Y. Lei, D. Zhou, C. Xiong, Z. Jiang, X. Li, H. Shang, Y. Zhao, W. Chen and B. Zhang, Interfacial engineering of 3D hollow $CoSe_2$@ultrathin $MoSe_2$ core@shell heterostructure for efficient pH-universal hydrogen evolution reaction, *Nano Res.*, 2021, **15**, 2895–2904.

163 B. Xia, T. Wang, X. Jiang, T. Zhang, J. Li, W. Xiao, P. Xi, D. Gao, D. Xue and J. Ding, Ar^{2+} beam irradiation-induced multivancancies in $MoSe_2$ nanosheet for enhanced electrochemical hydrogen evolution, *ACS Energy Lett.*, 2018, **3**, 2167–2172.

164 J. Zhang, Y. Chen, M. Liu, K. Du, Y. Zhou, Y. Li, Z. Wang and J. Zhang, 1T@2H-$MoSe_2$ nanosheets directly arrayed on Ti plate: an efficient electrocatalytic electrode for hydrogen evolution reaction, *Nano Res.*, 2018, **11**, 4587–4598.

165 X. Zhang, S. Wang, C. Wu, H. Li, Y. Cao, S. Li and H. Xia, Synthesis of S-doped AuPbPt alloy nanowire-networks as superior catalysts towards the ORR and HER, *J. Mater. Chem. A*, 2020, **8**, 23906–23918.

166 H. Zhao, D. Zhang, Y. Yuan, X. Wu, S. Li, Z. Li, J. Lai and L. Wang, Rapid and large-scale synthesis of ultra-small immiscible alloy supported catalysts, *Appl. Catal., B*, 2022, **304**, 120916.

167 S. Zhang, S. E. Saji, Z. Yin, H. Zhang, Y. Du and C. H. Yan, Rare-earth incorporated alloy catalysts: synthesis, properties, and applications, *Adv. Mater.*, 2021, **33**, 2005988.

168 Q. Kang, D. Lai, W. Tang, Q. Lu and F. Gao, Intrinsic activity modulation and structural design of NiFe alloy catalysts for an efficient oxygen evolution reaction, *Chem. Sci.*, 2021, **12**, 3818–3835.

169 Z. J. Wang, M. X. Li, J. H. Yu, X. B. Ge, Y. H. Liu and W. H. Wang, Low-iridium-content IrNiTa metallic glass films as intrinsically active catalysts for hydrogen evolution reaction, *Adv. Mater.*, 2020, **32**, 1906384.

170 A. Nairan, P. Zou, C. Liang, J. Liu, D. Wu, P. Liu and C. Yang, NiMo solid solution nanowire array electrodes for highly efficient hydrogen evolution reaction, *Adv. Funct. Mater.*, 2019, **29**, 1903747.

171 X. Zhao, Z. Zhang, X. Cao, J. Hu, X. Wu, A. Y. R. Ng, G.-P. Lu and Z. Chen, Elucidating the sources of activity and stability of FeP electrocatalyst for hydrogen evolution reactions in acidic and alkaline media, *Appl. Catal., B*, 2020, **260**, 118156.

172 A. Karmakar, K. Karthick, S. S. Sankar, S. Kumaravel, R. Madhu, K. Bera, H. N. Dhandapani, S. Nagappan, P. Murugan and S. Kundu, Stabilization of ruthenium nanoparticles over NiV-LDH surface for enhanced electrochemical water splitting: an oxygen vacancy approach, *J. Mater. Chem. A*, 2022, **10**, 3618–3632.

173 Q. Li, F. Huang, S. Li, H. Zhang and X. Y. Yu, Oxygen vacancy engineering synergistic with surface hydrophilicity modification of hollow Ru doped CoNi-LDH nanotube arrays for boosting hydrogen evolution, *Small*, 2022, **18**, 2104323.

174 C. Li, H. Jang, M. G. Kim, L. Hou, X. Liu and J. Cho, Ru-incorporated oxygen-vacancy-enriched MoO_2 electrocatalysts for hydrogen evolution reaction, *Appl. Catal., B*, 2022, **307**, 121204.

175 J. Zhang, E. Wang, S. Cui, S. Yang, X. Zou and Y. Gong, Single-atom Pt anchored on oxygen vacancy of monolayer $Ti_3C_2T_x$ for superior hydrogen evolution, *Nano Lett.*, 2022, **22**, 1398–1405.

176 Y. Qiu, S. Liu, C. Wei, J. Fan, H. Yao, L. Dai, G. Wang, H. Li, B. Su and X. Guo, Synergistic effect between platinum

single atoms and oxygen vacancy in MoO_2 boosting pH-universal hydrogen evolution reaction at large current density, *Chem. Eng. J.*, 2022, **427**, 131309.

177 D. Liu, C. Zhang, Y. Yu, Y. Shi, Y. Yu, Z. Niu and B. Zhang, Hydrogen evolution activity enhancement by tuning the oxygen vacancies in self-supported mesoporous spinel oxide nanowire arrays, *Nano Res.*, 2017, **11**, 603–613.

178 X. Han, X. Wu, Y. Deng, J. Liu, J. Lu, C. Zhong and W. Hu, Ultrafine Pt nanoparticle-decorated pyrite-type CoS_2 nanosheet arrays coated on carbon cloth as a bifunctional electrode for overall water splitting, *Adv. Energy Mater.*, 2018, **8**, 1800935.

179 W. Liu, E. Hu, H. Jiang, Y. Xiang, Z. Weng, M. Li, Q. Fan, X. Yu, E. I. Altman and H. Wang, A highly active and stable hydrogen evolution catalyst based on pyrite-structured cobalt phosphosulfide, *Nat. Commun.*, 2016, **7**, 10771.

180 J. Jiang, S. Bai, M. Yang, J. Zou, N. Li, J. Peng, H. Wang, K. Xiang, S. Liu and T. Zhai, Strategic design and fabrication of MXenes-Ti_3CNCl_2@CoS_2 core–shell nanostructure for high-efficiency hydrogen evolution, *Nano Res.*, 2022, **15**, 5977–5986.

181 J. Li, Z. Xia, Q. Xue, M. Zhang, S. Zhang, H. Xiao, Y. Ma and Y. Qu, Insights into the interfacial Lewis acid-base pairs in CeO_2-loaded CoS_2 electrocatalysts for alkaline hydrogen evolution, *Small*, 2021, **17**, 2103018.

182 C. Fu, L. Luo, L. Yang, S. Shen, G. Wei, J. Yin and J. Zhang, Theoretical exploration of the thermodynamic process competition between NRR and HER on transition-metal-doped CoP (101) facets, *J. Phys. Chem. C*, 2021, **125**, 17051–17057.

183 Z. Li, H. Feng, M. Song, C. He, W. Zhuang and L. Tian, Advances in CoP electrocatalysts for water splitting, *Mater. Today Energy*, 2021, **20**, 100698.

184 L. Zhang, J. Zhang, J. Fang, X. Y. Wang, L. Yin, W. Zhu and Z. Zhuang, Cr-doped CoP nanorod arrays as high-performance hydrogen evolution reaction catalysts at high current density, *Small*, 2021, **17**, 2100832.

185 S. Geng, F. Tian, M. Li, X. Guo, Y. Yu, W. Yang and Y. Hou, Hole-rich CoP nanosheets with an optimized d-band center for enhancing pH-universal hydrogen evolution electrocatalysis, *J. Mater. Chem. A*, 2021, **9**, 8561–8567.

186 G. Liu, M. Wang, Y. Xu, X. Wang, X. Li, J. Liu, X. Cui and L. Jiang, Porous CoP/Co_2P heterostructure for efficient hydrogen evolution and application in magnesium/seawater battery, *J. Power Sources*, 2021, **486**, 229351.

187 Y. Li, B. Zhang, W. Wang, X. Shi, J. Zhang, R. Wang, B. He, Q. Wang, J. Jiang, Y. Gong and H. Wang, Selective-etching of MOF toward hierarchical porous Mo-doped CoP/N-doped carbon nanosheet arrays for efficient hydrogen evolution at all pH values, *Chem. Eng. J.*, 2021, **405**, 126981.

188 B. You, N. Jiang, M. Sheng, M. W. Bhushan and Y. Sun, Hierarchically porous urchin-like Ni_2P superstructures supported on nickel foam as efficient bifunctional electrocatalysts for overall water splitting, *ACS Catal.*, 2015, **6**, 714–721.

189 Y. Wang, B. Zhang, W. Pan, H. Ma and J. Zhang, 3D porous nickel-cobalt nitrides supported on nickel foam as efficient electrocatalysts for overall water splitting, *ChemSusChem*, 2017, **10**, 4170–4177.

190 B. Deng, L. Zhou, Z. Jiang and Z.-J. Jiang, High catalytic performance of nickel foam supported Co_2P-Ni_2P for overall water splitting and its structural evolutions during hydrogen/oxygen evolution reactions in alkaline solutions, *J. Catal.*, 2019, **373**, 81–92.

191 H. Xu, B. Fei, G. Cai, Y. Ha, J. Liu, H. Jia, J. Zhang, M. Liu and R. Wu, Boronization-induced ultrathin 2D nanosheets with abundant crystalline-amorphous phase boundary supported on nickel foam toward efficient water splitting, *Adv. Energy Mater.*, 2019, **10**, 1902714.

192 J. Wang, P. He, Y. Shen, L. Dai, Z. Li, Y. Wu and C. An, FeNi nanoparticles on $Mo_2TiC_2T_x$ MXene@nickel foam as robust electrocatalysts for overall water splitting, *Nano Res.*, 2021, **14**, 3474–3481.

193 J. Li, Q. Zhang, J. Zhang, N. Wu, G. Liu, H. Chen, C. Yuan and X. Liu, Optimizing electronic structure of porous Ni/MoO_2 heterostructure to boost alkaline hydrogen evolution reaction, *J. Colloid Interface Sci.*, 2022, **627**, 862–871.

194 M. T. Chen, R. L. Zhang, J. J. Feng, L. P. Mei, Y. Jiao, L. Zhang and A. J. Wang, A facile one-pot room-temperature growth of self-supported ultrathin rhodium-iridium nanosheets as high-efficiency electrocatalysts for hydrogen evolution reaction, *J. Colloid Interface Sci.*, 2022, **606**, 1707–1714.

195 H. Wang, J. Li, K. Li, Y. Lin, J. Chen, L. Gao, V. Nicolosi, X. Xiao and J. M. Lee, Transition metal nitrides for electrochemical energy applications, *Chem. Soc. Rev.*, 2021, **50**, 1354–1390.

196 W. Sun, C. J. Bartel, E. Arca, S. R. Bauers, B. Matthews, B. Orvananos, B. R. Chen, M. F. Toney, L. T. Schelhas, W. Tumas, J. Tate, A. Zakutayev, S. Lany, A. M. Holder and G. Ceder, A map of the inorganic ternary metal nitrides, *Nat. Mater.*, 2019, **18**, 732–739.

197 R. Jamil, R. Ali, S. Loomba, J. Xian, M. Yousaf, K. Khan, B. Shabbir, C. F. McConville, A. Mahmood and N. Mahmood, The role of nitrogen in transition-metal nitrides in electrochemical water splitting, *Chem Catal.*, 2021, **1**, 802–854.

198 S. He, Y. Chen, M. Wang, K. Liu, P. Novello, X. Li, S. Zhu and J. Liu, Metal nitride nanosheets enable highly efficient electrochemical oxidation of ammonia, *Nano Energy*, 2021, **80**, 105528.

199 T. L. L. Doan, D. C. Nguyen, S. Prabhakaran, D. H. Kim, D. T. Tran, N. H. Kim and J. H. Lee, Single-atom Co-decorated MoS_2 nanosheets assembled on metal nitride nanorod arrays as an efficient bifunctional electrocatalyst for pH-universal water splitting, *Adv. Funct. Mater.*, 2021, **31**, 2100233.

200 J. Liang, B. Zhang, H. Shen, Y. Yin, L. Liu, Y. Ma, X. Wang, C. Xiao, J. Kong and S. Ding, Self-supported nickel nitride nanosheets as highly efficient electrocatalysts for hydrogen evolution, *Appl. Surf. Sci.*, 2020, **503**, 144143.

201 J. Li, B. Li, H. Huang, S. Yan, C. Yuan, N. Wu, D. Guo and X. Liu, Polyvinylpyrrolidone gel based Pt/Ni(OH)$_2$ heterostructures with redistributing charges for enhanced alkaline hydrogen evolution reaction, *J. Mater. Chem. A*, 2021, **9**, 27061–27071.

202 A. Kong, M. Peng, M. Liu, Y. Lv, H. Zhang, Y. Gao, J. Liu, Y. Fu, W. Li and J. Zhang, Robust Pt/TiO$_2$/Ni(OH)$_2$ nanosheet arrays enable outstanding performance for high current density alkaline water electrolysis, *Appl. Catal., B*, 2022, **316**, 121654.

203 H. Zhang, H. Guo, J. Ren, X. Jin, X. Li and R. Song, Synergistic engineering of morphology and electronic structure in constructing metal-organic framework-derived Ru doped cobalt-nickel oxide heterostructure towards efficient alkaline hydrogen evolution reaction, *Chem. Eng. J.*, 2021, **426**, 131300.

204 S. Chandrasekaran, D. Ma, Y. Ge, L. Deng, C. Bowen, J. Roscow, Y. Zhang, Z. Lin, R. D. K. Misra, J. Li, P. Zhang and H. Zhang, Electronic structure engineering on two-dimensional (2D) electrocatalytic materials for oxygen reduction, oxygen evolution, and hydrogen evolution reactions, *Nano Energy*, 2020, **77**, 105080.

205 E. J. Popczun, J. R. McKone, C. G. Read, A. J. Biacchi, A. M. Wiltrout, N. S. Lewis and R. E. Schaak, Nanostructured nickel phosphide as an electrocatalyst for the hydrogen evolution reaction, *J. Am. Chem. Soc.*, 2013, **135**, 9267–9270.

206 X. Wang, Y. V. Kolen'ko, X. Q. Bao, K. Kovnir and L. Liu, One-step synthesis of self-supported nickel phosphide nanosheet array cathodes for efficient electrocatalytic hydrogen generation, *Angew. Chem., Int. Ed.*, 2015, **54**, 8188–8192.

207 P. W. Menezes, A. Indra, C. Das, C. Walter, C. Göbel, V. Gutkin, D. Schmeißer and M. Driess, Uncovering the nature of active species of nickel phosphide catalysts in high-performance electrochemical overall water splitting, *ACS Catal.*, 2016, **7**, 103–109.

208 T. Xu, D. Jiao, L. Zhang, H. Zhang, L. Zheng, D. J. Singh, J. Zhao, W. Zheng and X. Cui, Br-induced P-poor defective nickel phosphide for highly efficient overall water splitting, *Appl. Catal., B*, 2022, **316**, 121686.

209 J. Zhou, C. Huang, Q. Zhou, Y. Xie, L. Yang, L. Yu and Y. Yu, Electronic structure regulation of nickel phosphide for efficient overall water splitting, *Inorg. Chem.*, 2022, **61**, 9318–9327.

210 B. Lu, D. Wang, C. Zhao, K. Zhu, J. Yan, G. Wang, D. Cao and K. Ye, The novel dual-category active sites of NiCoP/CoP as high-performance electrocatalyst for urea electrolysis and synergistic hydrogen production, *Mater. Chem. Front.*, 2022, **6**, 1681–1689.

211 Q. Yan, X. Chen, T. Wei, G. Wang, M. Zhu, Y. Zhuo, K. Cheng, K. Ye, K. Zhu, J. Yan, D. Cao and Y. Li, Hierarchical edge-rich nickel phosphide nanosheet arrays as efficient electrocatalysts toward hydrogen evolution in both alkaline and acidic conditions, *ACS Sustainable Chem. Eng.*, 2019, **7**, 7804–7811.

212 Y. Wang, L. Liu, X. Zhang, F. Yan, C. Zhu and Y. Chen, Self-supported tripod-like nickel phosphide nanowire arrays for hydrogen evolution, *J. Mater. Chem. A*, 2019, **7**, 22412–22419.

213 R. B. Wexler, J. M. P. Martirez and A. M. Rappe, Active role of phosphorus in the hydrogen evolving activity of nickel phosphide (0001) surfaces, *ACS Catal.*, 2017, **7**, 7718–7725.

214 W. Zhang, N. Han, J. Luo, X. Han, S. Feng, W. Guo, S. Xie, Z. Zhou, P. Subramanian, K. Wan, J. Arbiol, C. Zhang, S. Liu, M. Xu, X. Zhang and J. Fransaer, Critical role of phosphorus in hollow structures cobalt-based phosphides as bifunctional catalysts for water splitting, *Small*, 2022, **18**, 2103561.

215 C. C. Weng, J. T. Ren and Z. Y. Yuan, Transition metal phosphide-based materials for efficient electrochemical hydrogen evolution: a critical review, *ChemSusChem*, 2020, **13**, 3357–3375.

216 A. Parra-Puerto, K. L. Ng, K. Fahy, A. E. Goode, M. P. Ryan and A. Kucernak, Supported transition metal phosphides: activity survey for HER, ORR, OER, and corrosion resistance in acid and alkaline electrolytes, *ACS Catal.*, 2019, **9**, 11515–11529.

217 J. Duan, S. Chen, C. A. Ortiz-Ledon, M. Jaroniec and S. Z. Qiao, Phosphorus vacancies that boost electrocatalytic hydrogen evolution by two orders of magnitude, *Angew. Chem., Int. Ed.*, 2020, **59**, 8181–8186.

218 Q. Zhou, L. Liao, Q. Bian, F. Yu, D. Li, J. Zeng, L. Zhang, H. Wang, D. Tang, H. Zhou and Z. Ren, Engineering in-plane nickel phosphide heterointerfaces with interfacial sp H-P hybridization for highly efficient and durable hydrogen evolution at 2 A cm^{-2}, *Small*, 2022, **18**, 2105642.

219 W. Yang and S. Chen, Recent progress in electrode fabrication for electrocatalytic hydrogen evolution reaction: a mini review, *Chem. Eng. J.*, 2020, **393**, 124726.

220 Q. Shao, P. Wang, T. Zhu and X. Huang, Low dimensional platinum-based bimetallic nanostructures for advanced catalysis, *Acc. Chem. Res.*, 2019, **52**, 3384–3396.

221 F. Li and J.-B. Baek, Atomic tailoring of platinum catalysts, *Nat. Catal.*, 2019, **2**, 477–478.

222 X. Chen, X. An, L. Tang, T. Chen and G. Zhang, Confining platinum clusters in ZIF-8-derived porous N-doped carbon arrays for high-performance hydrogen evolution reaction, *Chem. Eng. J.*, 2022, **429**, 132259.

223 Y. Tan, R. Xie, S. Zhao, X. Lu, L. Liu, F. Zhao, C. Li, H. Jiang, G. Chai, D. J. L. Brett, P. R. Shearing, G. He and I. P. Parkin, Facile fabrication of robust hydrogen evolution electrodes under high current densities via Pt@Cu interactions, *Adv. Funct. Mater.*, 2021, **31**, 2105579.

224 Z. Zhu, H. Yin, C. T. He, M. Al-Mamun, P. Liu, L. Jiang, Y. Zhao, Y. Wang, H. G. Yang, Z. Tang, D. Wang, X. M. Chen and H. Zhao, Ultrathin transition metal dichalcogenide/3d metal hydroxide hybridized nanosheets to enhance hydrogen evolution activity, *Adv. Mater.*, 2018, **30**, 1801171.

225 G. Chen, T. Wang, J. Zhang, P. Liu, H. Sun, X. Zhuang, M. Chen and X. Feng, Accelerated hydrogen evolution

kinetics on NiFe-layered double hydroxide electrocatalysts by tailoring water dissociation active sites, *Adv. Mater.*, 2018, **30**, 1706279.

226 W. J. Jiang, T. Tang, Y. Zhang and J. S. Hu, Synergistic modulation of non-precious-metal electrocatalysts for advanced water splitting, *Acc. Chem. Res.*, 2020, **53**, 1111–1123.

227 J. Gao, L. Yang, D. Wang and D. Cao, Hollow nanotube Ru/$Cu_{2+1}O$ supported on copper foam as a bifunctional catalyst for overall water splitting, *Chemistry*, 2020, **26**, 4112–4119.

228 C. Song, Z. Zhao, X. Sun, Y. Zhou, Y. Wang and D. Wang, In situ growth of Ag nanodots decorated Cu_2O porous nanobelts networks on copper foam for efficient HER electrocatalysis, *Small*, 2019, **15**, 1804268.

229 Z. Yu, J. Xu, L. Meng and L. Liu, Efficient hydrogen production by saline water electrolysis at high current densities without the interfering chlorine evolution, *J. Mater. Chem. A*, 2021, **9**, 22248–22253.

230 R. Liu, Z. Gong, J. Liu, J. Dong, J. Liao, H. Liu, H. Huang, J. Liu, M. Yan, K. Huang, H. Gong, J. Zhu, C. Cui, G. Ye and H. Fei, Design of aligned porous carbon films with single-atom Co-N-C sites for high-current-density hydrogen generation, *Adv. Mater.*, 2021, **33**, 2103533.

231 S. Ma, X. Qu, J. Huang, C. Zhang, G. Chen, W. Chen, T. Li, T. Shao, K. Zheng, J. Tian, C. Li and K. Ostrikov, Compositional and crystallographic design of Ni-Co phosphide heterointerfaced nanowires for high-rate, stable hydrogen generation at industry-relevant electrolysis current densities, *Nano Energy*, 2022, **95**, 106989.

232 D. Gao, J. Ren, H. Wang, X. Wang, Y. Liu and R. Wang, An industry-applicable hybrid electrode for large current density hydrogen evolution reaction, *J. Power Sources*, 2021, **516**, 230635.

233 H. Q. Fu, M. Zhou, P. F. Liu, P. Liu, H. Yin, K. Z. Sun, H. G. Yang, M. Al-Mamun, P. Hu, H. F. Wang and H. Zhao, Hydrogen spillover-bridged Volmer/Tafel processes enabling ampere-level current density alkaline hydrogen evolution reaction under low overpotential, *J. Am. Chem. Soc.*, 2022, **144**, 6028–6039.

234 F. Wang, Y. Wu, B. Dong, K. Lv, Y. Shi, N. Ke, L. Hao, L. Yin, Y. Bai, X. Xu, Y. Xian and S. Agathopoulos, Robust porous WC-based self-supported ceramic electrodes for high current density hydrogen evolution reaction, *Adv. Sci.*, 2022, **9**, 2106029.

235 C. Zhang, Y. Luo, J. Tan, Q. Yu, F. Yang, Z. Zhang, L. Yang, H.-M. Cheng and B. Liu, High-throughput production of cheap mineral-based two-dimensional electrocatalysts for high-current-density hydrogen evolution, *Nat. Commun.*, 2020, **11**, 3724.

236 S. Li, M. Li and Y. Ni, Grass-like Ni/Cu nanosheet arrays grown on copper foam as efficient and non-precious catalyst for hydrogen evolution reaction, *Appl. Catal., B*, 2020, **268**, 118392.

237 M. Yao, B. Wang, B. Sun, L. Luo, Y. Chen, J. Wang, N. Wang, S. Komarneni, X. Niu and W. Hu, Rational design of self-supported Cu@WC core–shell mesoporous nanowires for pH-universal hydrogen evolution reaction, *Appl. Catal., B*, 2021, **280**, 119451.

238 C. Tong, R. Xiang, L. Peng, L. Tan, X. Tang, J. Wang, L. Li, Q. Liao and Z. Wei, Amorphous FeO_x (x = 1, 1.5) coated Cu_3P nanosheets with bamboo leaves-like morphology induced by solvent molecule adsorption for highly active HER catalysts, *J. Mater. Chem. A*, 2020, **8**, 3351–3356.

239 N. Xie, D.-D. Ma, Y.-L. Wu, X.-T. Wu and Q.-L. Zhu, Hierarchical Cu_2S hollow nanowire arrays for highly efficient hydrogen evolution reaction, *Sustainable Energy Fuels*, 2021, **5**, 2633–2639.

240 A. Hemmasian Ettefagh, S. Guo and J. Raush, Corrosion performance of additively manufactured stainless steel parts: A review, *Addit. Manuf.*, 2021, **37**, 101689.

241 L. Cui, F. Jiang, D. Deng, T. Xin, X. Sun, R. T. Mousavian, R. L. Peng, Z. Yang and J. Moverare, Cyclic response of additive manufactured 316L stainless steel: The role of cell structures, *Scr. Mater.*, 2021, **205**, 114190.

242 J. Mola, G. Luan, Q. Huang, C. Ullrich, O. Volkova and Y. Estrin, Dynamic strain aging mechanisms in a metastable austenitic stainless steel, *Acta Mater.*, 2021, **212**, 116888.

243 S. Choudhary, V. Cruz, A. Pandey, S. Thomas and N. Birbilis, Element-resolved electrochemical analysis of the passivity of additively manufactured stainless steel 316L, *Corros. Sci.*, 2021, **189**, 109576.

244 Y. Lei, Z. Zhan, M. Saakes, R. D. van der Weijden and C. J. N. Buisman, Electrochemical recovery of phosphorus from wastewater using tubular stainless-steel cathode for a scalable long-term operation, *Water Res.*, 2021, **199**, 117199.

245 M. Kim, J. Ha, Y.-T. Kim and J. Choi, Stainless steel: a high potential material for green electrochemical energy storage and conversion, *Chem. Eng. J.*, 2022, **440**, 135459.

246 J. Li, J. Luo, H. Chen, B. Qin, C. Yuan, N. Wu, G. Liu and X. Liu, Strong electronic metal-support interaction between Pt and stainless mesh for enhancing the hydrogen evolution reaction, *Chem. Commun.*, 2022, **58**, 9918–9921.

247 S. Zhu, G. Duan, C. Chang, Y. Chen, Y. Sun, Y. Tang, P. Wan and J. Pan, Fast electrodeposited nickle–iron hydroxide nanosheets on sintered stainless steel felt as bifunctional electrocatalyts for overall water splitting, *ACS Sustainable Chem. Eng.*, 2020, **8**, 9885–9895.

248 Y. Shi, Z. R. Ma, Y. Y. Xiao, Y. C. Yin, W. M. Huang, Z. C. Huang, Y. Z. Zheng, F. Y. Mu, R. Huang, G. Y. Shi, Y. Y. Sun, X. H. Xia and W. Chen, Electronic metal-support interaction modulates single-atom platinum catalysis for hydrogen evolution reaction, *Nat. Commun.*, 2021, **12**, 3021.

249 J. Yang, W. H. Li, S. Tan, K. Xu, Y. Wang, D. Wang and Y. Li, The electronic metal-support interaction directing the design of single atomic site catalysts: achieving high efficiency towards hydrogen evolution, *Angew. Chem., Int. Ed.*, 2021, **60**, 19085–19091.

250 M. Zhou, S. Bao and A. J. Bard, Probing size and substrate effects on the hydrogen evolution reaction by single

isolated Pt atoms, atomic clusters, and nanoparticles, *J. Am. Chem. Soc.*, 2019, **141**, 7327–7332.

251 J. Zhang, Y. Zhao, X. Guo, C. Chen, C.-L. Dong, R.-S. Liu, C.-P. Han, Y. Li, Y. Gogotsi and G. Wang, Single platinum atoms immobilized on an MXene as an efficient catalyst for the hydrogen evolution reaction, *Nat. Catal.*, 2018, **1**, 985–992.

252 P. Kuang, Y. Wang, B. Zhu, F. Xia, C. W. Tung, J. Wu, H. M. Chen and J. Yu, Pt single atoms supported on N-doped mesoporous hollow carbon spheres with enhanced electrocatalytic H_2-evolution activity, *Adv. Mater.*, 2021, **33**, 2008599.

253 J. Park, S. Lee, H. E. Kim, A. Cho, S. Kim, Y. Ye, J. W. Han, H. Lee, J. H. Jang and J. Lee, Investigation of the support effect in atomically dispersed Pt on WO_{3-x} for utilization of Pt in the hydrogen evolution reaction, *Angew. Chem., Int. Ed.*, 2019, **58**, 16038–16042.

254 J. Li, J. Wang, Y. Liu, C. Yuan, G. Liu, N. Wu and X. Liu, Sodium tungsten bronze-supported Pt electrocatalysts for the high-performance hydrogen evolution reaction, *Catal. Sci. Technol.*, 2022, **12**, 4498–4510.

255 T. N. J. I. Edison, R. Atchudan, N. Karthik, S. Chandrasekaran, S. Perumal, P. B. Raja, V. Perumal and Y. R. Lee, Deep eutectic solvent assisted electrosynthesis of ruthenium nanoparticles on stainless steel mesh for electrocatalytic hydrogen evolution reaction, *Fuel*, 2021, **297**, 120786.

256 Q. Tan, R. Xiao, X. Yao, T. Xiong, J. Li, Y.-W. Hu, Y. Huang and M. S. Balogun, Non-oxygen anion-regulated in situ cobalt based heterojunctions for active alkaline hydrogen evolution catalysis, *Chem. Eng. J.*, 2022, **433**, 133514.

257 Y. Hu, H. Yang, J. Chen, T. Xiong, M. J. T. Balogun and Y. Tong, Efficient hydrogen evolution activity and overall water splitting of metallic Co_4N nanowires through tunable d-orbitals with ultrafast incorporation of FeOOH, *ACS Appl. Mater. Interfaces*, 2019, **11**, 5152–5158.

258 M. Yao, B. Wang, N. Wang, S. Komarneni, Y. Chen, J. Wang, X. Niu and W. Hu, Self-supported composite of $(Ni,Co)_3C$ mesoporous nanosheets/N-doped carbon as a flexible electrocatalyst for pH-universal hydrogen evolution, *ACS Sustainable Chem. Eng.*, 2020, **8**, 5287–5295.

259 C. Jian, Q. Cai, W. Hong, J. Li and W. Liu, Edge-riched $MoSe_2/MoO_2$ hybrid electrocatalyst for efficient hydrogen evolution reaction, *Small*, 2018, **14**, 1703798.

260 T. Hu, K. Bian, G. Tai, T. Zeng, X. Wang, X. Huang, K. Xiong and K. Zhu, Oxidation-sulfidation approach for vertically growing MoS_2 nanofilms catalysts on molybdenum foils as efficient HER catalysts, *J. Phys. Chem. C*, 2016, **120**, 25843–25850.

261 Y. Xu, C. Zheng, S. Wang and Y. Hou, 3D arrays of molybdenum sulphide nanosheets on Mo meshes: efficient electrocatalysts for hydrogen evolution reaction, *Electrochim. Acta*, 2015, **174**, 653–659.

262 C. Jian, Q. Cai and W. Liu, A three-dimensional macroporous framework molybdenum disulfide-carbide heterojunction for highly efficient electrocatalytic hydrogen evolution at high current densities, *Chem. Commun.*, 2021, **57**, 11819–11822.

263 Y. Deng, Z. Liu, A. Wang, D. Sun, Y. Chen, L. Yang, J. Pang, H. Li, H. Li, H. Liu and W. Zhou, Oxygen-incorporated MoX (X: S, Se or P) nanosheets via universal and controlled electrochemical anodic activation for enhanced hydrogen evolution activity, *Nano Energy*, 2019, **62**, 338–347.

264 J. S. Kang, J. Kim, M. J. Lee, Y. J. Son, D. Y. Chung, S. Park, J. Jeong, J. M. Yoo, H. Shin, H. Choe, H. S. Park and Y. E. Sung, Electrochemically synthesized nanoporous molybdenum carbide as a durable electrocatalyst for hydrogen evolution reaction, *Adv. Sci.*, 2018, **5**, 1700601.

265 C. Jian, W. Hong, Q. Cai, J. Li and W. Liu, Surface electron state engineering enhanced hydrogen evolution of hierarchical molybdenum disulfide in acidic and alkaline media, *Appl. Catal., B*, 2020, **266**, 118649.

266 H. Zhao, Z. Li, J. Deng, X. Dai, M. Cui, F. Nie, X. Zhang, Z. Ren, Y. Wang, W. Song and J. Liu, Amorphous MoS_2 nanosheets on MoO_2 films/Mo foil as free-standing electrode for synergetic electrocatalytic hydrogen evolution reaction, *Int. J. Hydrogen Energy*, 2020, **45**, 17422–17433.

267 Z. Pu, Q. Liu, A. M. Asiri, Y. Luo, X. Sun and Y. He, 3D macroporous MoS_2 thin film: in situ hydrothermal preparation and application as a highly active hydrogen evolution electrocatalyst at all pH values, *Electrochim. Acta*, 2015, **168**, 133–138.

268 Y. Guo, X. Fu, B. Zhang and Z. Peng, Vertically standing MoP nanosheet arrays on Mo substrate: An integrated binder-free electrode for highly efficient and stable hydrogen evolution, *J. Alloys Compd.*, 2019, **792**, 732–741.

269 H. Zhao, Z. Li, X. Dai, M. Cui, F. Nie, X. Zhang, Z. Ren, Z. Yang, Y. Gan, X. Yin, Y. Wang and W. Song, Heterostructured CoP/MoO2 on Mo foil as high-efficiency electrocatalysts for the hydrogen evolution reaction in both acidic and alkaline media, *J. Mater. Chem. A*, 2020, **8**, 6732–6739.

270 Y. Luo, L. Tang, U. Khan, Q. Yu, H. M. Cheng, X. Zou and B. Liu, Morphology and surface chemistry engineering toward pH-universal catalysts for hydrogen evolution at high current density, *Nat. Commun.*, 2019, **10**, 269.

271 H. Sun, C. Tian, G. Fan, J. Qi, Z. Liu, Z. Yan, F. Cheng, J. Chen, C. P. Li and M. Du, Boosting activity on Co_4N porous nanosheet by coupling CeO_2 for efficient electrochemical overall water splitting at high current densities, *Adv. Funct. Mater.*, 2020, **30**, 1910596.

272 Y. Luo, Z. Zhang, F. Yang, J. Li, Z. Liu, W. Ren, S. Zhang and B. Liu, Stabilized hydroxide-mediated nickel-based electrocatalysts for high-current-density hydrogen evolution in alkaline media, *Energy Environ. Sci.*, 2021, **14**, 4610–4619.

273 C. Jian, W. Hong, Q. Cai and W. Liu, The local electronic structure modulation of the molybdenum selenide-nitride heterojunction for efficient hydrogen evolution reaction, *J. Mater. Chem. A*, 2021, **9**, 26113–26118.

274 C. Jian, Q. Cai, W. Hong and W. Liu, Large-scale production of a low-cost molybdenum dioxide-phosphide

seamless electrode for high-current-density hydrogen evolution, *J. Mater. Chem. A*, 2022, **10**, 3454–3459.

275 W. Liu, X. Wang, F. Wang, K. Du, Z. Zhang, Y. Guo, H. Yin and D. Wang, A durable and pH-universal self-standing MoC-Mo_2C heterojunction electrode for efficient hydrogen evolution reaction, *Nat. Commun.*, 2021, **12**, 6776.

276 N. Chen, W. Zhang, J. Zeng, L. He, D. Li and Q. Gao, Plasma-engineered MoP with nitrogen doping: electron localization toward efficient alkaline hydrogen evolution, *Appl. Catal., B*, 2020, **268**, 118441.

277 K. Jian, W. Ma, Z. Lv, M. Wang, X. Lv, Q. Li and J. Dang, Tuning the electronic structure of the CoP/Ni_2P nanostructure by nitrogen doping for an efficient hydrogen evolution reaction in alkaline media, *Inorg. Chem.*, 2021, **60**, 18544–18552.

278 J. Zhu, S. Li, M. Xiao, X. Zhao, G. Li, Z. Bai, M. Li, Y. Hu, R. Feng, W. Liu, R. Gao, D. Su, A. Yu and Z. Chen, Tensile-strained ruthenium phosphide by anion substitution for highly active and durable hydrogen evolution, *Nano Energy*, 2020, **77**, 105212.

279 S. Zhao, R. Xie, L. Kang, M. Yang, X. He, W. Li, R. Wang, D. J. L. Brett, G. He, G. Chai and I. P. Parkin, Enhancing hydrogen evolution electrocatalytic performance in neutral media via nitrogen and iron phosphide interactions, *Small Sci.*, 2021, **1**, 2100032.

280 Q. Zhou, Z. Shen, C. Zhu, J. Li, Z. Ding, P. Wang, F. Pan, Z. Zhang, H. Ma, S. Wang and H. Zhang, Nitrogen-doped CoP electrocatalysts for coupled hydrogen evolution and sulfur generation with low energy consumption, *Adv. Mater.*, 2018, **30**, 1800140.

281 Z. Liu, X. Yu, H. Xue and L. Feng, A nitrogen-doped CoP nanoarray over 3D porous Co foam as an efficient bifunctional electrocatalyst for overall water splitting, *J. Mater. Chem. A*, 2019, **7**, 13242–13248.

282 Y. Hua, Q. Xu, Y. Hu, H. Jiang and C. Li, Interface-strengthened CoP nanosheet array with Co_2P nanoparticles as efficient electrocatalysts for overall water splitting, *J. Energy Chem.*, 2019, **37**, 1–6.

283 X. Liu, Y. Pei, L. Huang, W. Lei, F. Li, Y. Li, H. Zhang, Q. Jia and S. Zhang, Rational design of ultrahigh porosity Co foam supported flower-like FeNiP-LDH electrocatalysts towards hydrogen evolution reaction, *Catal. Today*, 2022, **400**, 6–13.

284 Y. Pei, L. Huang, L. Han, H. Zhang, L. Dong, Q. Jia and S. Zhang, NiCoP/NiOOH nanoflowers loaded on ultrahigh porosity Co foam for hydrogen evolution reaction under large current density, *Green Energy Environ.*, 2022, **7**, 467–476.

285 X. Liu, Y. Yao, H. Zhang, L. Pan, C. Shi, X. Zhang, Z.-F. Huang and J.-J. Zou, In situ-grown cobalt–iron phosphide-based integrated electrode for long-term water splitting under a large current density at the industrial electrolysis temperature, *ACS Sustainable Chem. Eng.*, 2020, **8**, 17828–17838.

286 H. Ma, Z. Chen, Z. Wang, C. V. Singh and Q. Jiang, Interface engineering of Co/CoMoN/NF heterostructures for high-performance electrochemical overall water splitting, *Adv. Sci.*, 2022, **9**, 2105313.

287 L. Yang, R. Liu and L. Jiao, Electronic redistribution: construction and modulation of interface engineering on CoP for enhancing overall water splitting, *Adv. Funct. Mater.*, 2020, **30**, 1909618.

288 X. Luo, P. Ji, P. Wang, R. Cheng, D. Chen, C. Lin, J. Zhang, J. He, Z. Shi, N. Li, S. Xiao and S. Mu, Interface engineering of hierarchical branched Mo-doped Ni_3S_2/Ni_xP_y hollow heterostructure nanorods for efficient overall water splitting, *Adv. Energy Mater.*, 2020, **10**, 1903891.

289 T. Yu, Q. Xu, L. Luo, C. Liu and S. Yin, Interface engineering of NiO/RuO_2 heterojunction nano-sheets for robust overall water splitting at large current density, *Chem. Eng. J.*, 2022, **430**, 133117.

290 Y. Hu, H. Yu, L. Qi, J. Dong, P. Yan, T. Taylor Isimjan and X. Yang, Interface engineering of needle-like P-doped MoS_2/CoP arrays as highly active and durable bifunctional electrocatalyst for overall water splitting, *ChemSusChem*, 2021, **14**, 1565–1573.

291 F. Song, W. Li, J. Yang, G. Han, T. Yan, X. Liu, Y. Rao, P. Liao, Z. Cao and Y. Sun, Interfacial sites between cobalt nitride and cobalt act as bifunctional catalysts for hydrogen electrochemistry, *ACS Energy Lett.*, 2019, **4**, 1594–1601.

292 W. Hu, Q. Shi, Z. Chen, H. Yin, H. Zhong and P. Wang, Co_2N/$Co_2Mo_3O_8$ heterostructure as a highly active electrocatalyst for an alkaline hydrogen evolution reaction, *ACS Appl. Mater. Interfaces*, 2021, **13**, 8337–8343.

293 H. Wang, J. Xu, Q. Zhang, S. Hu, W. Zhou, H. Liu and X. Wang, Super-hybrid transition metal sulfide nanoarrays of Co_3S_4 nanosheet/P-doped WS_2 nanosheet/Co_9S_8 nanoparticle with Pt-like activities for robust all-pH hydrogen evolution, *Adv. Funct. Mater.*, 2022, **32**, 2112362.

294 Z. Feng, J. Pu, M. Liu, W. Zhang, X. Zhang, L. Cui and J. Liu, Facile construction of hierarchical Co_3S_4/CeO_2 heterogeneous nanorod array on cobalt foam for electrocatalytic overall water splitting, *J. Colloid Interface Sci.*, 2022, **613**, 806–813.

295 S. Hao, L. Chen, C. Yu, B. Yang, Z. Li, Y. Hou, L. Lei and X. Zhang, NiCoMo hydroxide nanosheet arrays synthesized via chloride corrosion for overall water splitting, *ACS Energy Lett.*, 2019, **4**, 952–959.

296 Y. Yan, J. Liu, K. Huang, L. Qiao, J. Sui, W. Cai and X. Zheng, Periodic corrosion turns bulk Ni into Zr-incorporated polycrystalline $Ni(OH)_2$ nanoarrays for overall water decomposition, *ACS Appl. Energy Mater.*, 2022, **5**, 5711–5718.

297 S. Duan, Z. Liu, H. Zhuo, T. Wang, J. Liu, L. Wang, J. Liang, J. Han, Y. Huang and Q. Li, Hydrochloric acid corrosion induced bifunctional free-standing NiFe hydroxide nanosheets towards high-performance alkaline seawater splitting, *Nanoscale*, 2020, **12**, 21743–21749.

298 Y. Zhao, Y. Gao, Z. Chen, Z. Li, T. Ma, Z. Wu and L. Wang, Trifle Pt coupled with NiFe hydroxide synthesized via corrosion engineering to boost the cleavage of water

molecule for alkaline water-splitting, *Appl. Catal., B*, 2021, **297**, 120395.

299 Z. Wu, Y. Zhao, H. Wu, Y. Gao, Z. Chen, W. Jin, J. Wang, T. Ma and L. Wang, Corrosion engineering on iron foam toward efficiently electrocatalytic overall water splitting powered by sustainable energy, *Adv. Funct. Mater.*, 2021, **31**, 2010437.

300 H. Lv, C. Fu, J. Fan, Y. Zhang and W. Hao, Mild construction of robust FeS-based electrode for pH-universal hydrogen evolution at industrial current density, *J. Colloid Interface Sci.*, 2022, **626**, 384–394.

301 T. Cui, X. Zhai, L. Guo, J.-Q. Chi, Y. Zhang, J. Zhu, X. Sun and L. Wang, Controllable synthesis of a self-assembled ultralow Ru, Ni-doped Fe_2O_3 lily as a bifunctional electrocatalyst for large-current-density alkaline seawater electrolysis, *Chin. J. Catal.*, 2022, **43**, 2202–2211.

302 J. Zhang, X. Shang, H. Ren, J. Chi, H. Fu, B. Dong, C. Liu and Y. Chai, Modulation of inverse spinel Fe_3O_4 by phosphorus doping as an industrially promising electrocatalyst for hydrogen evolution, *Adv. Mater.*, 2019, **31**, 1905107.

303 X.-Y. Zhang, F.-T. Li, R.-Y. Fan, J. Zhao, B. Dong, F.-L. Wang, H.-J. Liu, J.-F. Yu, C.-G. Liu and Y.-M. Chai, F, P double-doped Fe_3O_4 with abundant defect sites for efficient hydrogen evolution at high current density, *J. Mater. Chem. A*, 2021, **9**, 15836–15845.

304 X.-Y. Zhang, Y.-R. Zhu, Y. Chen, S.-Y. Dou, X.-Y. Chen, B. Dong, B.-Y. Guo, D.-P. Liu, C.-G. Liu and Y.-M. Chai, Hydrogen evolution under large-current-density based on fluorine-doped cobalt-iron phosphides, *Chem. Eng. J.*, 2020, **399**, 125831.

305 X.-Y. Zhang, F.-L. Wang, J.-Y. Fu, Y.-N. Zhen, B. Dong, Y.-N. Zhou, H.-J. Liu, D.-P. Liu, C.-G. Liu and Y.-M. Chai, Amorphous-crystalline catalytic interface of CoFeOH/CoFeP with double sites based on ultrafast hydrolysis for hydrogen evolution at high current density, *J. Power Sources*, 2021, **507**, 230279.

306 J. Li, W. Hong, C. Jian, Q. Cai and W. Liu, Seamless tungsten disulfide-tungsten heterojunction with abundant exposed active sites for efficient hydrogen evolution, *Appl. Catal., B*, 2019, **244**, 320–326.

307 J. Xie, H. Qu, J. Xin, X. Zhang, G. Cui, X. Zhang, J. Bao, B. Tang and Y. Xie, Defect-rich MoS_2 nanowall catalyst for efficient hydrogen evolution reaction, *Nano Res.*, 2017, **10**, 1178–1188.

308 D. Vikraman, S. Hussain, K. Akbar, K. Karuppasamy, S.-H. Chun, J. Jung and H.-S. Kim, Design of basal plane edges in metal-doped nanostripes-structured $MoSe_2$ atomic layers to enhance hydrogen evolution reaction activity, *ACS Sustainable Chem. Eng.*, 2018, **7**, 458–469.

309 Y.-N. Zhou, M.-X. Li, Z.-N. Shi, J.-C. Zhou, B. Dong, W. Jiang, B. Liu, J.-F. Yu and Y.-M. Chai, Crystal-amorphous NiO/MoO_2 with a high-density interface for hydrogen evolution, *Inorg. Chem. Front.*, 2022, **9**, 2087–2096.

310 M. A. R. Anjum, M. S. Okyay, M. Kim, M. H. Lee, N. Park and J. S. Lee, Bifunctional sulfur-doped cobalt phosphide electrocatalyst outperforms all-noble-metal electrocatalysts in alkaline electrolyzer for overall water splitting, *Nano Energy*, 2018, **53**, 286–295.

311 P. Wang, T. Jia and B. Wang, A critical review: 1D/2D nanostructured self-supported electrodes for electrochemical water splitting, *J. Power Sources*, 2020, **474**, 228621.

312 J.-S. Zhu, H. Yang, W. Zhang, Y. Mao, S.-S. Lyu and J. Chen, An In situ Raman study of intermediate adsorption engineering by high-index facet control during the hydrogen evolution reaction, *Inorg. Chem. Front.*, 2020, **7**, 1892–1899.

313 Y. Zhu, T.-R. Kuo, Y.-H. Li, M.-Y. Qi, G. Chen, J. Wang, Y.-J. Xu and H. M. Chen, Emerging dynamic structure of electrocatalysts unveiled by in situ X-ray diffraction/absorption spectroscopy, *Energy Environ. Sci.*, 2021, **14**, 1928–1958.

314 C. Lafforgue, F. Maillard, V. Martin, L. Dubau and M. Chatenet, Degradation of carbon-supported platinum-group-metal electrocatalysts in alkaline media studied by in situ Fourier transform infrared spectroscopy and identical-location transmission electron microscopy, *ACS Catal.*, 2019, **9**, 5613–5622.

315 J. Wang, H. Y. Tan, T. R. Kuo, S. C. Lin, C. S. Hsu, Y. Zhu, Y. C. Chu, T. L. Chen, J. F. Lee and H. M. Chen, In situ identifying the dynamic structure behind activity of atomically dispersed platinum catalyst toward hydrogen evolution reaction, *Small*, 2021, **17**, 2005713.

316 S. Hwang, X. Chen, G. Zhou and D. Su, In situ transmission electron microscopy on energy-related catalysis, *Adv. Energy Mater.*, 2019, **10**, 1902105.

317 J. Li, G. Johnson, S. Zhang and D. Su, In situ transmission electron microscopy for energy applications, *Joule*, 2019, **3**, 4–8.

318 Y. Wu, W. Luo, P. Gao, C. Zhu, X. Hu, K. Qu, J. Chen, Y. Wang, L. Sun, L. Mai and F. Xu, Unveiling the microscopic origin of asymmetric phase transformations in (de)sodiated Sb_2Se_3 with in situ transmission electron microscopy, *Nano Energy*, 2020, **77**, 105299.

319 B. Sheng, D. Cao, C. Liu, S. Chen and L. Song, Support effects in electrocatalysis and their synchrotron radiation-based characterizations, *J. Phys. Chem. Lett.*, 2021, **12**, 11543–11554.

320 M. Wang, L. Arnadottir, Z. J. Xu and Z. Feng, In situ X-ray absorption spectroscopy studies of nanoscale electrocatalysts, *Nanomicro Lett.*, 2019, **11**, 47.

321 J. Park and J. Cho, Advances in understanding mechanisms of perovskites and pyrochlores as electrocatalysts using *in situ* X-ray absorption spectroscopy, *Angew. Chem., Int. Ed.*, 2020, **59**, 15314–15324.

322 K. Murugappan, E. M. Anderson, D. Teschner, T. E. Jones, K. Skorupska and Y. Román-Leshkov, Operando NAP-XPS unveils differences in MoO_3 and Mo_2C during hydrodeoxygenation, *Nat. Catal.*, 2018, **1**, 960–967.

323 J. Chen, J. Kawai, K. Ozawa, R. Toyoshima, K. Tomishige and H. Kondoh, Substrate effect of Ir and Rh on surface ReO_x species under a hydrogen atmosphere studied by NAP-XPS, *J. Phys. Chem. C*, 2022, **126**, 11544–11552.

324 X. Zhang, R. You, Z. Wei, X. Jiang, J. Yang, Y. Pan, P. Wu, Q. Jia, Z. Bao, L. Bai, M. Jin, B. Sumpter, V. Fung, W. Huang and Z. Wu, Radical chemistry and reaction mechanisms of propane oxidative dehydrogenation over hexagonal boron nitride catalysts, *Angew. Chem., Int. Ed.*, 2020, **59**, 8042–8046.

325 Q.-X. Chen and S.-H. Yu, Ordering nanostructures enhances electrocatalytic reactions, *Trends Chem.*, 2020, **2**, 888–897.

326 L. Zhao, Z. Guo and Z. Liu, Facile synthesis and efficient electrochemical water splitting of bifunctional nanostructured Ni-based layered double hydroxide/sulfide composite, *J. Alloys Compd.*, 2022, **910**, 164880.

327 Y. Niu, Y. Yuan, Q. Zhang, F. Chang, L. Yang, Z. Chen and Z. Bai, Morphology-controlled synthesis of metal-organic frameworks derived lattice plane-altered iron oxide for efficient trifunctional electrocatalysts, *Nano Energy*, 2021, **82**, 105699.

328 F. Navarro-Pardo, J. Liu, O. Abdelkarim, G. S. Selopal, A. Yurtsever, A. C. Tavares, H. Zhao, Z. M. Wang and F. Rosei, 1D/2D cobalt-based nanohybrids as electrocatalysts for hydrogen generation, *Adv. Funct. Mater.*, 2020, **30**, 1908467.

329 X. Zang, W. Chen, X. Zou, J. N. Hohman, L. Yang, B. Li, M. Wei, C. Zhu, J. Liang, M. Sanghadasa, J. Gu and L. Lin, Self-assembly of large-area 2D polycrystalline transition metal carbides for hydrogen electrocatalysis, *Adv. Mater.*, 2018, **30**, 1805188.

330 S. Ding, Y. Sun, F. Lou, L. Yu, B. Xia, J. Duan, Y. Zhang and S. Chen, Plasma-regulated two-dimensional high entropy oxide arrays for synergistic hydrogen evolution: From theoretical prediction to electrocatalytic applications, *J. Power Sources*, 2022, **520**, 230873.

331 H. Zhou, F. Yu, J. Sun, R. He, S. Chen, C. W. Chu and Z. Ren, Highly active catalyst derived from a 3D foam of $Fe(PO_3)_2/Ni_2P$ for extremely efficient water oxidation, *Proc. Natl. Acad. Sci. U. S. A.*, 2017, **114**, 5607–5611.

332 Y. Liu, Q. Wang, J. Zhang, J. Ding, Y. Cheng, T. Wang, J. Li, F. Hu, H. B. Yang and B. Liu, Recent advances in carbon-supported noble-metal electrocatalysts for hydrogen evolution reaction: syntheses, structures, and properties, *Adv. Energy Mater.*, 2022, **12**, 2200928.

